Developing non-fouling and lubricious surface coatings for orthopedic implants

Prabhleen Kaur

A dissertation

submitted in partial fulfillment of the

requirements for the degree of

Doctor of Philosophy

University of Washington

2022

Reading Committee:

Buddy Ratner, Chair

Elizabeth Nance

Jorge Marchand

Program Authorized to Offer Degree:

Chemical Engineering

University of Washington

Abstract

Developing non-fouling and lubricious surface coatings for orthopedic implants

Prabhleen Kaur

Chair of the Supervisory Committee:
Professor Buddy Ratner
Departments of Bioengineering and Chemical Engineering

Foreign body response (FBR) remains a persistent challenge limiting the longevity of medical devices. Upon implantation, non-specific protein adsorption on the implant surface can trigger FBR and result in fouling. This necessitates frequent replacements and surgical procedures. Biological host responses are influenced primarily by atomic-scale surface properties like wettability, roughness and cytotoxicity. This dissertation introduces robust and versatile surface modification techniques designed to suitably alter these properties to enhance biocompatibility, applicable to commercially available, industrial-strength materials used in orthopedic implants.

Chemical modification *via* introduction of zwitterionic molecules is a proven strategy that greatly alters the thermodynamics of surface protein adsorption through strong interfacial hydration effects. This reduces non-specific protein adsorption and enhances surface lubricity

through robust hydration layers and fluidity of adhered water. The techniques demonstrated herein use poly (sulfobetaine methacrylate) (pSBMA) due to its low cost and ease of synthesis relative to other zwitterionic molecules. In grafting these species on to implant surfaces, we leverage versatile chemical modification methods based on RFGD plasma and ARGET ATRP.

The first part of this work thus focuses on surface modification protocols that involve surface activation using RFGD plasma deposition of HEMA, followed by macro-initiator covalent coupling and grafting pSBMA using ARGET ATRP (method 1). Next, we introduce a solvent free initiator for ARGET ATRP (method 2). A highly reactive bromoester, M3BP is deposited on the surface using RFGD plasma and used as initiator for synthesizing pSBMA coatings. Polyurethane and titanium are used as model substrates to demonstrate the versatility of these techniques.

This dissertation also details the performance evaluation of the fabricated coatings, including quantification of surface composition, wettability, protein adsorption and lubricity, in addition to *in vitro* and *in vivo* studies. Surfaces prepared using methodology 1 achieve a 93% reduction in albumin adsorption and 95% reduction in the friction coefficients relative to bare surfaces. They are chemically robust, non-cytotoxic, and show good *in vivo* performance in mice and chicken models. Surfaces prepared using methodology 2 also exhibit comparable results for both protein adsorption and friction coefficients, while providing an alternative ARGET ATRP initiator chemistry that does not require harsh solvents and is compatible with various materials irrespective of surface chemistry or geometry. These results signify the potential of these techniques for substantially improving biocompatibility and represent a proof-of-concept for simple and reproducible surface modification techniques with applicability at scale, serving a critical complementary function in maximizing the longevity and performance of orthopedic implants.

TABLE OF CONTENTS

LIST OF FIGURES

LIST OF TABLES

ACKNOWLEDGEMENTS

I am grateful to my Ph.D. advisor Prof. Buddy Ratner for giving me the opportunity to be a part of his lab and grow as an independent researcher. He always encouraged me to think critically and to find out of the box solutions to the problems at hand. His insightful comments and suggestions have gone a long way in improving the relevance and quality of my doctoral research. He was also instrumental in instilling in me the importance of constantly acquiring new skills. I am indebted to him for his guidance, support and advice during my graduate studies. I am also thankful to him for always presenting a positive and inclusive environment in the lab. I would also like to thank my dissertation committee members, Prof. Elizabeth Nance, Prof. Jorge Marchand and Prof. Cole DeForest for their valuable feedback and insightful discussions. Additionally, I would like to extend my sincere gratitude to Prof. Alshakim Nelson and Prof. Ashley Theberge who served as Graduate School Representatives on my committee.

I am thankful to our collaborator, Prof. Ravi Balasubramanian, for the opportunity to work on the research projects that comprise my PhD. I am especially thankful to him for always challenging me and pushing me to better my research. I have also benefited immensely from his mentorship and his constant encouragement to seek out opportunities for my professional development. My PhD project represented a combination of fundamental and applied research, and I am grateful for the opportunity to work on such a practical and interdisciplinary effort. I would also like to thank Justin Casebier, Forrest Ling and Hans Bestel from the Balasubramanian lab for all their help and productive discussions.

I would also like to extend my deep gratitude to the many individuals who provided invaluable assistance and support during my graduate school experience. Winston Ciridon spent

long hours and went out of his way to help me obtain the necessary training to smoothly operate the plasma reactors. I am grateful for his constant and prompt support in troubleshooting and resolving issues with the equipment anytime and every time, even if that required him to move his schedule around to accommodate my request. His dedication and commitment to helping students master this complex equipment went a long way in ensuring timely completion of my work. I would like to wholeheartedly thank our lab manager Sharon Creason for her relentless efforts to ensure the smooth and safe functioning of our lab. She went out of her way to make sure I always had what I needed to perform my experiments smoothly. From urgent procurement of supplies to accommodating last minute administrative and experimental requests, she has made invaluable contributions to my Ph.D. journey in more ways than one, for which I will forever be grateful. Her dedication and work ethic is inspirational and something I intend to emulate. I would also like to thank Gerry Hammer, Samantha Young, Micah Glaz and Heather Niles for all their assistance with instrument training and data analysis. Special thanks are also due to Allison Sherrill for her help in navigating the logistics of a Ph.D. program.

During my graduate school experience, I was fortunate to be a part of a supportive and collegial lab group, without whom my experience would not have been quite the same. A special shoutout to Julia King for being my support system throughout my journey. From deep discussions on science to the informal pep talks when I was feeling down, from random conversations to small thoughtful gestures, the past six years would have been very different if not for her support. I would also like to thank Dr. Lei Ye, Dr. Le Zhen, Dr. Marvin Mecwan, Dr. Razieh Khalifehzadeh and Dr. Kan Wu for their crucial assistance and mentorship. Sincere and honest thanks are also due to all my lab friends- Shijie, Guoyao, Sherry, KyungHoon, Louis, Meghan, Runbang, Jay, Irini and others for their support and useful feedback throughout my graduate school journey.

Sincere thanks are also due to my masters' advisor Prof. Yong Lak Joo under whose guidance I did my first independent research project. His training and mentorship went a long way towards preparing me for a top Ph.D. program. I would also like to extend my gratitude towards Dr. Yevgen Zhmayev, my Ph.D. mentor during my master's. His constant encouragement, support and mentorship was a major factor in my decision to pursue a doctorate.

I would like to thank and acknowledge Mrs. Suman Uppal, my high school mathematics teacher for always believing in me. The friends I made during different stages of my life deserve a special thanks as well. I would like to especially thank Anmol Behal for being a friend, mentor and guide since my high school. His positive life mantras never failed to lift my spirits and motivate me to keep going, no matter what. I would also like to acknowledge the friends I made in Seattle- Khushmeen, Akshay, Krutika, Antara, Abhinav, Reeya, Vidit, Rahul, Manan, Zeba and Ayushi amongst others. Special thanks to Akshay for always going above and beyond in helping me with all aspects of my studies and for being a friend in need. Khushmeen's positivity always brought a sense of normalcy and Krutika for cooking for me when I was busy finishing my dissertation.

I am truly grateful to my parents for always motivating and encouraging me to follow my chosen career path. I am thankful to them for always believing in me, even during the times when I did not believe in myself. Thank you Mumma and Papa for always being my driving force and my constant support. I would also like to thank my brother, Gurkaran for always being there by my side through thick and thin. I am indebted to them for everything I am today.

To Mumma and Papa

Chapter 1. MOTIVATION AND INTRODUCTION

1.1 MOTIVATION

Progress in the development of medical devices and implants is an important aspect of efforts to improve human life expectancy and quality. The global medical device market is projected to reach USD 718 billion by 2029, with the share of orthopedic devices expected to increase to USD 60 billion.[1,2] Medical devices and implants are made from different materials including polymers, metals, and ceramics.[3,4] These materials are required to perform in the acute internal environment of the human body. For instance, bones must endure a stress of approximately 4 MPa while the peak stresses on ligaments and tendons can be as high as 80 MPa. The body fluids in various tissues can exhibit a wide variation in pH with values between 1-9.[5] These numbers provide a glimpse into the extreme and dynamic conditions in which the implant materials must survive and perform, and thus signify the need for medical devices with the optimal combination of mechanical properties.

In addition to mechanical properties, chemical compatibility is a critical aspect of overall device biocompatibility. To be considered biocompatible, a material should not induce toxicity or irritation, must possess adhesive properties only towards specific cells or tissues, and have biomechanical properties comparable to those of surrounding organs and tissues. Low biocompatibility can cause infections, non-specific protein adsorption and inflammatory responses, which are an indication of rejection by the host body. Biological host response depends primarily on the interfacial interactions of biological systems and material surfaces. Therefore, compatibility and optimal performance of the material in the body is influenced by surface properties at atomic scale. Implant surface morphology, interfacial energy, wettability, and

cytotoxicity are some of the material properties that highly influence the amount and quality of cell adhesion, which in turn can cause surface fouling. Hence, surface modification of the materials is required to suitably alter one or more of these properties.[6]

The work in this dissertation is motivated by and focuses on surface modifications for implants under development by Balasubramanian et.al. at Oregon State University (OSU). These implants are envisaged as alternatives to conventional suturing surgery for patients suffering from median ulnar palsy, a condition in which patients can lose flexion in their fingers due to trauma or injury. Every year, approximately 20,000 tendon transfer hand surgeries are performed in the United States alone. The cumulative value of these surgeries is nearly USD 200 million. The current treatment for this condition involves taking a functioning tendon from the donor extensor carpis radialis longus (ECRL) muscle group and suturing it to all four damaged flexor tendons from the four fingers. This treatment couples the movements of the muscles and tendons, resulting in limited musculoskeletal function post-surgery due to uneven distribution of forces from the muscle across all tendons. Uneven force distribution can affect physical interaction tasks by preventing the fingers from naturally adapting to the shape of the object, resulting in incomplete grasp and limited hand function.

To address this problem, the proposed treatment by Balasubramanian et.al. makes use of an implant system to construct an *in situ* differential mechanism in the forearm using the implants and tendons. The implants act as passive engineered mechanisms by introducing a pulley-like system, which helps in differentially distributing the forces and movement from the donor muscle to all four tendons. This allows individual motion of the fingers and results in improved hand functions such as complete grasp (Figure 1.1).[7] The passive translation and rotation of the implant

around the tendon helps accommodate the difference in movement between the fingers, in contrast to the coupled finger motion produced by current suture-based procedures (Figure 1.2).

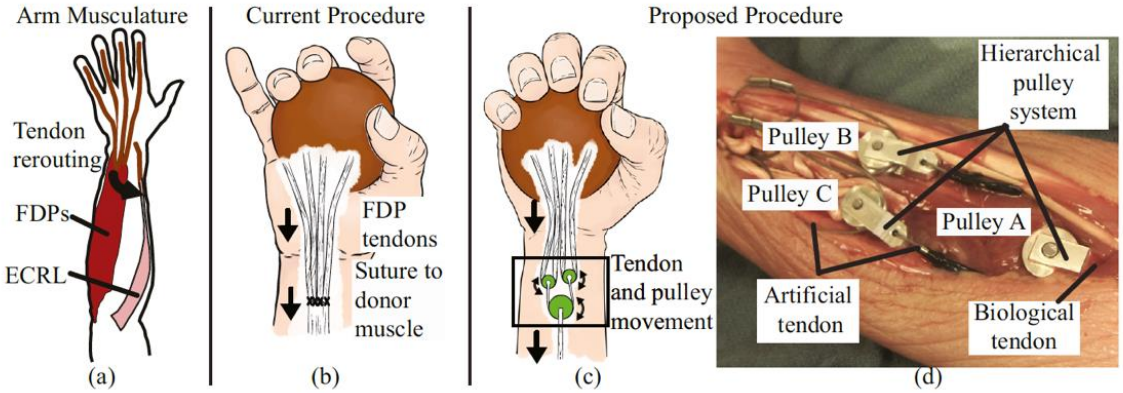

Figure 1.1. (a) Hand musculature and tendons. b) Current tendon transfer procedure using sutures. c) The proposed procedure using a pulley mechanism. d) Prototype pulley mechanism implanted in cadaver forearm for the study. *Reproduced from Ref.* 8 *under fair use.*

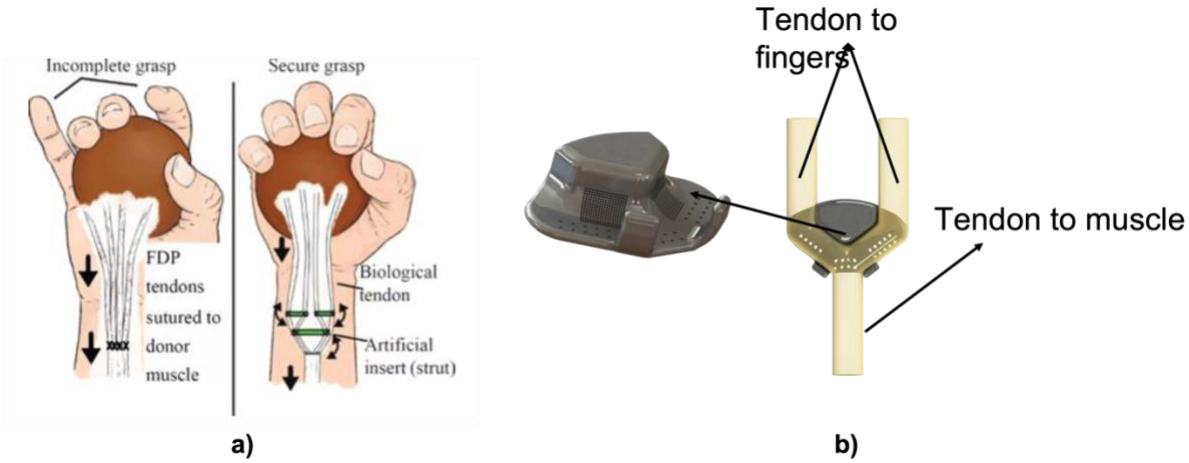

Figure 1.2. (a) Tendon transfer surgery for median ulnar nerve palsy for current suturing procedures (incomplete grasp) and the proposed procedure using implants (secure grasp).[9] b) proposed implant design.

In past studies by Balasubramanian et al., the implants were fabricated from ultra-high molecular weight polyethylene (UHMWPE), with the proposed procedure being tested in a

chicken feet model. The chicken foot extensor mechanism is specifically comparable to the human hand flexor mechanism. The chickens were implanted for 5-8 weeks with untreated UHMWPE implants. Upon explantation, severe fibrosis was observed around the implants, indicating substantial foreign body response (FBR) induced by non-specific protein and cell adsorption and surface friction (Figure 1.3).[6] While limitations in implant design and the implantation procedures are also likely contributing factors, this primarily signifies the need for surface modification of the implant material to maximize longevity.

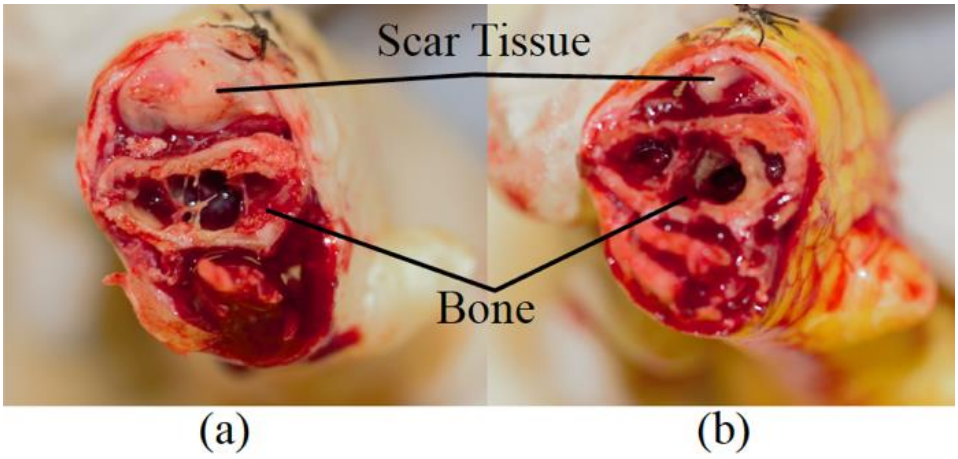

Figure 1.3. Cross-sectional view of chicken around the surgical site showing the dense scar tissue from the tendon transfer surgery performed using (a) current suturing procedure (b) proposed procedure using implant system.[10]

This research thus focuses on surface modification of the materials used in these implants. The main objective for surface modification herein is the favourable alteration of surface properties to prevent FBR by resisting non-specific protein adsorption. A secondary objective is increasing surface lubricity to facilitate the smooth rotation of implants around the tendons. To achieve these aims, we leveraged super hydrophilic zwitterionic poly (sulfobetaine methacrylate) (pSBMA) coatings, which have been demonstrated to achieve ultralow protein adsorption on substrates such as gold.[11] In addition, SBMA is lower-cost and easier to synthesize and handle relative to other

zwitterionic alternatives.[12] In fabricating these polymeric coatings, we used versatile surface modification techniques based on radio frequency glow discharge (RFGD) plasma and Activators ReGenerated by Electron Transfer atom transfer radical polymerization (ARGET ATRP).[13–15] These techniques enable the attachment of chemically robust, delamination resistant and reproducible hydrophilic coatings while also possessing significant advantages over alternative functionalization techniques, such as a reduced requirement of toxic metallic catalyst and tolerance to ambient conditions.[15–17] The overall strategy is thus integration of these concepts to develop simple yet effective surface modification methodologies that can help achieve key biocompatibility aims for a variety of implant materials.

This dissertation discusses our efforts in optimization and application of these surface modification techniques to two materials commonly used in medical implants and of interest to Balasubramanian et al.– polyurethanes, and titanium. In addition to descriptions of systematic protocols based on these techniques, this work also describes the characterization of the modified surfaces. Relevant variables studied in this work include surface composition, protein adsorption, lubricity, and *in vitro* and *in vivo* performance – critical determinants of implant biocompatibility and of direct relevance to research objectives.

1.2 FOREIGN BODY RESPONSE

Medical devices implants are used for a variety of clinical applications and their efficient performance is critical for successful medical procedures and overall patient health. The implantation of a medical device, i.e., a foreign object inside the human body, activates a cascade of complex events, which can eventually lead to the formation of a thick fibrous capsule around the device. This reaction by the immune system of the host body is known as the foreign body response (FBR).[18] Micro-vasculature and tissues surrounding the implanted devices usually suffer

injury during surgical procedures, initiating localized, nonspecific acute and chronic inflammatory responses. The extent of these injuries in turn affects the degree of the host response.[19] In addition, non-specific protein adsorption from the blood plasma and other biological fluids begins almost immediately on the surface of the material following implantation. This is a dynamic process that includes protein adsorption, rearrangement and displacement. The composition and arrangement of the adsorbed protein can affect subsequent cell and biomolecule adhesion, thus affecting the inflammatory responses.[18–21] This entire cascade of events can lead to the formation of a thick collagenous capsule. The insulating encapsulation of the implant can impede further interaction of the device with the surrounding tissue, thus rendering it futile.

The steps leading to FBR are depicted in Figure 1.4. The tissue and vasculature injuries from the surgery immediately trigger an inflammatory response. Seconds after device implantation, the device surface is covered with extravasated blood, which leads to non-specific adsorption of proteins like albumin and fibrinogen, forming a provisional matrix around the implant. This provisional matrix of proteins acts as a guiding signal for the cells gathering around the implant and begins cell adhesion. With time, the smaller proteins get displaced by larger molecules through a dynamic process of adsorption-desorption. The amount and composition of the adsorbed proteins can affect the extent of FBR around different implant materials. During the second ‘acute’ phase of FBR, inflammatory signals at the implant site result in the transport, adhesion, and activation of neutrophils around the adhered proteins. Neutrophils are known as the early responders in any kind of tissue injury. They begin to release factors such as reactive oxygen sites and proteolytic enzymes, which further promote the inflammatory process.

Following protein adsorption, the next stage of FBR is marked by rapid replacement of neutrophils by relatively abundant and motile monocytes which migrate to the wound site and

transform into macrophages, which form the second line of defense. The macrophages adhere to a material and try to digest or phagocytose it, to eliminate invading threats and mediate tissue repair. Upon failure to do so with the implant, macrophages undergo fusion to improve their efficacy and form multinucleated foreign body giant cells (FBGCs). Macrophages also release factors such as reactive oxygen sites and degrading enzymes in an attempt to break down the implant, which they recognize as a foreign body. This can affect implant stability and form cracks on its surface. This can in turn lead to implant breakdown and leaching of toxins from the bulk of the material. Chronic inflammatory response follows the acute response. Vascular endothelial growth factor (VEGF) is released by the macrophages and FBGCs, which triggers the formation of an immature vascular network. The next steps involve formation of granulation tissue and fibroblasts along with endothelial cells. The fibroblasts act as collagen synthesizers and form a thick fibrous capsule around the implant, isolating it from the body tissue and rendering it futile. This process of capsule formation and foreign body reaction is called fibrosis.[18,22] The FBR progresses into fibrosis over a period of weeks and stays active till the implant disintegrates or is removed.

In addition to patient health, some other factors that control the extent and severity of the host immune response include the surgical techniques used for implantation, the extent of surgical injury, and the surgical site. In addition, the implant shape and physicochemical properties of the implant surface also affect non-specific protein and cell adsorption.[18,20] The extent of the host response can thus be controlled by improved surgical techniques and altering the implant surface chemistry to mitigate non-specific protein adsorption.

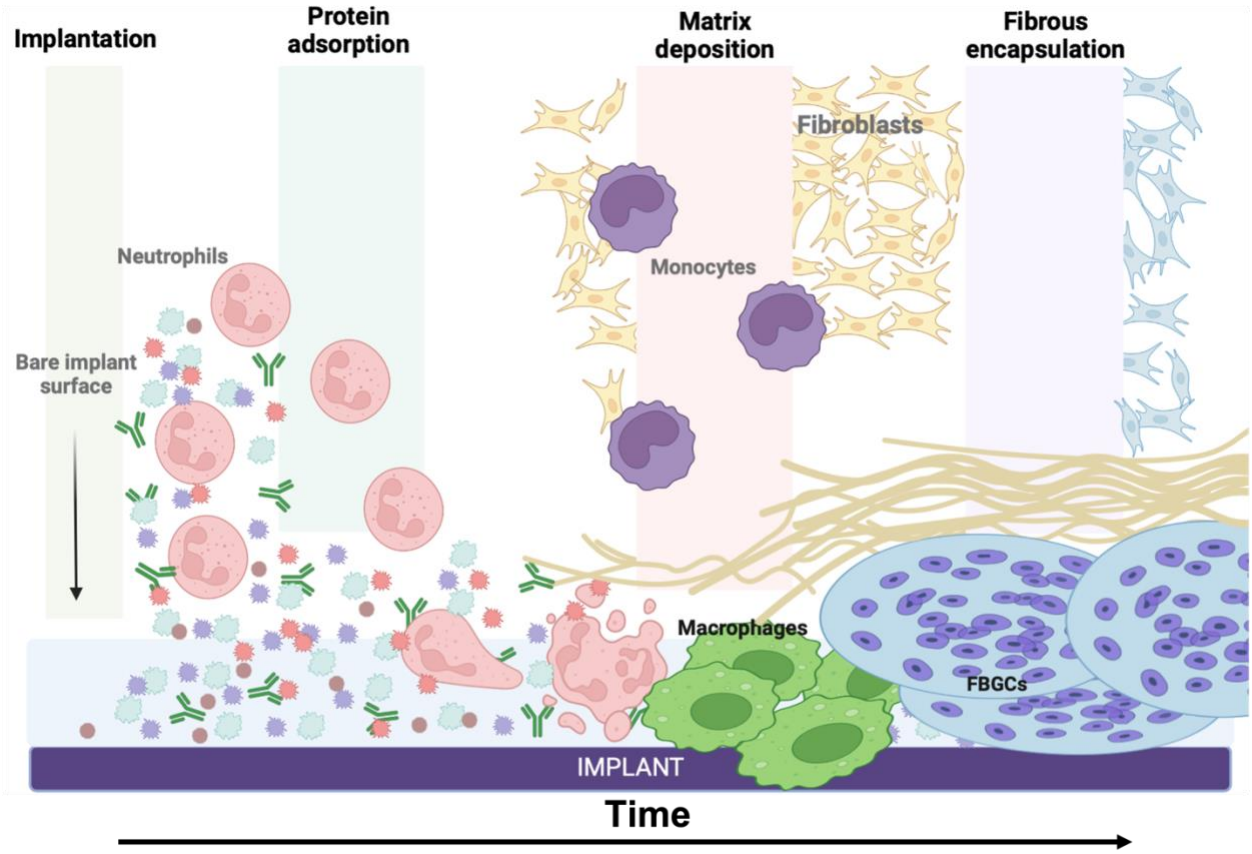

Figure 1.4. Natural innate immune response following implantation of a foreign material.

1.3 NEED FOR SURFACE MODIFICATION

The overall device performance and stability in the host body is highly influenced by the extent and severity of FBR. It also affects the chemical and structural stability of the implant. FBGCs can degrade the implant through surface oxidation and enzymatic reactions. Implant performance is also greatly weakened during the period of formation of the fibrous capsule, which can be of the order of weeks. The initial stages of FBR are highly controlled by the non-specific adsorption of proteins and biomolecules, followed by leukocyte adhesion. It is hypothesized that preventing non-specific protein adsorption or fouling can help mitigate subsequent inflammatory response and leukocyte activation, thus preventing fibrosis.[19]

The need to ensure sustained *in vivo* implant performance and minimize surgeries necessitates the development of treatments that can suppress inflammatory responses, primarily by resisting non-specific protein adsorption. Proteins undergo conformational change when in contact with a hydrophobic foreign material. They tend to orient their hydrophobic head with the material surface and the hydrophilic tail towards the biological medium to reduce surface energy. This reduction thermodynamically favors the adsorption of proteins, since it outweighs the decrease in entropy caused by the conformation change of the proteins. Hydrophilic functionalized surfaces generally provide low interfacial free energy resulting in reduced protein adsorption and increased biocompatibility.[23] In addition to hydrophilicity, interfacial interactions between the implant surface and host body also depend on atomic-scale surface properties such as cytotoxicity, roughness, morphology and interfacial energy.[6] Favorable modification of surface properties of implant material can thus resist non-specific protein adsorption and prevent fibrosis.

Synthetic polymer coatings have seen extensive use to modify the surface properties of implants with the goal of limiting non-specific protein adsorption ("non-fouling" surfaces).[18] Many hydrophilic surfaces are known to reduce protein adsorption due to the formation of an interfacial hydration layer on the implant surface, which helps prevent the proteins and biomolecules from attaching to the surface. Poly (ethylene glycol) (PEG) is one of the main synthetic materials used for making protein-resistant surface coatings. PEG-modified surfaces exhibit the combined effect of "steric repulsion" and a hydration layer formed via hydrogen bonding around the polymer chains. However, it has now been recognized that PEG decomposes into reactive aldehyde moieties in the presence of oxygen and transition metal ions, species typically found in biologically relevant solvents.[11] The discovery of new failure mechanisms for PEG-based implants signifies the need for alternative hydrophilic polymers.

1.4 ZWITTERIONIC POLYMERS

Recently, zwitterionic polymers have attracted considerable attention as ultra-low fouling materials, due to their advantages over PEG-based antifouling materials, including improved specificity, stability and sensitivity to protein detection in complex conditions. Zwitterionic materials are considered biomimetic due to the abundant presence of phosphorylcholine (PC) headgroups, found on the external surface of the mammalian cell membrane (Figure 1.5).[11,24,25]

Zwitterionic surfaces can increase surface wettability and prevent non-specific protein adsorption by forming a strong hydration layer at the interface, which is bound through the solvation of the charged terminal groups along with hydrogen bonding.[26–29] Polybetaine (PB) polymers like poly (sulfobetaine methacrylate) (pSBMA) and poly(carboxybetaine methacrylate) (pCBMA) are structurally very similar to that of PC-based polymers, with both cationic and anionic entities present on the same monomer backbone. This results in the formation of a strong dipole moment and abundant quantities of charged groups. Although the overall charge on the zwitterionic molecular chains is neutral, the concurrence of positively and negatively charged groups results in high polarity and strong hydrophilicity.[28,30]

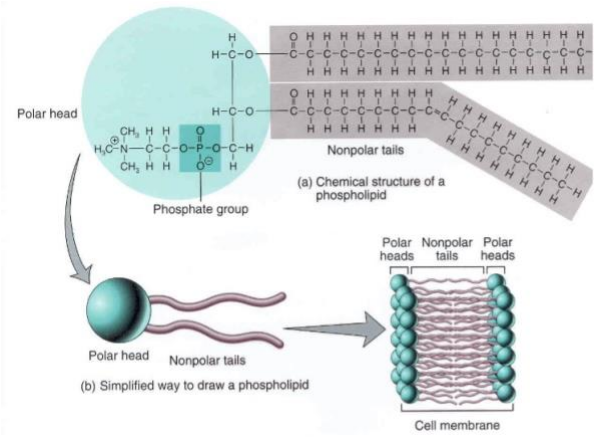

Figure 1.5. Structure of the lipid bilayer. Phosphatidylcholine (a phospholipid) is composed of hydrophilic polar “heads” and hydrophobic nonpolar “tails.” Adapted from Ref. 31 under fair use.

Zwitterionic polymers based on sulfobetaine (SB) and carboxybetaine (CB) are emerging as popular alternatives to PC derivatives which are complex to synthesize and result in low yield, making them expensive. SB monomers have structural similarities to PC molecules, while offering the advantages of easy synthesis, applicability and stability. These consist of a sulfonate anion and quarternary ammonium cation on the same side chain, similar to PC molecules. The most studied sulfobetaine, poly (sulfobetaine methacrylate) consists of a methacrylate main chain and an analog of the taurine betaine as pendant group. Like sulfobetaine, carboxybetaines also possess positively charged quarternary ammonium groups, but the negative charge is present as a carboxylate group instead of a sulfonic acid group (Figure 1.6). In addition to their resulting biomimetic and non-fouling properties, both classes of polymers possess unique strengths. The strong hydration abilities resulting from tightly bound and structured water layers around the zwitterionic pendant in SB-based polymers contribute to substantial biological inertness, low endotoxicity and low cytotoxicity. The presence of robust hydration layers also reduces the adhesion of biomolecules, preventing surface fouling.[12,32,33] On the other hand, CB derivatives such as poly(carboxybetaine) (pCBMA) are the only zwitterionic polymers with demonstrated ultra-low fouling as well as biorecognition capabilities. The presence of the carboxylate group, which is easy to convert to other functional groups, is ideal for biorecognition applications. Additionally, the carboxyl group in pCBMA can be easily esterified, which can then be hydrolyzed to generate zwitterionic polymers with the desired combination of properties.[12,34–36]

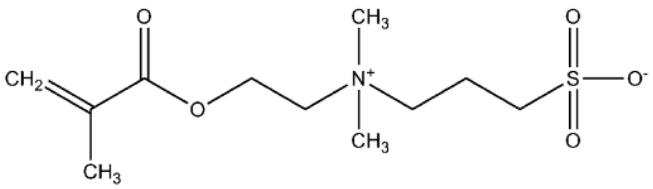

Sulfobetaine methacrylate (SBMA)

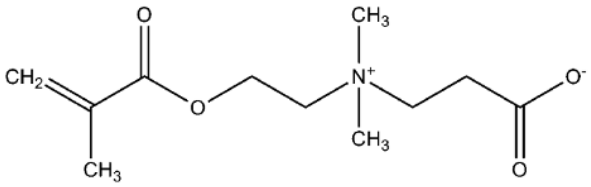

Carboxybetaine methacrylate (CBMA)

Figure 1.6. Structure of sulfobetaine and carboxybetaine zwitterionic monomers.

Synthesizing zwitterionic polymer surface coatings is a versatile and popular method of incorporating these hydrophilic entities on the material surface to enhance biocompatibility. Zwitterionic polymers can be grafted either using physical methods such as physisorption or chemical methods such as controlled radical polymerization techniques including surface-initiated atom transfer radical polymerization (SI-ATRP) or **A**ctivators **ReG**enerated by **E**lectron **T**ransfer atom transfer radical polymerization (ARGET ATRP). In addition to the design of the implant materials, the molecular design of the polymer coatings also plays a significant role in determining the non-fouling and lubricating properties of the surface. With optimal grafting density and chain length, pSBMA polymer brushes have been demonstrated to achieve substantially reduced non-specific protein adsorption and increased surface lubricity, both in diluted and full-strength plasma solutions.[12,24]

1.5 POLYMER BRUSHES

Polymer brushes are special macromolecular structures with one end of the polymer chain anchored to the surface or another polymer chain via stable covalent or non-covalent bonding.[37]

The polymer chains can typically exist in three different conformations depending on the grafting density and the molecular weight of the polymer on the substrate – from the 'mushroom regime' at low grafting density to 'brush regime' at high grafting density, as shown in Figure 1.7.[24,38] The mushroom regime is characterized by entangled polymer chains whereas the strong steric repulsion between dense chains in the brush regime results in vertically stretched out chains. The specific polymer chain regime depends on the surface-polymer-solvent interactions. In poor solvents, the polymer chains tend to collapse into the mushroom regime, whereas in a good solvent, the chains tend to stretch away from the surface into a brush-like regime due to osmotic and steric repulsions. Geometric indicators of the specific brush conformation are the ratio of distance between the anchor points (a), and the radius of gyration of polymers (R_{gyr}). When $a > 2R_{gyr,}$ there is no interaction between two single polymer chains and the chains tend to collapse into the mushroom configuration. Increasing the grafting density first produces mushroom-to brush transition structures which change to polymer brushes beyond a threshold grafting density.[30,37–39]

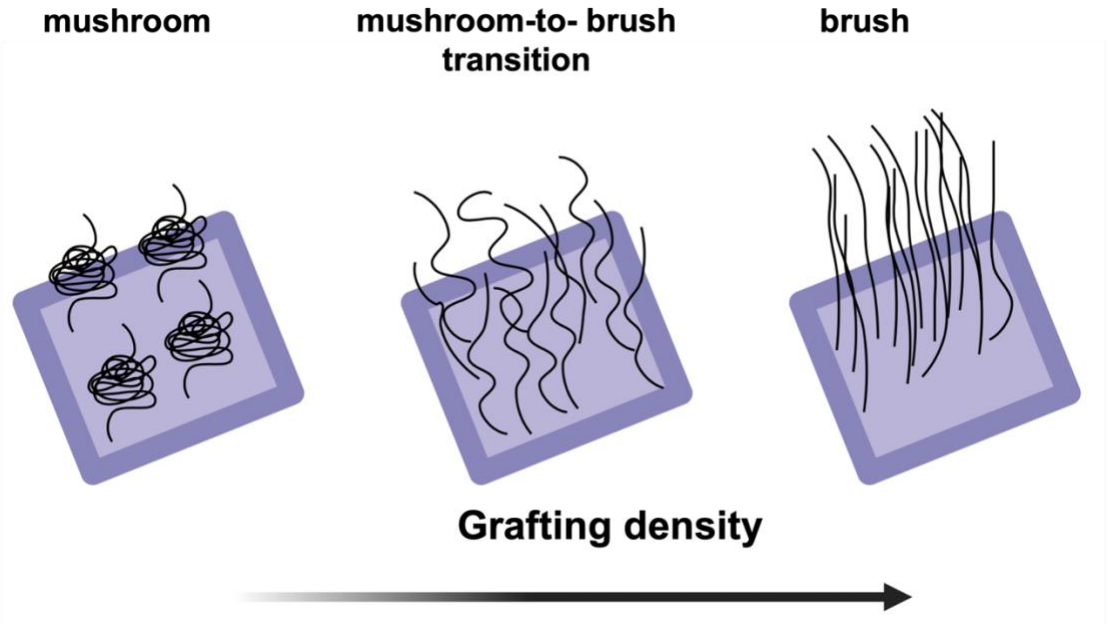

Figure 1.7. Schematic of the conformations of tethered polymer chains on the surface as a function of grafting density: mushroom, mushroom-to-brush transition, brush.

1.6 PREPARATION OF POLYMER BRUSHES

Polymer chains can be anchored to the substrate surface either via physical or covalent bonding (Figure 1.8). Physical adsorption involves using methods like dip coating, in which the polymer films are attached to the surface through noncovalent interactions like electrostatic forces, hydrophobic interactions and hydrogen bonding. Since the forces tethering polymer chains to the surfaces are weak forces, these attachment processes are reversible, and the polymer films can delaminate as an effect of solvation or fluid force shear.[38,40]

For covalent attachment of polymer brushes, most fabrication strategies use either "grafting-to" or "grafting-from" methods. "Grafting-to" methods involve the attachment of pre-synthesized end-functionalized polymer chains to a functionalized surface. In general, this method results in loose attachments, limited film thickness and low grafting densities due to steric repulsion from surrounding polymer chains and an unfavorable reaction direction. "Grafting-from", on the other hand, is a bottom-up strategy which involves functionalizing the surface with an initiator and then growing polymer chains using surface-initiated polymerization (SIP).[30,38,40,41] These methods can thus be used for tuning the brush thickness, grafting density and chain length by adjusting the initiator density, making it suitable for various surface modification applications, e.g. creating non-fouling and lubricated surfaces, allowing reversible cell attachment etc.

Living radical polymerization techniques allow for successful grafting of a variety of polymers from the surface and precise tailoring of the molecular weight, brush architecture and composition of polymer chains. Some of the frequently used SIP techniques include surface-initiated atom transfer radical polymerization (SI-ATRP), reversible addition-fragmentation chain transfer radical polymerization (RAFT), ring opening metathesis polymerization and nitroxide-mediated polymerization (NMP).[40,41] SI-ATRP is the most widely used living radical

polymerization technique, owing to the mild reaction conditions, simple experimental setup and compatibility with both aqueous and organic solvents.

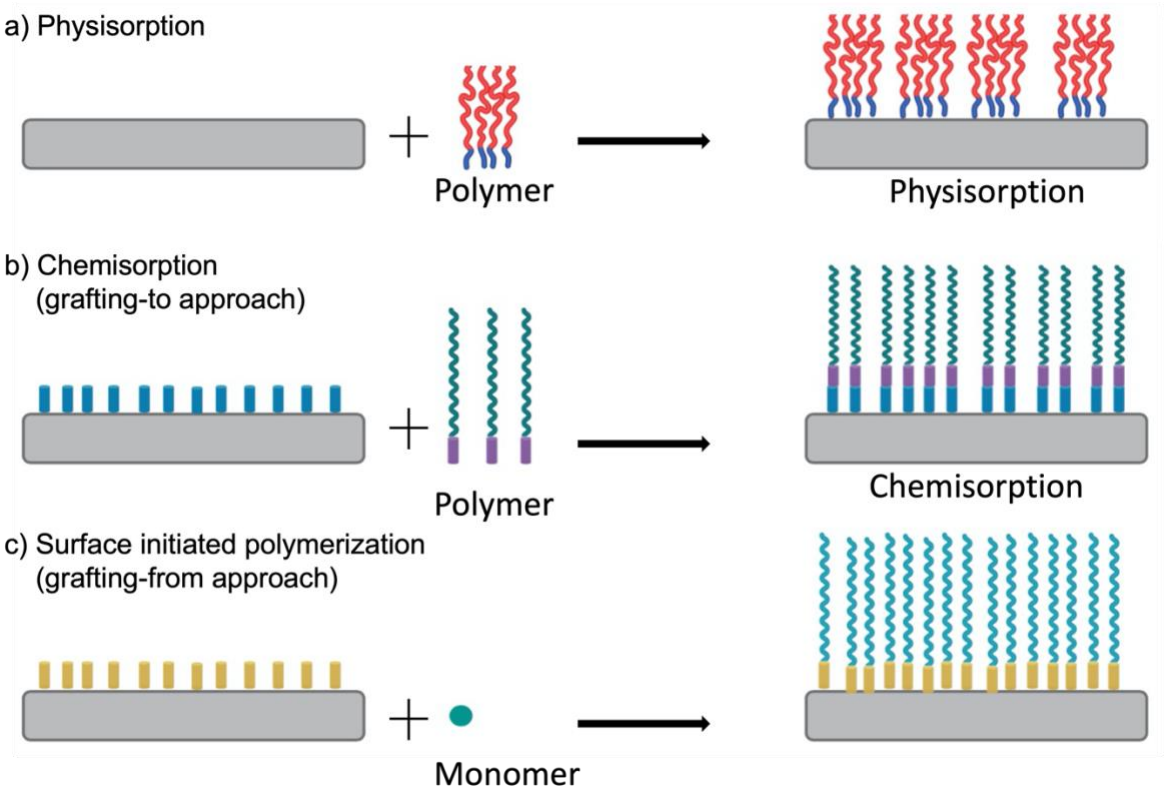

Figure 1.8. Different methods of grafting polymer chains on the surface.

ATRP involves the use of a redox-active transition metal complex (Mt^m), which is typically a copper catalyst. The general mechanism of the process is based on an equilibrium between dormant species, i.e. dormant alkyl halide terminated polymer chain ends (P_n-X), and active radicals (P_n^*), as shown in Figure 1.9. During the activation step the activator, which is a transition metal complex (Mt^m/L) (catalyst and ligand complex), reacts with the dormant species (alkyl halide initiators), generating living radicals (P_n^*) and thereby stimulating chain propagation (kact). This step also involves the formation of the higher oxidation state metal complex with a coordinated halide ligand (X-Mt^{m+1}/L) which acts as the deactivator. The deactivators formed

during this process can react with the active radicals in the reverse reaction, reforming the dormant species and the activator (k_{deact}). The radical termination reduces as the reaction progresses, due to persistent radical effect, increased chain length, conversion, and viscosity. The rate of chain propagation depends on the propagation and deactivation rate constants, and ratio of concentrations of transition metal complex in the lower and the higher oxidation states. Overall, the polymerization process is strongly affected by several factors including the initiator, ligand, catalyst and solvent.[38,42–45]

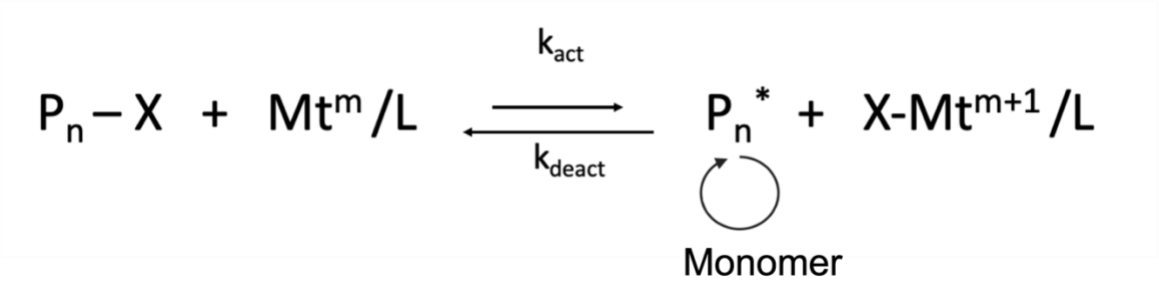

Figure 1.9. Mechanism of ATRP.

There are several factors associated with the ATRP process that hinder control and raise concerns about the use of this technique in biomedical applications. ATRP is highly sensitive to the presence of oxygen since it can lead to the conversion of the transition metal to a higher oxidation state (Mt^m to Mt^{m+1}). Since the rate of polymerization theoretically depends on the ratio of the concentrations of transition metal in lower oxidation state to that in the higher oxidation state ($[Mt^m]/[Mt^{m+}1]$), even a small amount of oxygen can significantly lower the rate of polymerization. Deoxygenation of the polymer solution is a tedious step and increases the overall complexity of the experimental process. In addition, the process requires the use of large amounts of transition metal catalyst (usually copper-based), which if not carefully removed can prove toxic for biomedical applications.[42,46]

These limitations of ATRP can be overcome by using **A**ctivators **ReG**enerated by **E**lectron **T**ransfer (ARGET) ATRP. This procedure utilizes a reducing agent in the reaction mixture which helps in *in situ* regeneration of the activator (Cu (I)) from the deactivator (Cu (II)) (Figure 1.10). This allows the catalyst concentration to be reduced to parts per million (ppm) levels, thus reducing the risk of toxicity. The advantages of ARGET ATRP over conventional ATRP make it an attractive candidate for a "grafted-from" approach for various surface modification applications. The addition of reducing agent also makes the reaction mixture considerably tolerant towards oxygen, greatly reducing the need for deoxygenation. This process can also be successfully conducted in aqueous media, reducing the need for toxic solvent systems. In sum, the more permissive experimental conditions, low catalyst concentrations, and relatively benign chemical reagents (solvents and reducing agents) make this polymerization technique suitable for use at industrial scale and safe for biomedical applications.[16]

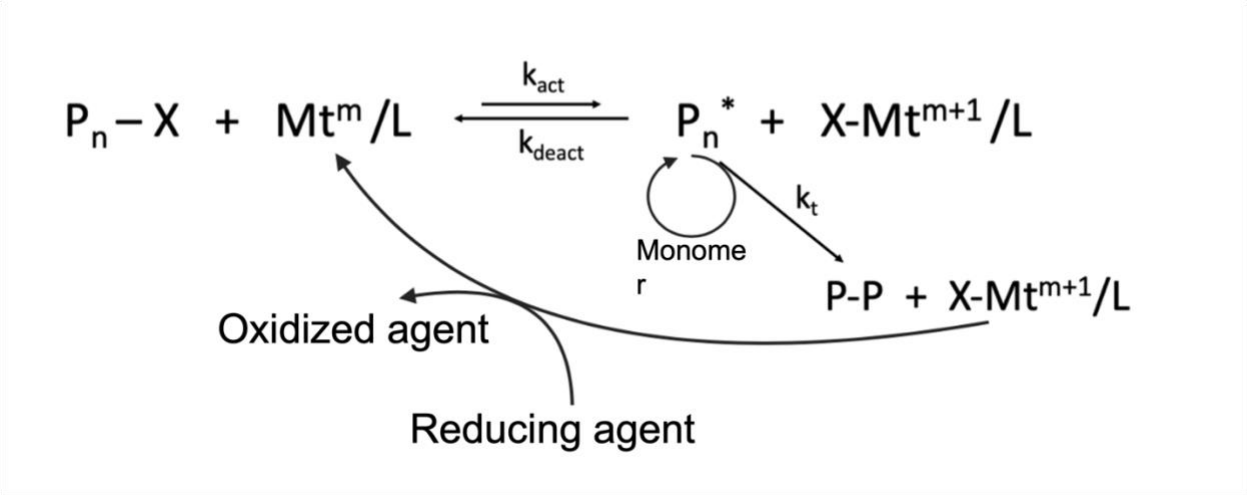

Figure 1.10. Mechanism of ARGET ATRP.

1.7 EFFECT OF MOLECULAR DESIGN OF POLYMER BRUSHES ON ANTIFOULING PROPERTIES

It is a well-established concept that hydrophilic surfaces have lower interfacial energy, leading to relatively looser protein binding at the surface.[23] In recent studies, surfaces grafted with zwitterionic polymer brushes have shown extremely low non-specific protein adsorption owing to their super-hydrophilic nature.[11,24,47] Grafted zwitterionic polymer brushes tend to block protein adsorption by allowing the formation of a strong hydration layer and utilizing the steric excluded volume effect (Figure 1.11). A tightly bound hydration layer acts as a physical and energy barrier between the material surface and the biological environment, thus preventing protein adsorption. The hydration layer is only sustained if there is enough hydration pressure to serve as an energy barrier to non-specific adsorption. In addition, the polymer brushes need to be flexible in order to create configurational mobility to block the potential protein adsorption sites by steric exclusion.[23,48,49]

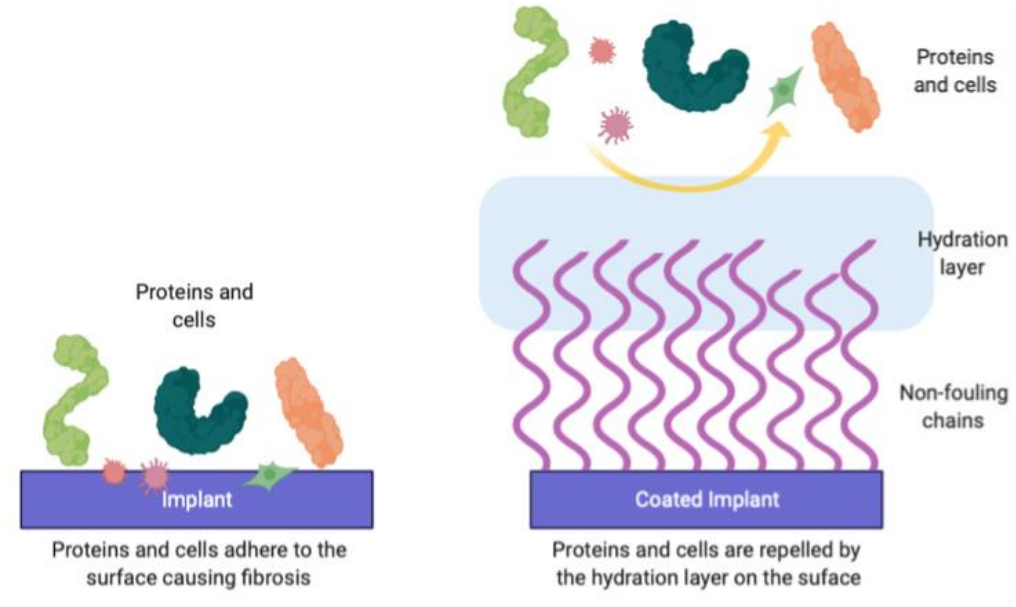

Figure 1.11. Flexible chains with continuous movement block protein adsorption by allowing the formation of a hydration layer and utilization of steric excluded volume effects.

In addition to the functionality of the hydrophilic material, the molecular structure and design of the polymer brushes are also paramount for resisting non-specific protein adsorption since they affect the polymer chain flexibility. Packing density and chain length can also strongly affect the hydration layer at the interface and the steric hindrance between the polymer brushes.[12] Previous studies have shown that high brush density is the key to resisting non-specific protein adsorption on the surface.[12,50] Extremely low protein adsorption has been observed for polySBMA (pSBMA) grafted surfaces with low molecular weight (M_w) polymer chains. Higher M_w brushes were found to be associated with increased surface packing defects. Large SBMA segments were found to form aggregates, creating large cavities between the surrounding brushes which resulted in low surface coverage and higher protein adsorption.[12,34,51,52]In a study by Jiang et al. on the effect of grafting density of pSBMA, it was observed that backfilling the cavities formed by high $M_{w\ pSBMA}$ brushes with low M_w copolymer chains resulted in reduced protein adsorption.[50] This observation confirms the need of higher grafting density for minimal protein adsorption.

In another study by Ladd et al., pCBMA grafted surfaces showed lower protein adsorption compared to pSBMA grafted surfaces. This observation can be explained based on the chemistry of these monomers. In CBMA, the charged moieties are separated by only two carbon atoms, leading to stronger interactions between the hydration shells surrounding the two ionic groups. This results in the formation of a stronger and more spatially uniform hydration layer. On the other hand, in SBMA the oppositely charged segments are separated by a three-carbon atom long chain. This results in more spaced-out hydration shells, causing weaker interactions and reduced uniformity of the hydration layer. These observations signify the importance of the polymer chain chemistry in resisting non-specific protein adsorption.[34]

In addition to grafting density, chain length is also shown to have a significant effect on the robustness of the hydration layer. In a study by Chang et. al., thicker pSBMA coatings were found to show lower protein adsorption because of increased surface hydration. Uniform brushes and full surface coverage lead to the formation of a strong hydration layer as a result of full water surface contact.[12,53] In a study by Sin et al., it was observed that the conformational structure and surface density of the brush anchoring agent layer also strongly affects the formation of well-spaced and flexible polymer brushes.[54] Such structures result in better surface hydration and grafting density of the polymer chains. Studies have also shown that excessively high chain density can lead to compression and entanglement of polymer brushes, reducing chain flexibility, and leading to a weak hydration layer. Still another study showed that longer chains at low grafting density, or shorter chains at high grafting density are ideal for high protein resistance.[55,56] All these observations illustrate the need for optimal grafting density and chain length to achieve the formation of a robust extended interfacial hydration layer and adequate chain flexibility.

1.8 ORGANIZATION OF THIS DISSERTATION

Owing to their unique physiochemical properties and versatility, polymer brush coatings have found applications in many emerging areas including nanotechnology, photonic applications, catalysis, tribological and non-fouling applications. Since the focus of this study is surface modification for creating non-fouling and lubricated surfaces for orthopedic implants, these two applications are discussed in detail in the following chapters. The remainder of this document is thus organized around studies systematically investigating zwitterionic polymers for the above applications.[30,57–61]

The overall research effort is chiefly summarized in chapters 2-4. Chapter 2 discusses the grafting of pSBMA coatings on radio frequency glow discharge (RFGD) plasma activated surfaces using ARGET ATRP. The surface characterization, protein adsorption and *in vitro* and *in vivo* performance is also discussed in detail. Chapter 3 describes the use of an RFGD plasma deposited haloester, methyl-3-bromopropionate as a ARGET ATRP initiator to graft pSBMA coatings. The evaluation of the surfaces thus prepared is also discussed in detail in terms of surface characterization, protein adsorption and *in vitro* stability. Chapter 4 discusses the lubricity evaluation of the surfaces prepared using techniques discussed in Chapters 2 and 3. Finally Chapter 5 concludes the dissertation with a summary of the methodologies developed in this work, a discussion of limitations, and directions for improvements and future work.

1.9 REFERENCES

(1) *With 5.0% CAGR, Orthopedic Implants Market Size worth USD 60.90 Billion by 2029*. https://www.globenewswire.com/en/news-release/2022/08/09/2494655/0/en/With-5-0-CAGR-Orthopedic-Implants-Market-Size-worth-USD-60-90-Billion-by-2029.html (accessed 2022-11-21).

(2) *Medical Devices Market*. https://www.fortunebusinessinsights.com/industry-reports/medical-devices-market-100085 (accessed 2022-11-21).

(3) Bazaka, K.; Jacob, M. v. Implantable Devices: Issues and Challenges. *Electronics (Switzerland)*. 2012. https://doi.org/10.3390/electronics2010001.

(4) Teo, A. J. T.; Mishra, A.; Park, I.; Kim, Y. J.; Park, W. T.; Yoon, Y. J. Polymeric Biomaterials for Medical Implants and Devices. *ACS Biomater Sci Eng* 2016, *2* (4), 454–472. https://doi.org/10.1021/acsbiomaterials.5b00429.

(5) Ramakrishna, S.; Mayer, J.; Wintermantel, E.; Leong, K. W. Biomedical Applications of Polymer-Composite Materials: A Review. *Compos Sci Technol* 2001, *61* (9). https://doi.org/10.1016/S0266-3538(00)00241-4.

(6) Ul Ahad, I.; Bartnik, A.; Fiedorowicz, H.; Kostecki, J.; Korczyc, B.; Ciach, T.; Brabazon, D. Surface Modification of Polymers for Biocompatibility via Exposure to Extreme Ultraviolet Radiation. *Journal of Biomedical Materials Research - Part A*. 2014. https://doi.org/10.1002/jbm.a.34958.

(7) Homayouni, T.; Underwood, K. N.; Beyer, K. C.; Martin, E. R.; Allan, C. H.; Balasubramanian, R. Modeling Implantable Passive Mechanisms for Modifying the Transmission of Forces and Movements between Muscle and Tendons. *IEEE Trans Biomed Eng* 2015, *62* (9), 2208–2214. https://doi.org/10.1109/TBME.2015.2419223.

(8) Mardula, K. L.; Balasubramanian, R.; Allan, C. H. Implanted Passive Engineering Mechanism Improves Hand Function after Tendon Transfer Surgery: A Cadaver-Based Study. *Hand* 2015, *10* (1), 116–122. https://doi.org/10.1007/s11552-014-9676-0.

(9) Mandich, J.; Casebier, J.; Francis, J.; Chandramouli, S.; Balasubramanian, R.; Warnock, J. Implantable Mechanisms for Orthopedic Surgery: Validation Using Biomechanical Simulation and Cadaver Study in Chicken Foot. In *Proceedings of the Veterinary Orthopedics Society*; 2017.

(10) Le, A. J.; Casebier, J.; Mandich, J.; Larson, M. K.; Warnock, J.; Sweeney, J.; Balasubramanian, R. Evaluation of Postoperative Healing for Novel Tendon-Transfer Surgery Using an Implantable Passive Mechanism: A Pilot In Vivo Study. In *Proceedings of the Veterinary Orthopedics Society*; 2017.

(11) Zhang, Z.; Chen, S.; Chang, Y.; Jiang, S. Surface Grafted Sulfobetaine Polymers via Atom Transfer Radical Polymerization as Superlow Fouling Coatings. *Journal of Physical Chemistry B* 2006, *110* (22), 10799–10804. https://doi.org/10.1021/jp057266i.

(12) Sin, M. C.; Chen, S. H.; Chang, Y. Hemocompatibility of Zwitterionic Interfaces and Membranes. *Polym J* 2014, *46* (8), 436–443. https://doi.org/10.1038/pj.2014.46.

(13) Kim, D. D.; Takeno, M. M.; Ratner, B. D.; Horbett, T. A. Glow Discharge Plasma Deposition (GDPD) Technique for the Local Controlled Delivery of Hirudin from Biomaterials. *Pharmaceutical Research*. 1998, pp 783–786. https://doi.org/10.1023/A:1011987423502.

(14) Matyjaszewski, K.; Patten, T. E.; Xia, J. Controlled/'living' Radical Polymerization. Kinetics of the Homogeneous Atom Transfer Radical Polymerization of Styrene. *J Am Chem Soc* 1997, *119* (4), 674–680. https://doi.org/10.1021/ja963361g.

(15) Matyjaszewski, K.; Hongchen, D.; Jakubowski, W.; Pietrasik, J.; Kusumo, A. Grafting from Surfaces for "Everyone": ARGET ATRP in the Presence of Air. *Langmuir* 2007, *23* (8), 4528–4531. https://doi.org/10.1021/la063402e.

(16) Simakova, A.; Averick, S. E.; Konkolewicz, D.; Matyjaszewski, K. Aqueous ARGET ATRP. *Macromolecules* 2012, *45* (16), 6371–6379. https://doi.org/10.1021/ma301303b.

(17) Biederman, H.; Slavínská, D. Plasma Polymer Films and Their Future Prospects. *Surf Coat Technol* 2000, *125* (1–3), 371–376. https://doi.org/10.1016/S0257-8972(99)00578-2.

(18) Chandorkar, Y.; Ravikumar, K.; Basu, B. The Foreign Body Response Demystified. *ACS Biomater Sci Eng* 2019, *5* (1), 19–44. https://doi.org/10.1021/acsbiomaterials.8b00252.

(19) Bridges, A. W.; García, A. J. Anti-Inflammatory Polymeric Coatings for Implantable Biomaterials and Devices. *J Diabetes Sci Technol* 2008, *2* (6), 984–994. https://doi.org/10.1177/193229680800200628.

(20) Anderson, J. M.; Rodriguez, A.; Chang, D. T. Foreign Body Reaction to Biomaterials. *Seminars in Immunology*. 2008. https://doi.org/10.1016/j.smim.2007.11.004.

(21) Williams, D. F. On the Nature of Biomaterials. *Biomaterials* 2009, *30* (30), 5897–5909. https://doi.org/10.1016/j.biomaterials.2009.07.027.

(22) Carnicer-Lombarte, A.; Chen, S. T.; Malliaras, G. G.; Barone, D. G. Foreign Body Reaction to Implanted Biomaterials and Its Impact in Nerve Neuroprosthetics. *Frontiers in Bioengineering and Biotechnology*. Frontiers Media S.A. April 15, 2021. https://doi.org/10.3389/fbioe.2021.622524.

(23) Ngo, B. K. D.; Grunlan, M. A. Protein Resistant Polymeric Biomaterials. *ACS Macro Lett* 2017, *6* (9), 992–1000. https://doi.org/10.1021/acsmacrolett.7b00448.

(24) Schlenoff, J. B. Zwitteration: Coating Surfaces with Zwitterionic Functionality to Reduce Nonspecific Adsorption. *Langmuir* 2014, *30* (32), 9625–9636. https://doi.org/10.1021/la500057j.

(25) Iwata, R.; Suk-In, P.; Hoven, V. P.; Takahara, A.; Akiyoshi, K.; Iwasaki, Y. Control of Nanobiointerfaces Generated from Well-Defined Biomimetic Polymer Brushes for Protein and Cell Manipulations. *Biomacromolecules* 2004, *5* (6), 2308–2314. https://doi.org/10.1021/bm049613k.

(26) Wu, J.; Lin, W.; Wang, Z.; Chen, S. Investigation of the Hydration of Nonfouling Material Poly (Sulfobetaine Methacrylate) by Low-Field Nuclear Magnetic Resonance. *Langmuir* 2012, *28* (4), 2137–2144. https://doi.org/10.1021/la203827h.

(27) Leng, C.; Hung, H. C.; Sun, S.; Wang, D.; Li, Y.; Jiang, S.; Chen, Z. Probing the Surface Hydration of Nonfouling Zwitterionic and PEG Materials in Contact with Proteins. *ACS Appl Mater Interfaces* 2015, *7* (30), 16881–16888. https://doi.org/10.1021/acsami.5b05627.

(28) Zhang, Y.; Liu, Y.; Ren, B.; Zhang, D.; Xie, S.; Chang, Y.; Yang, J.; Wu, J.; Xu, L.; Zheng, J. Fundamentals and Applications of Zwitterionic Antifouling Polymers. *J Phys D Appl Phys* 2019, *52* (40), 403001. https://doi.org/10.1088/1361-6463/ab2cbc.

(29) Golabchi, A.; Wu, B.; Cao, B.; Bettinger, C. J.; Cui, X. T. Zwitterionic Polymer/Polydopamine Coating Reduce Acute Inflammatory Tissue Responses to Neural Implants. *Biomaterials* 2019, *225* (September), 119519. https://doi.org/10.1016/j.biomaterials.2019.119519.

(30) Qu, K.; Yuan, Z.; Wang, Y.; Song, Z.; Gong, X.; Zhao, Y.; Mu, Q.; Zhan, Q.; Xu, W.; Wang, L. Structures, Properties, and Applications of Zwitterionic Polymers. *ChemPhysMater* 2022, *1* (4), 294–309. https://doi.org/10.1016/j.chphma.2022.04.003.

(31) *Phospholipid Bilayer*. https://ibiologia.com/phospholipid-bilayer/ (accessed 2022-11-27).

(32) Chang, Y.; Chang, W. J.; Shih, Y. J.; Wei, T. C.; Hsiue, G. H. Zwitterionic Sulfobetaine-Grafted Poly (Vinylidene Fluoride) Membrane with Highly Effective Blood Compatibility via Atmospheric Plasma-Induced Surface Copolymerization. *ACS Appl Mater Interfaces* 2011, *3* (4), 1228–1237. https://doi.org/10.1021/am200055k.

(33) Zhang, Z.; Chao, T.; Chen, S.; Jiang, S. Superlow Fouling Sulfobetaine and Carboxybetaine Polymers on Glass Slides. *Langmuir* 2006, *22* (24), 10072–10077. https://doi.org/10.1021/la062175d.

(34) Ladd, J.; Zhang, Z.; Chen, S.; Hower, J. C.; Jiang, S. Zwitterionic Polymers Exhibiting High Resistance to Nonspecific Protein Adsorption from Human Serum and Plasma. *Biomacromolecules* 2008, *9* (5), 1357–1361. https://doi.org/10.1021/bm701301s.

(35) Vaisocherová, H.; Yang, W.; Zhang, Z.; Cao, Z.; Cheng, G.; Piliarik, M.; Homola, J.; Jiang, S. Ultralow Fouling and Functionalizable Surface Chemistry Based on a Zwitterionic Polymer Enabling Sensitive and Specific Protein Detection in Undiluted Blood Plasma. *Anal Chem* 2008, *80* (20), 7894–7901. https://doi.org/10.1021/ac8015888.

(36) Yang, W.; Xue, H.; Li, W.; And, J. Z.; Jiang, S. Pursuing “Zero” Protein Adsorption of Poly (Carboxybetaine) from Undiluted Blood Serum and Plasma. *Langmuir* 2009, *25* (19), 11911–11916. https://doi.org/10.1021/la9015788.

(37) Feng, C.; Huang, X. Polymer Brushes: Efficient Synthesis and Applications. *Acc Chem Res* 2018, *51* (9), 2314–2323. https://doi.org/10.1021/acs.accounts.8b00307.

(38) Yang, W.; Zhou, F. Polymer Brushes for Antibiofouling and Lubrication. *Biosurf Biotribol* 2017, *3* (3), 97–114. https://doi.org/10.1016/j.bsbt.2017.10.001.

(39) Yu, Y. Switchable Adhesion and Friction by Stimulus Responsive Polymer Brushes, 2017.

(40) Kocak, G.; Butun, V.; Tuncer, C. PH-Responsive Polymers. *Polym Chem* 2017, *8*, 144–176.

(41) Kim, M.; Schmitt, S. K.; Krutty, J. D.; Gopalan, P. From Self-Assembled Monolayers to Coatings: Advances in the Synthesis and Nanobio Applications of Polymer Brushes. *Polymers (Basel)* 2015, *7* (7), 1346–1378.

(42) Matyjaszewski, K. Atom Transfer Radical Polymerization (ATRP): Current Status and Future Perspectives. *Macromolecules* 2012, *45* (10), 4015–4039. https://doi.org/10.1021/ma3001719.

(43) *ATRP*. https://www.cmu.edu/maty/chem/fundamentals-atrp/atrp.html (accessed 2022-11-25).

(44) Matyjaszewski, K.; Tsarevsky, N. v. Macromolecular Engineering by Atom Transfer Radical Polymerization. *Journal of the American Chemical Society*. American Chemical Society May 7, 2014, pp 6513–6533. https://doi.org/10.1021/ja408069v.

(45) Tang, W.; Kwak, Y.; Braunecker, W.; Tsarevsky, N. v.; Coote, M. L.; Matyjaszewski, K. Understanding Atom Transfer Radical Polymerization: Effect of Ligand and Initiator Structures on the Equilibrium Constants. *J Am Chem Soc* 2008, *130* (32), 10702–10713. https://doi.org/10.1021/ja802290a.

(46) Krys, P.; Matyjaszewski, K. Kinetics of Atom Transfer Radical Polymerization. *Eur Polym J* 2017, *89*, 482–523. https://doi.org/10.1016/j.eurpolymj.2017.02.034.

(47) Li, G.; Cheng, G.; Xue, H.; Chen, S.; Zhang, F.; Jiang, S. Ultra Low Fouling Zwitterionic Polymers with a Biomimetic Adhesive Group. *Biomaterials* 2008, *29* (35), 4592–4597. https://doi.org/10.1016/j.biomaterials.2008.08.021.

(48) Jeon, S. I.; Lee, J. H.; Andrade, J. D.; de Gennes, P. G. Protein-Surface Interactions in the Presence of Polyethylene Oxide I. Simplified Theory. *J Colloid Interface Sci* 1991, *142* (1), 149–158.

(49) Hucknall, A.; Rangarajan, S.; Chilkoti, A. In Pursuit of Zero: Polymer Brushes That Resist the Adsorption of Proteins. *Advanced Materials* 2009, *21* (23), 2441–2446. https://doi.org/https://doi.org/10.1002/adma.200900383.

(50) Chang, Y.; Chen, S.; Zhang, Z.; Jiang, S. Highly Protein-Resistant Coatings from Well-Defined Diblock Copolymers Containing Sulfobetaines. *Langmuir* 2006, *22* (5), 2222–2226. https://doi.org/10.1021/la052962v.

(51) Uchida, K.; Otsuka, H.; Kaneko, M.; Kataoka, K.; Nagasaki, Y. A Reactive Poly (Ethylene Glycol) Layer to Achieve Specific Surface Plasmon Resonance Sensing with a High S/N Ratio: The Substantial Role of a Short Underbrushed PEG Layer in Minimizing Nonspecific Adsorption. *Anal Chem* 2005, *77* (4), 1075–1080. https://doi.org/10.1021/ac0486140.

(52) Kuo, W. H.; Wang, M. J.; Chien, H. W.; Wei, T. C.; Lee, C.; Tsai, W. B. Surface Modification with Poly (Sulfobetaine Methacrylate-Co-Acrylic Acid) to Reduce Fibrinogen Adsorption, Platelet Adhesion, and Plasma Coagulation. *Biomacromolecules* 2011, *12* (12), 4348–4356. https://doi.org/10.1021/bm2013185.

(53) Chang, Y.; Chang, Y.; Higuchi, A.; Shih, Y. J.; Li, P. T.; Chen, W. Y.; Tsai, E. M.; Hsiue, G. H. Bioadhesive Control of Plasma Proteins and Blood Cells from Umbilical Cord Blood onto the Interface Grafted with Zwitterionic Polymer Brushes. *Langmuir* 2012, *28* (9), 4309–4317. https://doi.org/10.1021/la203504h.

(54) Sin, M. C.; Sun, Y. M.; Chang, Y. Zwitterionic-Based Stainless Steel with Well-Defined Polysulfobetaine Brushes for General Bioadhesive Control. *ACS Appl Mater Interfaces* 2014, *6* (2). https://doi.org/10.1021/am4041256.

(55) Ostaci, R. V.; Damiron, D.; al Akhrass, S.; Grohens, Y.; Drockenmuller, E. Poly (Ethylene Glycol) Brushes Grafted to Silicon Substrates by Click Chemistry: Influence of PEG Chain Length, Concentration in the Grafting Solution and Reaction Time. *Polym Chem* 2011, *2* (2), 348–354. https://doi.org/10.1039/c0py00251h.

(56) Pata, V.; Dan, N. The Effect of Chain Length on Protein Solubilization in Polymer-Based Vesicles (Polymersomes). *Biophys J* 2003, *85* (4), 2111–2118. https://doi.org/10.1016/S0006-3495(03)74639-6.

(57) Ishihara, K. Biomimetic Materials Based on Zwitterionic Polymers toward Human-Friendly Medical Devices. *Sci Technol Adv Mater* 2022, *23* (1), 498–524. https://doi.org/10.1080/14686996.2022.2119883.

(58) Puerta-Oteo, R.; Ojeda-Amador, A. I.; Jiménez, M. V.; Pérez-Torrente, J. J. Catalytic Applications of Zwitterionic Transition Metal Compounds. *Dalton Transactions* 2022, *51* (3), 817–830. https://doi.org/10.1039/d1dt03746c.

(59) Zhang, M.; Yu, P.; Xie, J.; Li, J. Recent Advances of Zwitterionic-Based Topological Polymers for Biomedical Applications. *J Mater Chem B* 2022, *10* (14), 2338–2356. https://doi.org/10.1039/d1tb02323c.

(60) Zheng, L.; Sundaram, H. S.; Wei, Z.; Li, C.; Yuan, Z. Applications of Zwitterionic Polymers. *React Funct Polym* 2017, *118*, 51–61. https://doi.org/10.1016/j.reactfunctpolym.2017.07.006.

(61) Harijan, M.; Singh, M. Zwitterionic Polymers in Drug Delivery: A Review. *Journal of Molecular Recognition* 2022, *35* (1), e2944. https://doi.org/https://doi.org/10.1002/jmr.2944.

Chapter 2. GRAFTING pSBMA COATINGS ON RADIOFREQUENCY GLOW DISCHARGE PLASMA ACTIVATED SURFACES USING ARGET ATRP TO RESIST NON-SPECIFIC PROTEIN ADSORPTION

Abstract: Most materials employed for orthopedic implants on account of their mechanical strength tend to be hydrophobic and often cause foreign body response. This leads to reduced implant lifetime and necessitates frequent surgical replacements. With a view to overcoming these limitations, this chapter introduces a surface modification technique applicable to a plethora of industrial-strength materials used in orthopedics. The introduction of hydrophilic species such as zwitterionic poly (sulfobetaine methacrylate) (pSBMA) greatly alters the thermodynamics of interfacial protein adsorption by forming a strong hydration layer, successfully preventing protein adsorption. Here, these species were introduced using radio frequency glow discharge (RFGD) plasma deposition of 2-hydroxyethyl methacrylate (HEMA), followed by macro-initiator covalent coupling using α-bromoisobutyryl bromide and pSBMA coating synthesis with ARGET ATRP. Polyurethane (RPU) and titanium were used as model substrates to demonstrate the versatility of the RFGD plasma deposition. The chemical composition of the modified surfaces was analyzed using X-ray photoelectron spectroscopy. The coating thickness was measured using a profilometer and found to be 71 ± 4.1 nm after HEMA deposition and 116 ± 3.9 nm after pSBMA grafting. The contact angle for titanium was measured to be 12.8 ± 2.2° after pSBMA grafting. In addition, the coated RPU samples showed a 93% reduction in protein adsorption relative to bare substrates, as measured using *I-125* tagged albumin. The coated RPU samples were also implanted in mice and chickens and showed negligible to mild fibrosis upon explantation, indicating increased biocompatibility.

2.1 INTRODUCTION

Recent years have witnessed significant progress in the development of materials that can be used in biomedical implants and devices.[1] However, myriad inflammatory 'Foreign Body Response' (FBR) mechanisms continue to impede further performance improvements.[2–5] The limited lifetime of biomedical implants due to suboptimal biocompatibility thus necessitates frequent surgical procedures and replacements.[6,7] Implant rejection due to FBR is primarily the result of the unfavorable interfacial properties of implant materials, including surface wettability, roughness and cytotoxicity.[8] Most mechanically robust industrial materials used for fabricating medical implants are hydrophobic in nature, such as polypropylene (PP), polyurethane (PU), polytetrafluoroethylene (PTFE), titanium and stainless steel. Hydrophobic surfaces are more prone to non-specific protein adsorption, the triggering event for FBR, due to unfavorable energetics.[9] In contrast, the low interfacial energy of hydrophilic surfaces in biological environments allows for reduced non-specific protein adsorption and fouling, thereby mitigating FBR mechanisms.[10] Surface modification is thus essential to alter the interfacial properties of these implant materials and improve biocompatibility. This necessitates reasonably simple surface modification protocols applicable to a wide range of industrial materials.[11–13]

In fabricating non-fouling surfaces, polyethylene glycol (PEG) continues to find extensive use both for surface coatings, and as a constituent of copolymers to minimize FBR, due to its ability to form strong hydration layers at the interface *via* hydrogen bonding.[14] However, the long-term performance of PEGylated materials is limited due to reduced specificity and therapeutic efficacy, chemical degradation due to reactive oxygen species, and long-term immunogenicity.[15–18] Biomimetic zwitterionic polymers are thus being explored as super hydrophilic alternatives, and molecules such as phosphatidyl choline, carboxybetaine, and sulfobetaine have been studied

extensively.[19–23] Zwitterionic materials are rich in phosphorylcholine (PC) headgroups, which resemble the surface of the mammalian cell membrane.[23–25] Synthetic polybetaine (PB) polymers like poly(sulfobetaine methacrylate) (pSBMA) and poly(carboxybetaine methacrylate) (pCBMA) are very similar to PC-based polymers in terms of structure, with both cationic and anionic groups present on the same monomer backbone.[26,27]

Zwitterionic surfaces are believed to resist non-specific protein adsorption *via* a strong and stable hydration layer attached through the solvation of the charged terminal groups, in addition to hydrogen bonding.[28–31] In previous studies performed in our group, subcutaneous implantation of pCBMA hydrogels in mice showed no signs of fibrosis even after 3 months, indicating that zwitterionic materials can prevent the formation of dense collagenous capsules. This greatly enhances device performance over extended periods of time.[32] Surfaces coated with sulfobetaine polymers have shown high resistance to non-specific protein adsorption with fibrinogen adsorption levels < 0.3 ng/cm^2, as measured by surface plasmon resonance.[23] Sulfobetaine-based polymers have substantial biological inertness and low cytotoxicity in addition to their strong hydration abilities. In addition, while sulfobetaine-based monomers possess structural similarities to certain PC derivatives, they also possess the advantages of low cost and ease of synthesis and handling.[33] Past work from many groups has demonstrated the ability of robust pSBMA coatings to prolong the lifetime of medical implants.[12,20,34,35] Given these considerations, SBMA was chosen as the polymer for this study.

There exist a variety of methods for the attachment of polymer coatings to solid substrates such as the ones discussed herein. The simplest class of methods utilizes physical bonding by way of weak intermolecular forces such as electrostatic forces, hydrogen bonding, and hydrophobic dispersive interactions. Given the weak strength of these interactions, the tethered polymer chains

can easily be removed or delaminated because of solvation effects or shearing action.[36] In contrast, covalent attachment *via* surface initiated controlled radical polymerization techniques like atom transfer radical polymerization (ATRP) results in more robust and permanent films.[37] These methods typically involve immobilization of an initiator molecule on an activated surface followed by monomer polymerization.[38–40] Thiol and silane chemistries are commonly used for initiator immobilization on substrates such as gold and silicon.[38] These chemistries are however incompatible with a variety of materials with inert surfaces like plastics that can degrade or dissolve upon soaking in solvents like methylene chloride that are commonly used for initiator immobilization.[40–42] Therefore, as an alternative, we have utilized radio frequency glow discharge (RFGD) plasma deposition for surface activation and immobilization of ATRP initiators. RFGD plasma deposition has been widely used for creating strongly bound thin films for surface functionalization.[43–46] In addition, activators regenerated by electron transfer (ARGET) ATRP was used for polymerization in place of conventional ATRP, which requires oxygen free inert conditions and larger amounts of toxic Cu (I) transition metal to carry out the reaction.[47,48] In contrast, ARGET ATRP utilizes a reserve of reducing agent to regenerate Cu (I) from Cu (II) *in situ*, thus significantly reducing the amount of required Cu (I), in addition to increased tolerance towards oxygen.[49–51]

In this work the implant material surfaces were first activated by creating thin films of 2-hydroxyethyl methacrylate (HEMA) *via* RFGD plasma deposition to introduce hydroxyl groups. This step is based on the adaptation of plasma polymerization techniques introduced and extensively refined in our group.[46,52–54] The polymerization initiator α-bromoisobutyryl bromide (BIBB) was then immobilized by esterification of hydroxyl groups with BIBB to introduce bromine groups on the surface, which were then used to synthesize pSBMA coatings *via* ARGET

ATRP. This is a reliable method that can be easily optimized for different substrates and varied surface chemistries. This work thus describes the application and efficacy of a versatile surface modification technique for a variety of materials used in orthopedic implants, irrespective of surface chemistry or geometry. Reinforced polyurethane (RPU-70) and titanium (Ti) were explored as materials of interest. A schematic of the process, depicting the initiator immobilization and polymerization steps applied in this study is shown in Figure 2.1.

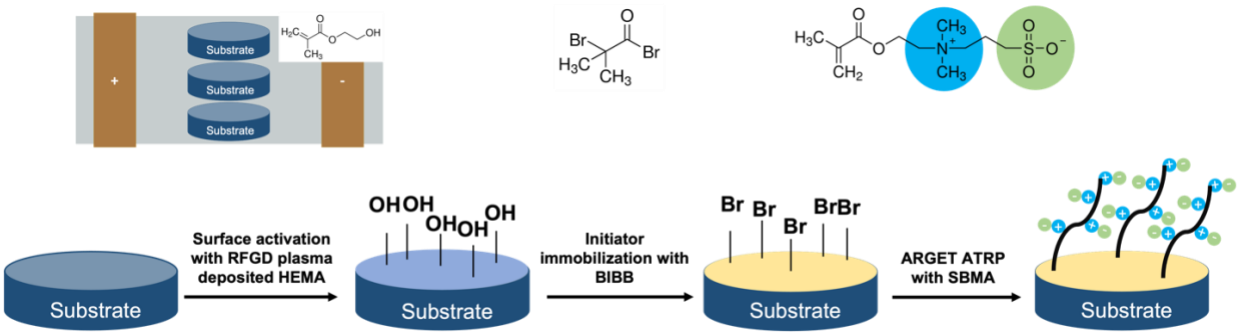

Figure 2.1. Schematic of the general coating process. In step 1, a clean, bare substrate of the given implant material is functionalized with hydroxyl groups by means of RFGD plasma deposition of HEMA. In step 2, the ATRP initiator, BIBB is immobilized on the surface. Finally, in step 3, SBMA is grafted from the surface using ARGET ATRP.

2.2 MATERIALS

2-hydroxyethyl methacrylate, ophthalmic grade (HEMA, CAS No.: 868-77-9) was purchased from polysciences. α-Bromoisobutyryl bromide (BIBB, CAS No.: 20769-85-1), copper (II) bromide ($CuBr_2$, CAS No.: 7789-45-9), 2,2-bipyridyl (bpy, CAS No.: 366-18-7), L-ascorbic acid (CAS No.: 50-81-7), [2-(methacryloyloxy)ethyl]dimethyl-(3-sulfopropyl)ammonium hydroxide (SBMA, CAS No.: 3637-26-1), triethylamine (TEA, CAS No.: 121-44-8), human serum albumin (HSA, ≥99%, CAS No.: 70024-90-7), sodium azide (CAS No.: 26628-22-8), and sodium iodide (CAS No.: 7681-82-5) were purchased from Sigma-Aldrich and used as received. Boric

acid (CAS No.: 10043-35-3), sodium phosphate monobasic (CAS No.: 7558-80-7), sodium hydroxide (CAS No.: 1310-73-2) and all solvents were purchased from Fisher Scientific and used as received. Citric acid monohydrate (CAS No.: 5949-29-1) was purchased from J.T. Baker. Iodine-125 radionuclide (Specific Activity: ~17 Ci/mg) was purchased from Perkin Elmer. Sodium chloride (CAS No.: 7647-14-5) was purchased from EMD Millipore. Chromatography columns (10DG Desalting Columns, CAS No.: 7322010) were purchased from Bio-Rad. 8 mm discs of RPU-70 were 3D by Dependable Plastics (Fairfield, CA). Titanium sheets were purchased from McMaster-Carr.

2.3 EXPERIMENTAL METHODS

2.3.1 SAMPLE PREPARATION

2.3.1.1 Substrate preparation and cleaning

Titanium sheets were first cut into 0.5-inch squares. To remove any surface impurities, the samples were thoroughly washed by sonication in n-hexane, methylene chloride, acetone and methanol for 15 min each. The cycle was repeated three times. The solvents were changed after every cycle. RPU-70 discs were washed by sonicating only in n-hexane for 15 min, repeating the cycle three times. All samples were then dried under vacuum and stored in a desiccator until further use. The process for polypropylene substrates is described in Appendix A.

2.3.1.2 Surface activation using RFGD plasma

The substrate surfaces were first activated by deposition of a layer of hydroxyl groups (-OH) using plasma deposition of HEMA. These hydroxyl groups act as anchors for the successive initiator immobilization reactions. A custom-built plasma reactor based on the design reported by Lopez et. al. was used for all plasma-based experiments in this study (Figure 2.2).[52] The plasma

reactor parameters used for RPU-70 were slightly different from those used for titanium substrates. This was due to the presence of a thick oxide layer on the titanium surfaces, which can lead to easy delamination of coatings. The process parameters thus needed to be optimized for titanium substrates.

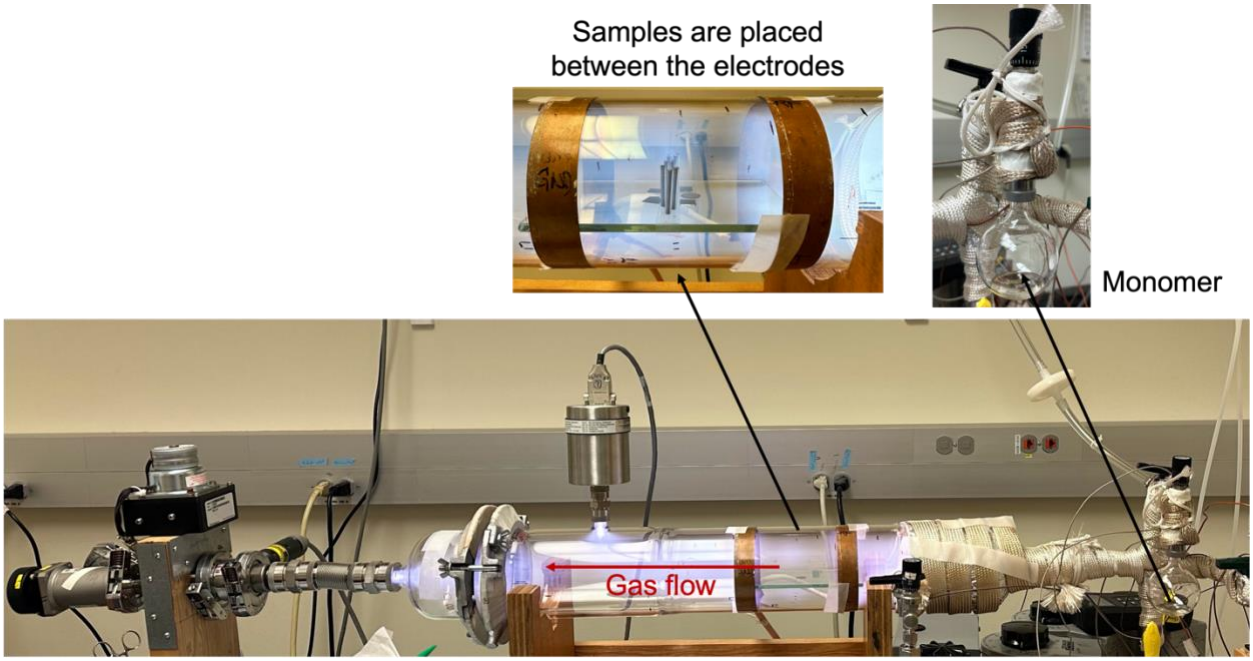

Figure 2.2. Image of the RFGD plasma setup.

After thorough cleaning, the substrates were loaded in the plasma reactor and placed between the two electrodes (powered and grounded) positioned 100 mm apart. An automatic impedance matching network and a 13.57 MHz radio frequency power source were connected to the powered electrode. A mechanical pump was used to pump down the reactor to a base pressure of 6-7 mTorr. A cold trap cooled using liquid nitrogen was installed between the mechanical pump and the reactor to condense any waste organic vapors.

For RPU-70, after the reactor attained the base pressure, the samples were first argon-etched for 5 min at 60 W while maintaining a pressure of 250 mTorr. This was done to clean the sample surfaces of any organic impurities. After this step, methane gas was bled into the chamber

and a methane layer was plasma deposited at 80 W for 5 min, while maintaining a stable pressure of 140 mTorr. The methane layer enables strong adhesion of subsequent plasma coatings to the substrates, thus preventing delamination. After the deposition of the methane layer, the reactor was again pumped down to base pressure. HEMA monomer was then added in a glass flask attached to the reactor and was vaporized by heating to 65°C using a water bath. The monomer vapors were then introduced into the reactor and allowed to reach a stable pressure of 250 mTorr. An initial adhesion layer was first formed by plasma depositing the HEMA at 100 W for 1 min, after which the power was reduced to 6 W for 10 min, while maintaining a stable pressure of 250 mTorr. The plasma generator was then turned off and the samples were quenched in the monomer vapors for 5 min at a pressure of 250 mTorr. This was done to achieve complete utilization of the free radicals generated by the plasma. The chamber was then pumped down to base pressure and flushed with argon thrice, to prevent any organic vapors from escaping into the atmosphere upon opening the reactor. The plasma-deposited samples were retrieved under argon and kept in vacuum overnight to lessen surface chemical reactivity.

For titanium substrates, the above procedure was applied albeit with minor optimizations for the durations of argon etching and adhesion layer deposition. For titanium, the samples were argon etched for 15 min at 60 W, while maintaining a stable pressure of 250 mTorr. After this, a layer of methane was plasma deposited for 8 min at 80 W and a pressure of 140 mTorr. The HEMA monomer was then plasma deposited for 2 min at 100 W and 10 min at 6 W, at a stable pressure of 250 mTorr, and quenched for 5 min before collecting under argon. The Argon etching was performed for a longer duration for titanium to reduce the thickness of the surface oxide layer and thus minimize surface roughness.[55] The longer duration for methane deposition and HEMA deposition at 100 W is expected to help in the adhesion of the subsequent layers.

Following surface activation, the HEMA coated samples (hereafter denoted as RPU-HEMA for RPU-70 and Ti-HEMA for titanium) were first soaked in deionized (DI) water for 1 h followed by drying overnight under vacuum before further use in experiments. This was to remove any unreacted monomer from the surface.

2.3.1.3 Immobilization of macroinitiator for ARGET ATRP

Surface activation using RFGD plasma deposited HEMA was followed by the immobilization of a macroinitiator. ARGET ATRP initiator, α-bromoisobutyryl bromide (BIBB) was immobilized by esterification of hydroxyl groups with BIBB to introduce bromine groups on the surface, which were then used to synthesize pSBMA coatings *via* ARGET ATRP. To do this, the HEMA-activated substrates were respectively soaked in a solution of 10 ml extra dry methylene chloride and 350 µl triethylamine (TEA) (Ti-HEMA) and 10 ml ice-cold n-hexane (RPU-HEMA). This was followed by the dropwise addition of 350 µl BIBB. The reaction was allowed to run for a total duration of 24 h. The titanium samples were stored at room temperature under constant stirring for 4 h and at 4°C for the remaining 20 h. For RPU, the samples were kept at 4°C for the 24 h duration. At the end of the reaction, the samples were thoroughly washed with methylene chloride (Ti-HEMA) or n-hexane (RPU-HEMA) to remove any unreacted BIBB. The BIBB-immobilized discs (Ti-HEMA-BIBB or RPU-HEMA-BIBB) were allowed to dry overnight under vacuum before further use. For RPU-70, n-hexane was used since polyurethanes tend to swell and disintegrate in harsh solvents such as methylene chloride.

2.3.1.4 Surface-initiated ARGET ATRP of SBMA

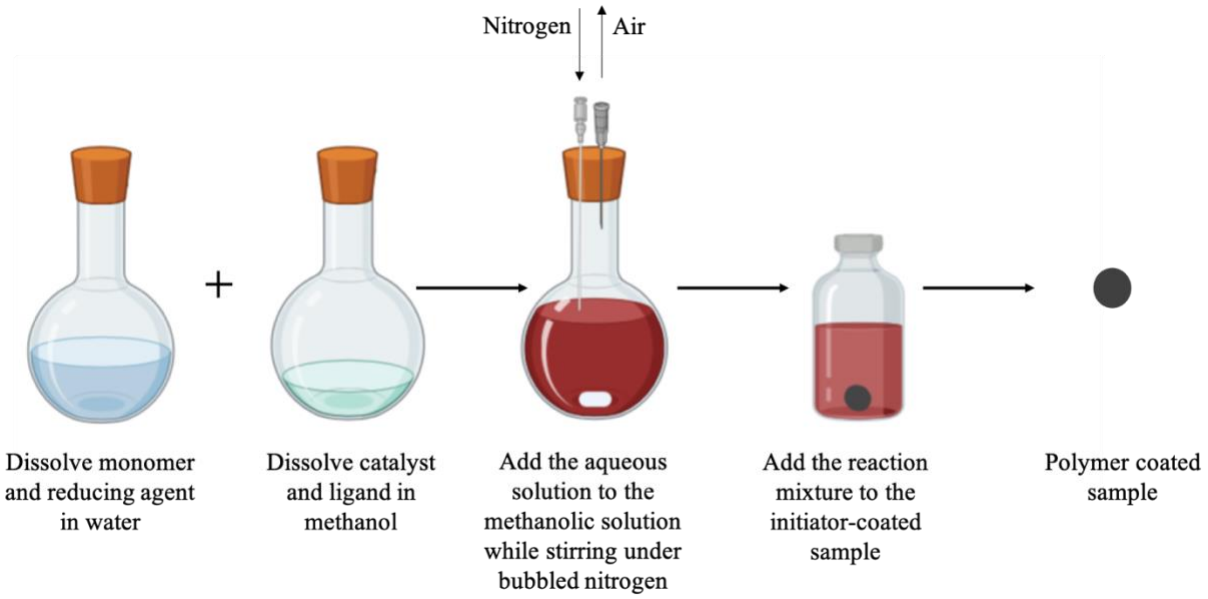

Figure 2.3.Schematic of ARGET ATRP.

A schematic of ARGET ATRP is shown in Figure 2.3. The polymerization was performed in air under ambient conditions. Glass vials and round bottomed flasks were used for conducting these experiments, since no specialized equipment or setup is required for ARGET ATRP, unlike conventional ATRP. Since SBMA is a polar molecule, a mixture of water and methanol was used as the solvent mixture. To prepare the reaction mixture, a predetermined amount of SBMA (0.72 mmol) and L-ascorbic acid (0.27 mmol) were first dissolved in DI water and $CuBr_2$ (0.03 mmol) and bpy (0.19 mmol) were dissolved in methanol. The denser aqueous mixture was then added to the methanolic mixture, and the solution was degassed with nitrogen for 1 h under constant stirring. The reaction mixture was then added to glass vials containing the initiator-immobilized substrates and kept on a slow shaker at room temperature. The reaction was allowed to run for 2.5 h. Deionized water and methanol were used in a 60:40 ratio as the solvent mixture for this reaction. 3 ml of the prepared solution was used for each sample. At the end of the reaction time, the samples

were removed from the vials and washed with a 1:1 mixture of methanol and water at least six times. pSBMA grafted samples (Ti-HEMA-pSBMA and RPU-HEMA-pSBMA) were then dried under vacuum and stored in a desiccator until further analysis.

2.3.2 SAMPLE ANALYSIS METHODS

2.3.2.1 X-ray photoelectron spectroscopy (XPS)

The elemental composition of all the prepared RPU surfaces was characterized using X-ray photoelectron spectroscopy. XPS was performed on an S-Probe photoelectron spectrometer (Surface Science Instruments) equipped with a monochromatic Al Kα source operated at 20 mA emission current and 10 kV anode potential. Charge neutralization was performed using a low energy electron flood gun. A circular X-ray analysis area for all the acquisitions was set to a diameter of 800 μm. During the spectral acquisition the pressure in the analytical chamber was maintained below 5×10^{-9} Torr. Low resolution survey scans were obtained in the energy range of 0 to 1100 eV with a step size of 1 eV and a pass energy of 150 eV. High resolution C 1s scans were obtained from 270 to 290 eV, N 1s scans from 390 eV to 410 eV, and S 2p scans were obtained from 160 eV to 180 eV. The scans were analyzed for elemental composition and high-resolution peak fitting using the Service Physics Hawk version 7 software and fitted with a Shirley background. All binding energies were referenced to that of the C 1s orbital at 284 eV.

All XPS spectra for titanium samples were collected on a Kratos Axis-Ultra DLD spectrometer equipped with a monochromatized Al Kα X-ray source operated at 10 mA emission current and 12 kV anode potential. Charge neutralization was done using a low energy electron flood gun. The X-ray analysis area for all acquisitions was set at 700 x 300 μm. During the spectral acquisition the pressure in the analytical chamber was maintained at a value less than 5×10^{-9} Torr. Pass energy for survey scans was set at 80 eV and that for the high-resolution scans was 20 eV.

The take-off angle, i.e. the angle between the sample normal and the input axis of the energy analyzer was set to 0°, which allows for a sampling depth of ~ 100 Å. The Kratos Vision 2 software was used to determine peak areas for calculating the elemental composition. Casa XPS software was used for peak fitting of the high-resolution spectra. All binding energies were referenced to the aliphatic carbon (C 1s) at 285 eV. All high-resolution spectra were fitted with a Shirley background.

2.3.2.2 Profilometry

The thickness of the prepared surface coatings was measured using a Bruker-DektakXT Profilometer with a 2 μm radius diamond stylus. Thickness was measured for dry samples using the hill-and-valley profile acquisition setting across a scratch made on the surface with a razor blade. For all thickness measurements, silicon wafers were used as the substrates.

2.3.2.3 Contact Angle

The contact angle of the prepared surfaces was measured in air using an NRL contact angle goniometer (Model A-100, Rame-Hart, Inc.). Water droplets were transferred to the sample surfaces using a pipette. The contact angle measurements were repeated n=6 times for each sample group.[56]

2.3.2.4 Radiolabeling of human serum albumin using ICL method

Human serum albumin (HSA) was radiolabeled by tagging with iodine-125 (I-125) using the iodine monochloride (ICl) method, based on protocols previously established in our lab and described by Horbett et.al. and Mecwan et. al.[46,57] Briefly, to tag the HSA with I-125, 1 mCi of I-125 radionuclide was added to 0.5 ml of 2X borate buffer which was immediately added to 0.5 ml of a 3:1 mixture of ICl/NaCl. This mixture was then finally added to 0.5 ml of 10 mg/ml HSA

solution prepared in 1X borate. The mixture was placed on ice for 20 min for the tagging reaction to occur. The solution was then passed through a chromatography column for purification. 40 fractions of the purified tagged protein were collected, and the activity measured using a Perkin Elmer 2470 WIZARD 2 gamma counter. This was done to capture the free iodine peaks and evaluate the efficiency of iodination. The three or four fractions with the highest activity were collected, pooled together, and run through a second chromatography column for further purification followed by a second fraction collection and activity measurement for peak identification. The three or four fractions with the highest activity were again collected and pooled together. The purified radiolabeled protein was placed in a lead pig and stored at -80°C until further use.

2.3.2.5 I-125 radiolabeled HSA adsorption

Non-specific protein adsorption was measured for the coated surfaces using bare substrates as negative controls. Human serum albumin was used as the model protein for this study. A sample set of n=4 was used for all studies. First, all samples were incubated in 0.75 ml of degassed citrate phosphate buffer saline with sodium azide (cPBSzI) for 2 h at 37°C in 2 ml cups. This was performed to equilibrate the surfaces. The radiolabeled albumin was then thawed and added to a 0.6 mg/ml stock solution of HSA in degassed cPBSzI, to prepare the "hot" protein solution. The activity of the hot solution (HSA containing radiolabeled protein) was measured to obtain a minimum 2:1 signal-to-noise ratio, with an activity of ~ 100 CPM/ng. After the 2 h incubation period, 0.75 ml of the hot protein solution was added to each sample and incubated for another 2 h at 37°C. After this step, the samples were thoroughly washed with cPBSzI using a rinsing setup to remove any excess non-adsorbed protein from the sample surface. The samples were then transferred to gamma counter tubes and carefully capped. The radioactivity of each sample was

measured for 1 min using the gamma counter. The amount of the protein adsorbed was measured based on the activity of the hot protein solution and surface area of the samples and was calculated in ng/cm^2.

2.3.2.6 Cytotoxicity studies

NIH-3T3 mouse fibroblasts were used to determine the toxicity of the coated samples. RPU and titanium samples grafted with pSBMA (n=3) were first sterilized by soaking in 70% ethanol for 1 h. The sterilized samples were then aseptically placed in 12-well plates along with 1 ml of complete growth medium (DMEM-high glucose + 1 v% L-glutamine + 1 v% antibiotic/antimycotic + 10 v% fetal bovine serum) and allowed to elute for 24 h by incubation at 37°C. After elution, 1 ml eluates were transferred from the samples to another 12-well plate with the sub-confluent cultured cells. The samples were again incubated at 37°C for an additional 72 h and removed for microscopic examination at 24, 48 and 72 h time points. The well plates were periodically swirled during the incubation period. Blank wells of a tissue culture polystyrene (TCPS) plate incubated in normal media were used as negative control while latex was used as positive control. The cells were observed for visible signs of toxicity as indicated by changes in cell morphology by way of comparison with the negative control cells. The samples were rated on a reactivity grade from 0 to 4 using guidelines developed by the US Pharmacopeia (USP) or ISO 10993-5, with 0 denoting no reactivity and 4 indicating severe reactivity.

2.3.3 *IN VIVO* STUDIES

2.3.3.1 In vivo implantation in mice

A mouse model was used to evaluate the FBR to pSBMA grafted RPU discs. For this study, 8 mm RPU discs were used as the model implant. The samples were sterilized by soaking in 70% ethanol. All animal experiments strictly adhered to federal guidelines and were

approved by the Animal Care and Use Committee at the University of Washington. 8 mm RPU discs coated with pSBMA were implanted in 8-10 weeks old male Balb/C mice (n=10) for 4 weeks. All implantations were performed subcutaneously. The mice were administered with buprenorphine before being anesthetized with isoflurane. To implant the discs, the backs of the mice were first shaved and sterilized with betadine and cleaned with alcohol wipes before making the incisions. This was to clean the incision site of any mice hair or other impurities. Subcutaneous pockets were then formed under both shoulders of each mouse and one implant was placed on each side. The incisions were closed with surgical staples and mice were carefully monitored until explantation.

After 4 weeks of implantation, all mice were euthanized by asphyxiation with carbon dioxide, carefully following the protocols provided by the Animal Care and Use Committee at the University of Washington. The implants were explanted by making midline incisions. After dissection, the samples were fixed in a zinc fixative and embedded in paraffin blocks. 7 µm sections were prepared on glass slides by sectioning the paraffin blocks with a microtome. The samples were then baked in an oven at 60°C for 20 min and allowed to cool down before deparaffinizing the slides. The slides were then stained with Masson's trichrome using previously established protocols in our lab. The stained slides were imaged in brightfield using a Nikon E800 camera.

2.3.3.2 In vivo implantation in chickens

The chicken experiments were performed at Oregon State University using 4 months old Freedom Ranger chickens (n=10). The surgeries were performed by veterinary surgeons. 3-D implants made using RPU-70 were implanted in the chicken feet to test the biomechanics of the

actual implant design and more importantly the effect of pSBMA coatings on FBR. All samples were sterilized before implantation using ethylene oxide.

2.4 RESULTS AND DISCUSSION

This section is a discussion and analysis of the proposed protocol for grafting of zwitterionic pSBMA coatings on polyurethane (RPU) and titanium (Ti) based substrates using the surface modification techniques discussed previously (RFGD plasma and ARGET ATRP). The surfaces were first activated by depositing 2-hydroxyethyl methacrylate using RFGD plasma, followed by immobilization of a macroinitiator, BIBB and synthesis of pSBMA coatings using ARGET ATRP. A schematic of this three-step methodology is shown in Figure 2.1. Polypropylene (PP) was the initial substrate of interest, and some initial protocol development and testing was performed on PP. The results for PP samples are discussed in section A.6. However, the use of PP was later discontinued in favor of RPU-70, which possesses the advantage of being 3-D printable with better design resolution for implant features, in addition to superior mechanical properties. The majority of the testing, characterization, and analysis reported herein is thus based on RPU substrates, including the *in vivo* studies. Titanium was later introduced as an alternative implant material because of its wide use and relative familiarity to regulatory agencies. The results for RPU and titanium substrates are discussed in the following sections.

2.4.1 SURFACE CHARACTERIZATION USING XPS

To begin with, hydroxyl groups were introduced on clean RPU and titanium surfaces, using RFGD plasma deposited HEMA (RPU-HEMA, Ti-HEMA) using methods described in section 2.3.1.2. The hydroxyl groups act as anchors for the macroinitiator immobilization. BIBB was attached through the esterification of the hydroxyl groups to introduce bromine on the surface

(RPU-HEMA-BIBB, Ti-HEMA-BIBB). The bromine is then used to initiate ARGET ATRP to graft pSBMA coatings (RPU-HEMA-pSBMA, Ti-HEMA-pSBMA). XPS was used to analyze the surface composition after each modification step to verify the success of surface modification. The atomic compositions of various surfaces before and after surface treatments are summarized in Table 2.1 and Table 2.2. XPS survey scans are depicted in Figure 2.4 and Figure 2.5. All scans were collected after soaking the samples in DI water for 1 h to ensure the measured values are only those of robustly attached species.

For clean bare RPU, only carbon (C), oxygen (O) and nitrogen (N) were observed on the surface, as expected for a clean polyurethane surface. After the introduction of HEMA, C and O were expectedly the only observed species. Bromine was observed only after the immobilization of BIBB, indicating successful esterification of the hydroxyl groups. No nitrogen or sulfur species were observed after HEMA deposition and BIBB attachment. After the successful confirmation of the presence of a bromine initiator, pSBMA coatings were synthesized using ARGET ATRP. Stoichiometrically, a uniform pSBMA coating should contain 5.6 % (atom percentage) of both N and S. The values measured for pSBMA-grafted RPU, and titanium surfaces are in close agreement with the theoretical values, confirming successful grafting of pSBMA brush coatings. In addition, bromine was undetected after pSBMA grafting, indicating complete utilization of the initiator and the presence of a dense pSBMA coating with thickness greater than 100 Å. Additionally, no unexpected contamination was detected, further confirming the presence and quality of the pSBMA coating on the surfaces.

Table 2.1. Summary of the surface composition of bare and functionalized RPU surfaces as obtained by survey and high-resolution C 1s scans from XPS (n=3).

Sample	Elemental composition (%)					C 1s (%)		
	C 1s	O 1s	Br 3d	N 1s	S 2p	CH	CN, CO	COOR
RPU	83 ± 0.5	13.9 ± 0.4	-	3.1 ± 0.2	-	62.4 ± 0.9	31.6 ± 1.9	6.1 ± 0.9
RPU-HEMA	69 ± 0.9	31 ± 0.2	-	-	-	50.4 ± 0.1	33.3 ± 0.8	16.3 ± 0.6
RPU-HEMA-BIBB	69.6 ± 0.6	27 ± 0.3	3.4 ± 0.8	-	-	68.1 ± 0.1	22.1 ± 0.1	9.8 ± 0.3
RPU-HEMA-pSBMA	66.3 ± 0.9	24 ± 1.1	-	5.1 ± 0.2	4.6 ± 0.3	54.2 ± 1.1	38.5 ± 0.6	7.4 ± 0.5

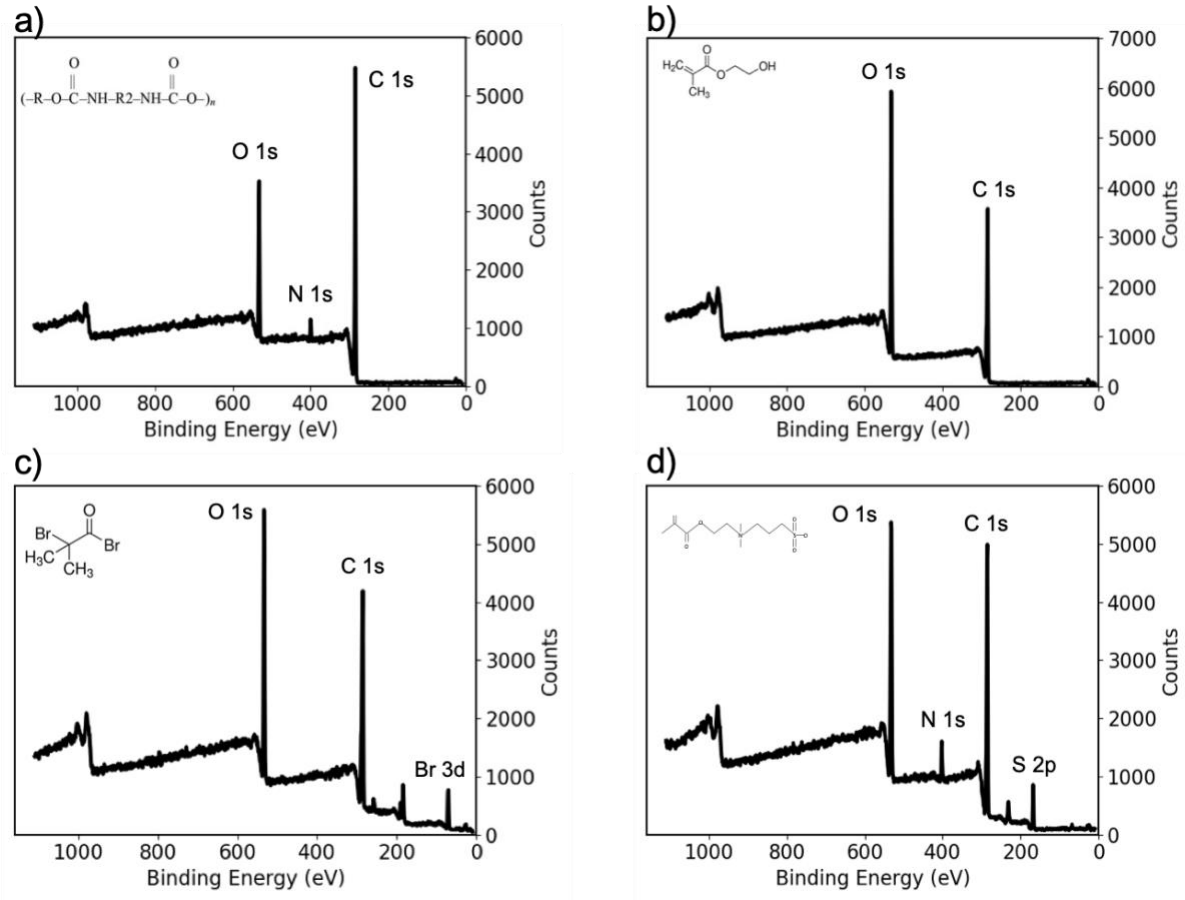

Figure 2.4. Representative XPS survey scans of RPU surfaces before and after functionalization. a) Bare RPU b) RPU-HEMA c) RPU-HEMA-BIBB d) RPU-HEMA-pSBMA. Major peaks are labeled in each scan.

Table 2.2. Summary of the surface composition of bare and functionalized titanium surfaces as obtained by survey and high-resolution C 1s scans from XPS (n=3).

Sample	Elemental composition (%)						C 1s (%)		
	C 1s	O 1s	Br 3d	N 1s	S 2p	Ti 2p	CH	CO	COOR
Ti	34.7 ± 3	49.1 ± 1.6	-		-	16.2 ± 1.3	76.3 ± 0.3	13.9 ± 1.3	9.8 ± 1.0
Ti-HEMA	73.5 ± 0.1	26.5 ± 0.1	-	-	-	-	55.1 ± 0.8	30.7 ± 0.6	14.2 ± 1.4
Ti-HEMA-BIBB	69.5 ± 0.3	26.8 ± 0.4	3.7 ± 0.2	-	-	-	51.3 ± 1.3	30.0 ± 0.9	18.7 ± 0.4
Ti-HEMA-pSBMA	67.9 ± 0.6	23 ± 0.6	-	4.7 ± 0.3	4.4 ± 0.3	-	49.4 ± 0.8	39.8 ± 0.7	10.8 ± 0.8

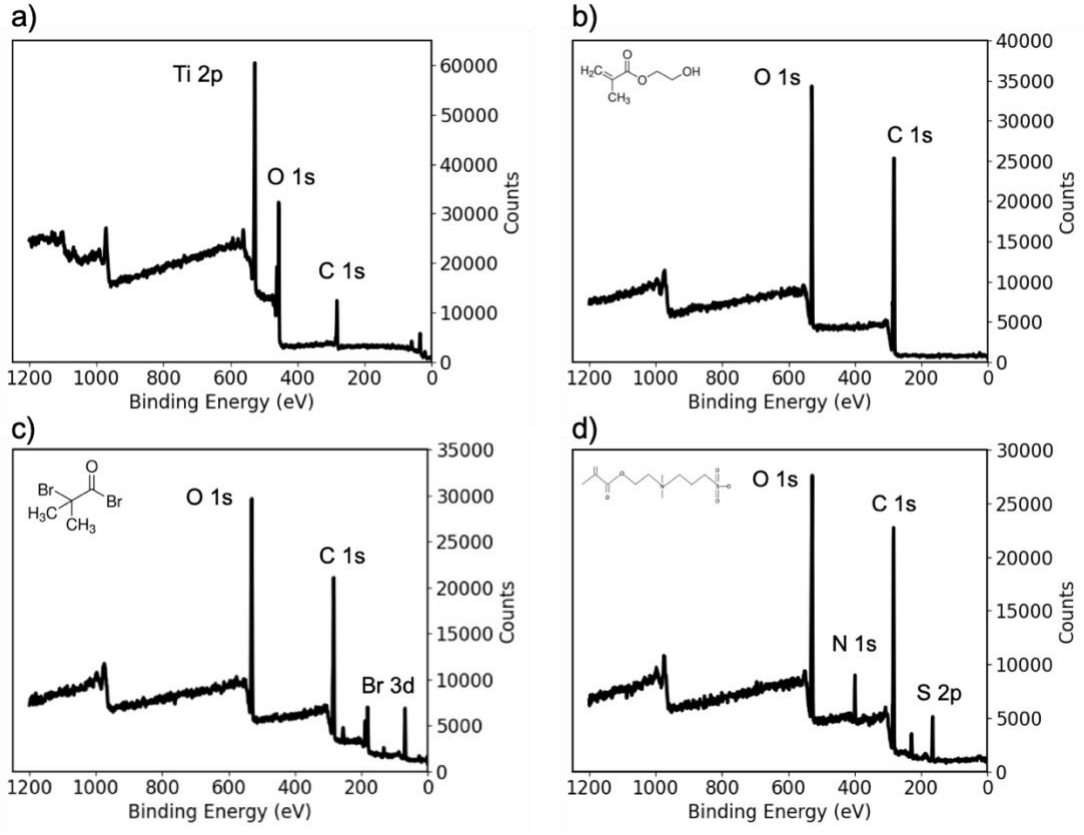

Figure 2.5. Representative XPS survey scans of titanium surfaces before and after functionalization. a) Bare Ti b) Ti-HEMA c) Ti-HEMA-BIBB d) Ti-HEMA-pSBMA. Major peaks are labeled in each scan.

To obtain further insight into the chemical bonding environment of the prepared surfaces, high resolution C 1s spectra were also collected for RPU and titanium surfaces before and after the surface treatments. Characteristic shifts were observed in carbon peaks for all samples, based on the chemical structure of the coating compound. The contributions of each chemical state of carbon on various surfaces are summarized in Table 2.1 and Table 2.2. The shape and features of high-resolution C 1s spectra of RPU and titanium surfaces at various stages of modification are depicted in Figure 2.6 and Figure 2.7, respectively.

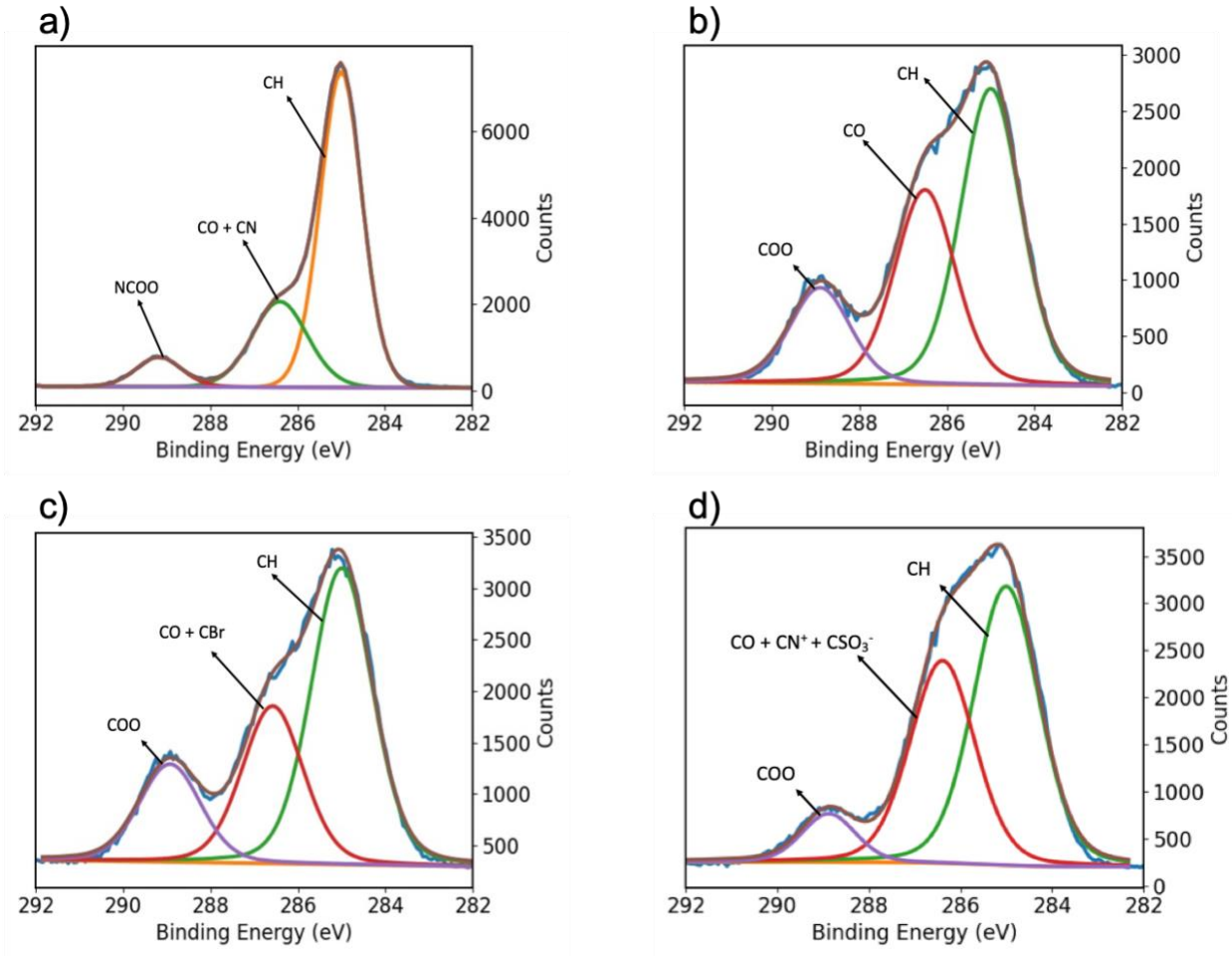

Figure 2.6. Representative high-resolution spectra of the C1s peak on various RPU surfaces. a) bare RPU b) RPU-HEMA c) RPU-HEMA-BIBB d) RPU-HEMA-pSBMA. Fitted peaks are labeled to represent different bonding environments within each chemical structure.

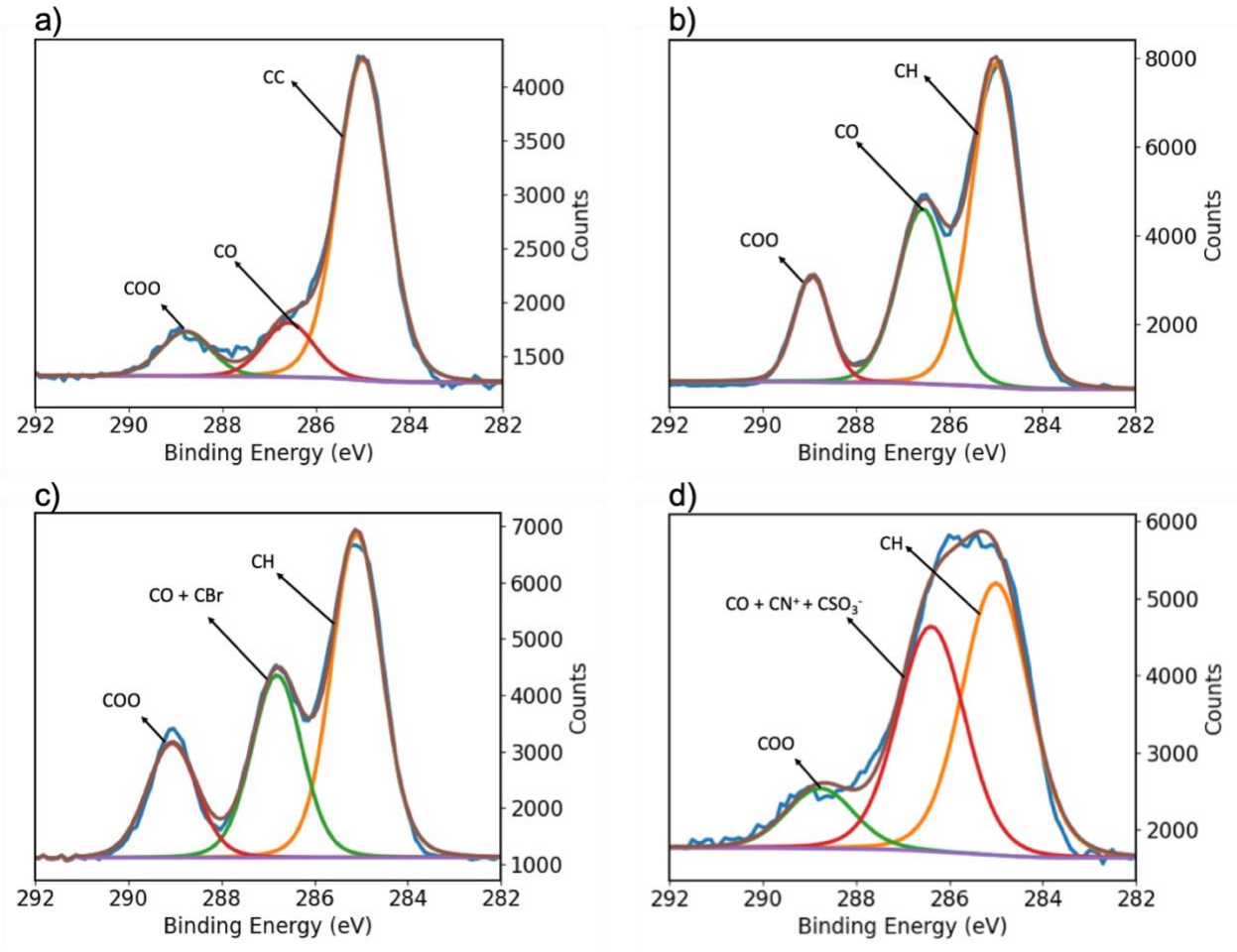

Figure 2.7. Representative high-resolution spectra of the C1s peak on various titanium surfaces. a) bare Ti b) Ti-HEMA c) Ti-HEMA-BIBB d) Ti-HEMA-pSBMA. Fitted peaks are labeled to represent different bonding environments within each chemical structure.

All spectra were fitted with three width-constrained peaks, each corresponding to different bonding environments based on the chemical structure of the surface coating. For bare surfaces, C-H or C-C was fitted at 285 eV, CO and CN at 286.5 eV, and NCOO or COO were fitted at 289 eV. For HEMA-grafted surfaces, the C-H peak was fitted at 285 eV, CO at 286.5 eV, and the peak corresponding to COO at 289 eV. For BIBB-immobilized surfaces, the peak at 286.5 eV represented overlapping CO and C-Br peaks. For pSBMA grafted surfaces, the peak at 286.5 eV represents an overlap of CO, CN^+, and CSO_3^-, confirming the presence of pSBMA on the surface.

To gain further insight into the bonding environments of bare and pSBMA-coated RPU surfaces, high resolution N 1s spectra were also collected, since both surfaces contain nitrogen (Figure 2.8). The N 1s peak (400 eV) in the bare RPU spectrum can reasonably be attributed to the NCO and NCOO groups, which are generally present in the polyurethane structure, whereas in case of pSBMA-grafted surfaces, the N 1s peak represents the nitrogen from the positively charged quarternary amine species in the pSBMA structure.[58,59]

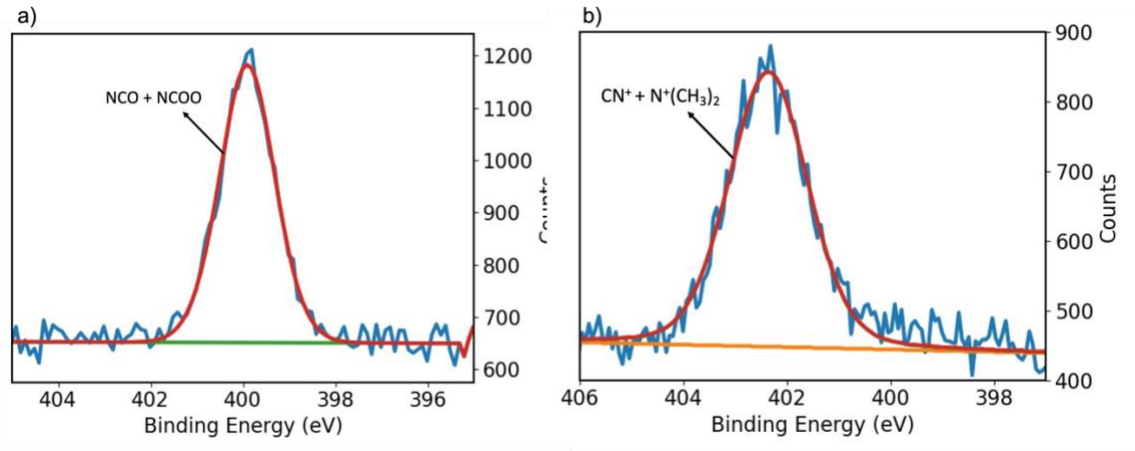

Figure 2.8. Representative high-resolution spectra of the N1s peak on a) bare RPU and b) RPU-HEMA-pSBMA surfaces. Fitted peaks are labeled to represent different bonding environments within each chemical structure.

N 1s and S 2p high resolution spectra were also collected and analyzed for pSBMA-grafted titanium (Figure 2.9). The nitrogen spectrum showed one N 1s peak at around 400 eV, which could be assigned to the quarternary amine groups present in pSBMA. Similarly, the sulfur spectrum shows 2 peaks, S $2p_{3/2}$ at 167.5 eV and S $2p_{1/2}$ at 168.5 eV. Both peaks represent the same bonding environment in the 2p orbital and can be attributed to the negatively charged sulfonate group present in the pSBMA molecule.[58,59]

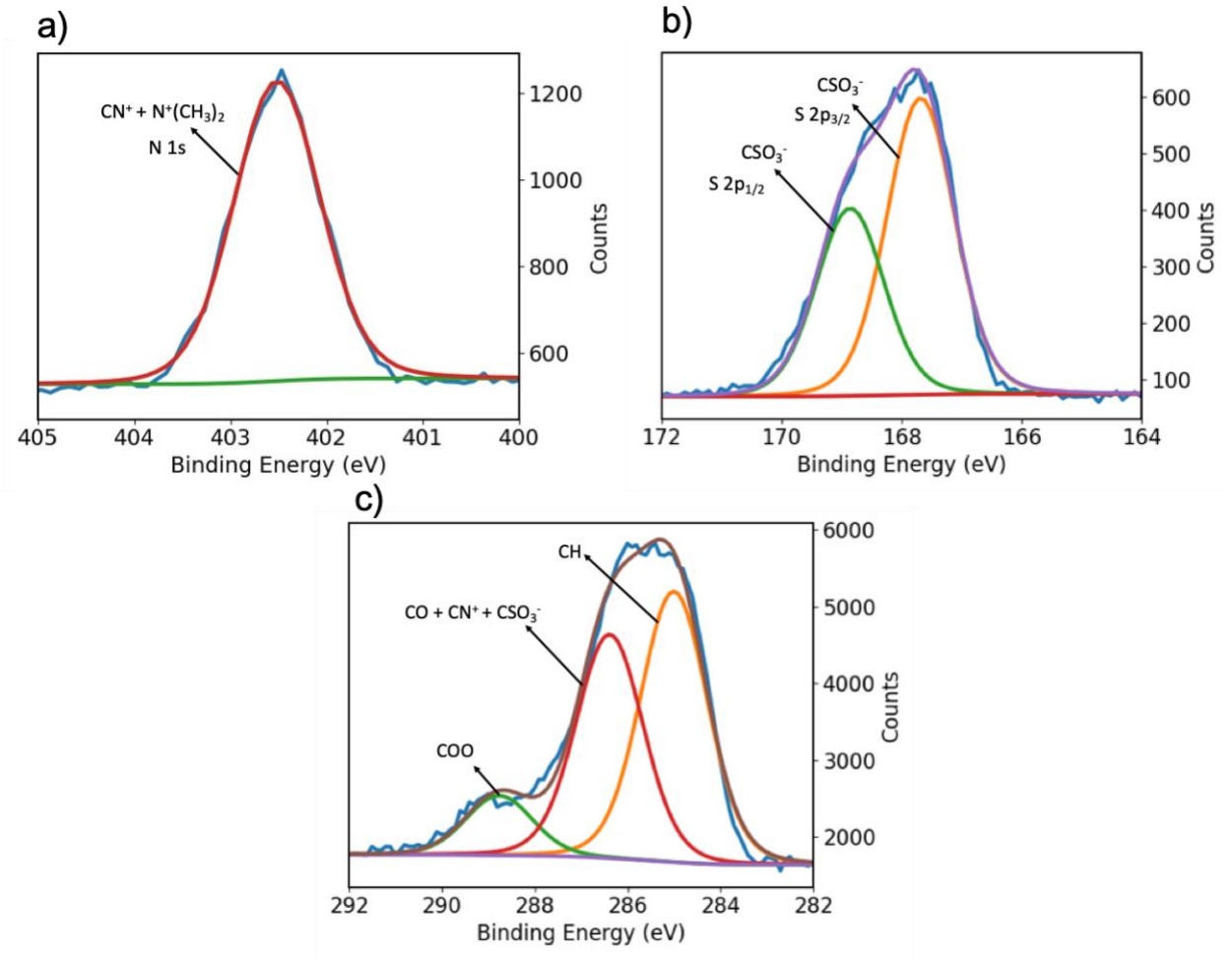

Figure 2.9. Representative high-resolution spectra of the pSBMA grafted titanium surface a) N 1s b) S 2p and c) C 1s. Fitted peaks are labeled to represent different bonding environments within each chemical structure.

These observations confirm the successful chemical transformations associated with the grafting of a uniform zwitterionic coating on the substrate surfaces. Following this, further analysis was performed to study the effect of chemical processing on the structure of RPU, given its plastic nature and possible vulnerability to the chemicals used, such as the n-hexane used for washing and initiator attachment. In addition, the robustness and delamination resistance of the prepared surfaces needs to be confirmed, and this was studied by soaking the samples in saline solutions and evaluating the chemical composition using XPS. To study the effect of n-hexane wash, XPS

survey and high-resolution C 1s spectra were collected for an RPU disc before and after washing with n-hexane. The results of elemental composition from XPS survey scans are summarized in Table 2.3 and Figure 2.10. The high-resolution C 1s scans are summarized in Table 2.3 and depicted in Figure 2.11. Comparison of the samples indicated no difference, suggesting chemical compatibility of RPU with n-hexane. This observation also validates the use of n-hexane in the initiator immobilization reaction for RPU.

Table 2.3. Summary of the surface composition of RPU surfaces before and after washing with n-hexane as obtained by survey and high-resolution C 1s scans from XPS.

Sample	**Elemental composition (%)**				**C 1s (%)**		
	C 1s	**O 1s**	**N 1s**	**Si 2p**	**CH**	**CN, CO**	**COOR**
Before hexane wash	77.3	15.1	3.7	3.9	62.4	31.6	6.1
After hexane wash	77.1	15.8	2.6	4.5	61.1	34.3	4.6

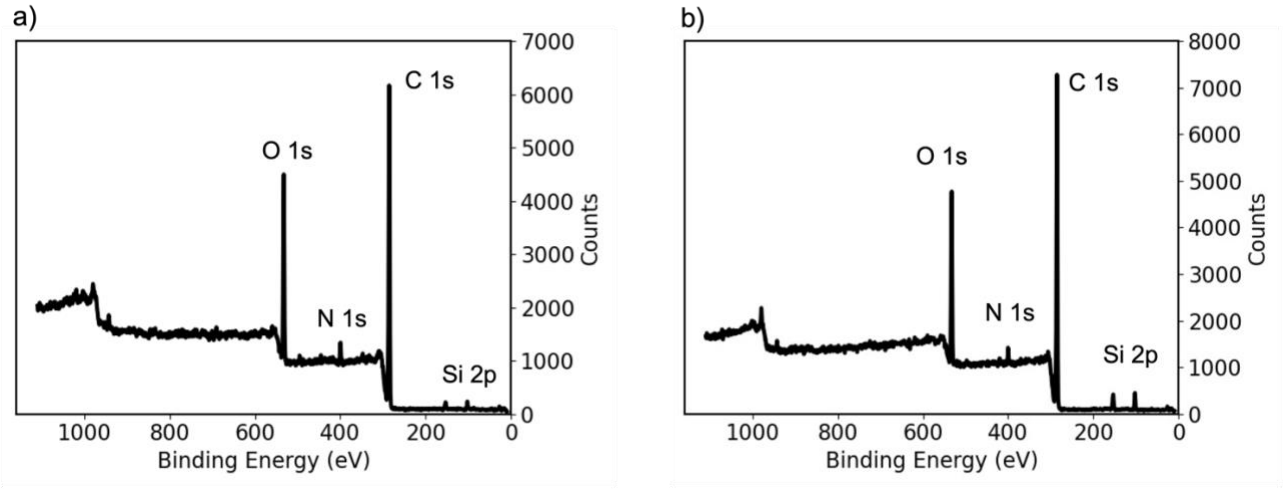

Figure 2.10. Representative XPS survey scans of RPU surfaces a) before and b) after washing with n-hexane. Major peaks are labeled in each scan.

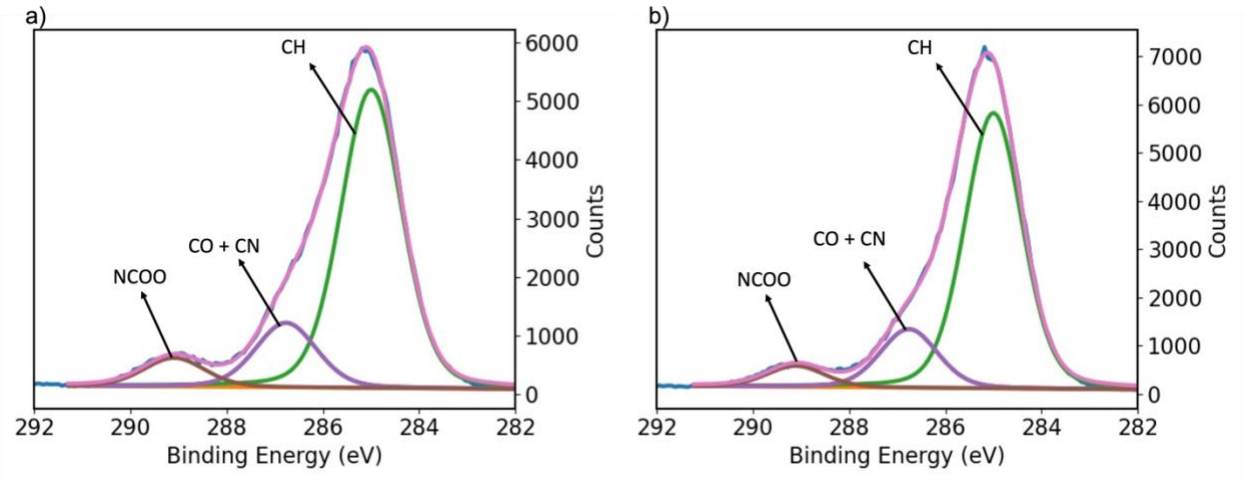

Figure 2.11. Representative high-resolution spectra of the C 1s peak on RPU surfaces a) before and b) after washing with n-hexane. Fitted peaks are labeled to represent different bonding environments within each chemical structure.

To study the *in vitro* stability of the grafted surfaces, the samples were soaked in saline solutions and tested for elemental composition using XPS. RPU samples were soaked in PBS for 48 h before analysis. The results of the surface composition are summarized in Table 2.4 and the survey scans are depicted in Figure 2.12. The XPS spectra of the RPU surfaces before and after soaking in PBS are similar. Both samples contain comparable amounts of N and S, values that are in agreement with theoretically expected values for pSBMA-grafted surfaces. In addition, trace amounts of sodium and copper were observed on the samples after the PBS soak, which can be attributed to the PBS solution, since the samples were not washed after the PBS soak to rule out any artifacts due to further chemical exposure. The high-resolution C 1s spectra are depicted in Figure 2.13. As summarized in Table 2.4, the composition of various C 1s functional groups in both samples have comparable values, with the differences well within the range of error of XPS. These observations confirm the *in vitro* stability of pSBMA-grafted RPU surfaces.

Table 2.4. Summary of the surface composition of RPU surfaces before and after soaking in PBS as obtained by survey and high-resolution C 1s scans from XPS (n=3).

Sample	Elemental composition (%)							C 1s (%)		
	C 1s	O 1s	Br 3d	N 1s	S 2p	Na 1s	Cu $2p_{3/2}$	CH	CN/ CO	COOR
RPU-HEMA-pSBMA	66.3 ± 0.9	24 ± 1.1	-	5.1 ± 0.2	4.6 ± 0.3	-	-	54.2 ± 1.1	38.5 ± 0.6	7.4 ± 0.5
RPU-HEMA-pSBMA_PBS soak	64.3 ± 1.3	22.8 ± 0.7	-	4.9 ± 0.5	4.2 ± 0.4	1.9 ± 0.4	0.5	52.8 ± 0.8	39.2 ± 0.5	8.3 ± 0.4

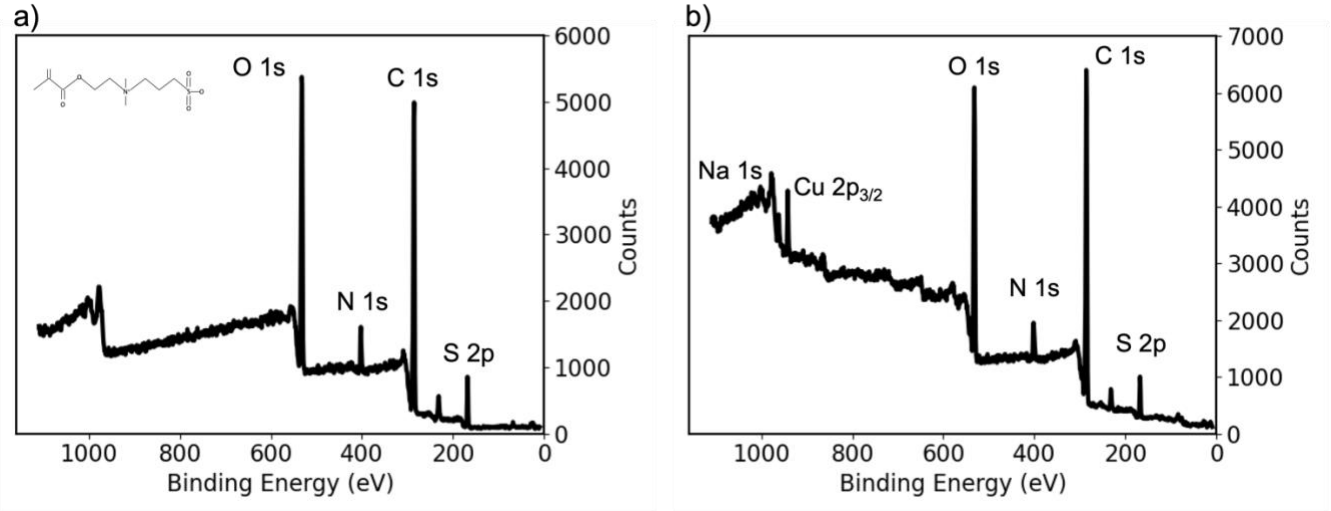

Figure 2.12. Representative XPS survey scans of pSBMA grafted RPU surfaces a) before and b) after soaking in PBS. Major peaks are labeled in each scan.

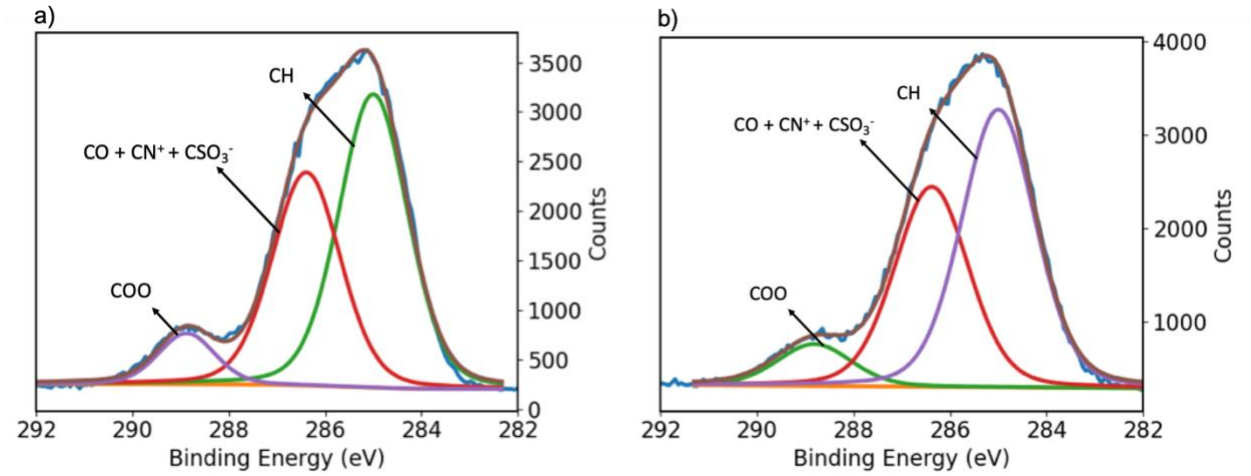

Figure 2.13. Representative high-resolution spectra of the C 1s peak on pSBMA grafted RPU surfaces a) before and b) after soaking in PBS. Fitted peaks are labeled to represent different bonding environments within each chemical structure.

In vitro stability test results for the pSBMA-coated titanium samples are summarized in Table 2.5. For this study, the prepared pSBMA grafted samples were soaked in 0.9% saline at 37ºC for 10 days, at the end of which the samples were analyzed with XPS. It can be observed that the titanium atomic % on the bare samples has reduced to 5% after soaking in saline, in contrast to 16% for an unsoaked sample. In addition, sodium and chlorine were also observed on the saline-soaked samples in trace amounts. These changes can be attributed to the deposition of a salt layer on the titanium surface after the 10-day soak, since the samples were not washed after the salt soak to avoid further processing. Similar changes can be seen for the pSBMA-grafted surfaces as well.

Table 2.5. Summary of the surface composition of titanium surfaces before and after soaking in 0.9% saline solution as obtained by survey and high-resolution C 1s scans from XPS (n=3).

Sample	Elemental composition (%)								C 1s (%)		
	C 1s	O 1s	Br 3d	N 1s	S 2p	Ti 2p	Na 1s	Cl 2p	CH	CO	COOR
Ti	34.7 ± 2.8	49.1 ± 1.6	-	-	-	16.2 ± 1.3	-	-	76.3 ± 0.3	13.9 ± 1.3	9.8 ± 1
Ti_salt soaked	72.8 ± 1.3	18.4 ± 1.2	-	2.2 ± 0.8	-	5.1 ± 0.35	1.5 ± 0.42	0.3 ± 0.3	78.1	16.2	5.8 ± 1
Ti-HEMA-pSBMA	67.9 ± 0.6	23.1 ± 0.6	-	4.7 ± 0.3	4.4 ± 0.3	-	-	-	49.4 ± 0.8	39.8 ± 0.7	10.8 ± 1
Ti-HEMA-pSBMA_salt soaked	63.8 ± 2.1	23.1 ± 0.2	-	4.8 ± 0.1	3.9 ± 0.2	-	2.5 ± 1.1	2.1 ± 1.1	48.3 ± 2	43.1 ± 1.7	8.6 ± 0.3

High-resolution C 1s scans were also collected for these samples and are depicted in Figure 2.14. As summarized in Table 2.5, the differences in composition of various C 1s functional groups are within the margin of error. High-resolution N and S spectra were also collected for Ti-HEMA-pSBMA samples, after soaking in the saline solution, and are depicted in Figure 2.15. The representative N 1s and S 2p peaks in the respective high-resolution spectra also show trends similar to the unsoaked samples, as depicted in Figure 2.9 and discussed above. These observations confirm the *in vitro* stability of titanium surfaces grafted with pSBMA.

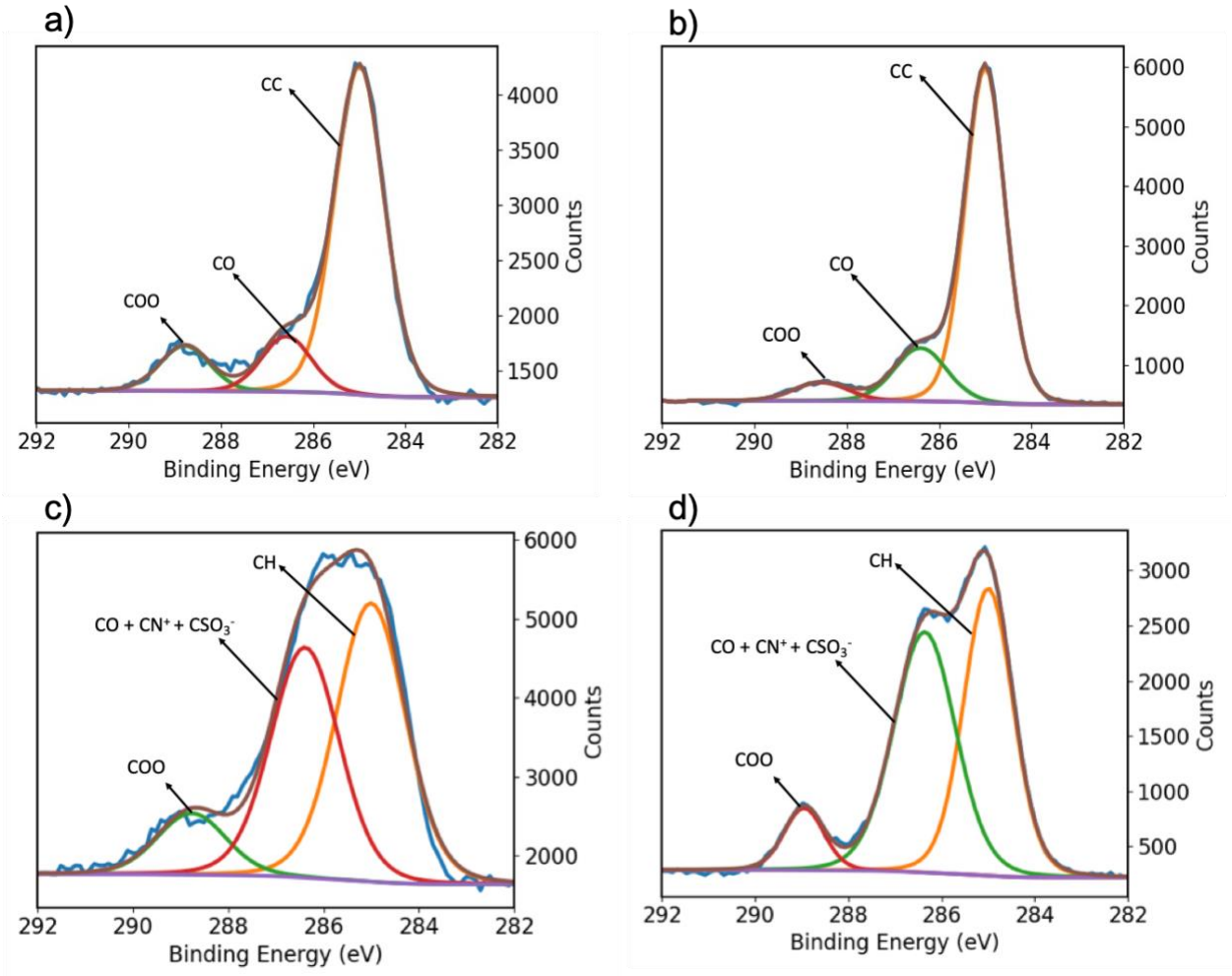

Figure 2.14. Representative high-resolution spectra of the C 1s peak on bare titanium a) before b) after soaking in 0.9 % saline solution and pSBMA grafted titanium c) before and d) after soaking in 0.9% saline solution. Fitted peaks are labeled to represent different bonding environments within each chemical structure.

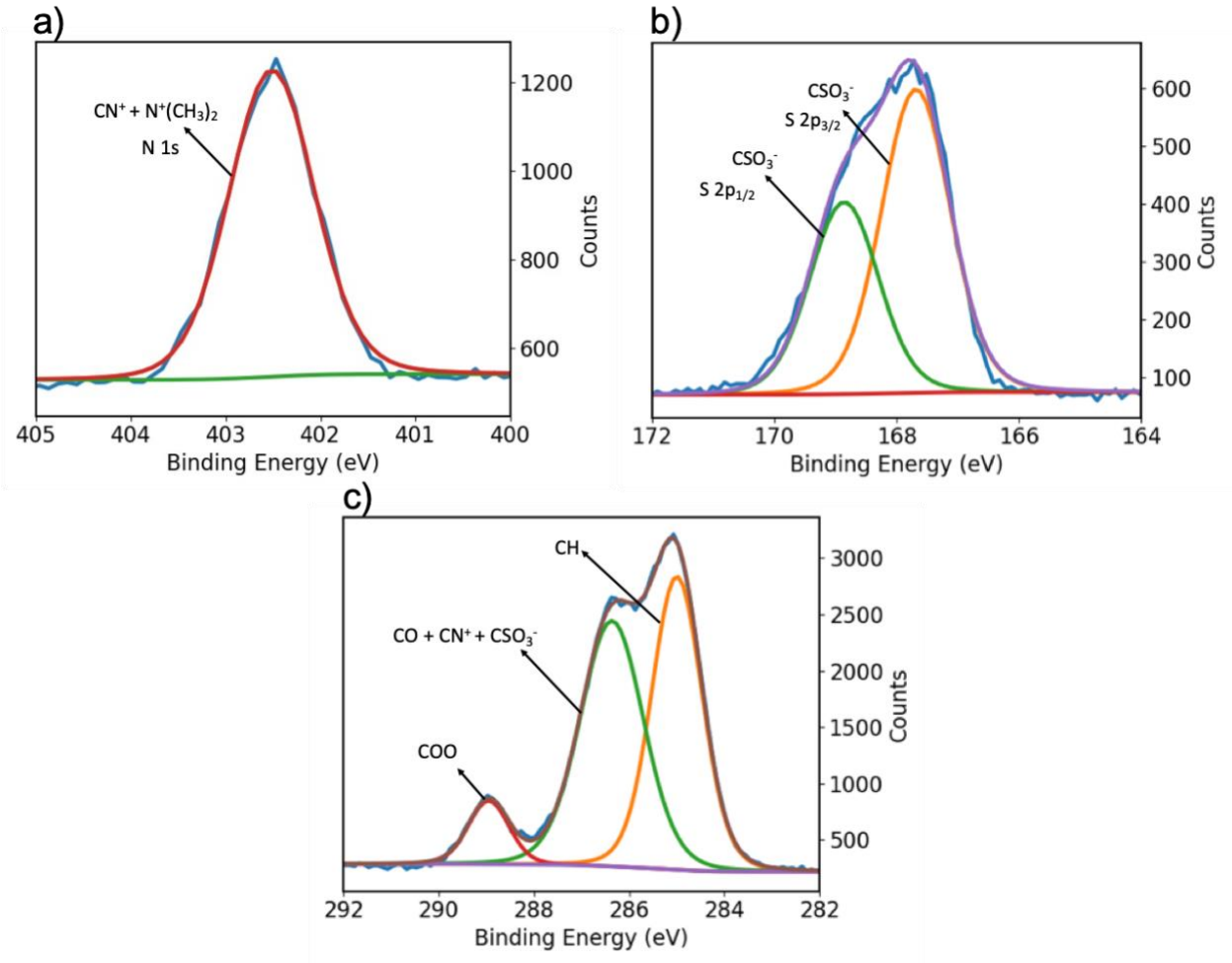

Figure 2.15. Representative high-resolution spectra of the pSBMA grafted titanium surfaces soaked in 0.9% saline solution: a) N 1s b) S 2p and c) C 1s. Fitted peaks are labeled to represent different bonding environments within each chemical structure.

After validation of the proposed protocol in terms of expected chemical composition trends, and verification of *in vitro* stability of the prepared hydrophilic coatings, the next step was the *in vivo* performance evaluation of the surface-modified implants. The *in vivo* tests in chicken model were performed at Oregon State University and are detailed in section 2.3.3.2. However, given *in vivo* studies typically involve extensive sterilization of the device before implantation in the host body, we must establish the effect of these treatments on the chemical composition and integrity of the pSBMA surfaces. This is required to prevent the pretreatment steps from potentially

confounding the *in vivo* performance analysis. In the chicken studies discussed in this work, the RPU implants were sterilized using ethylene oxide (EtO). To establish the effect on the coating structure, RPU implants were EtO-sterilized and analyzed using XPS. The composition of the bare and pSBMA coated samples, before and after EtO sterilization, is summarized in Table 2.6 and Table 2.7. The XPS survey scans and high-resolution C 1s and N 1s spectra are shown in Figure 2.16 and Figure 2.17, respectively.

The XPS results indicate some changes in the surface composition of both bare and pSBMA-grafted RPU samples after EtO sterilization. For bare RPU, a 50% increase in the atomic percentage of O 1s can be observed, while the C 1s percentage has decreased by >10% (Table 2.6). Similar changes occur in the bonding environment of C1s for bare RPU (Table 2.7). This is likely due to the interaction of the implant surface with EtO gas. The pSBMA-grafted samples exhibit smaller changes in elemental composition, but reasonable changes are observable in the N 1s bonding environment (Table 2.6 and Table 2.7). Despite these changes in the composition, the presence of significantly detectable amounts of characteristic elements and functional groups clearly indicates that the coating remains substantially intact, indicating reasonable robustness to the sterilization pretreatments.

Table 2.6. Summary of the representative surface composition results of RPU surfaces before and after EtO sterilization as obtained by survey scans from XPS.

Sample	Elemental composition (%)				
	C 1s	O 1s	Br 3d	N 1s	S 2p
RPU	83	13.9	-	3.1	-
RPU_Sterilized	74.5	23.1	-	2.4	-
RPU-HEMA-pSBMA	66.3	24	-	5.1	4.6
RPU-HEMA-pSBMA_Sterilized	68	21.1	1.2	6.6	3.1

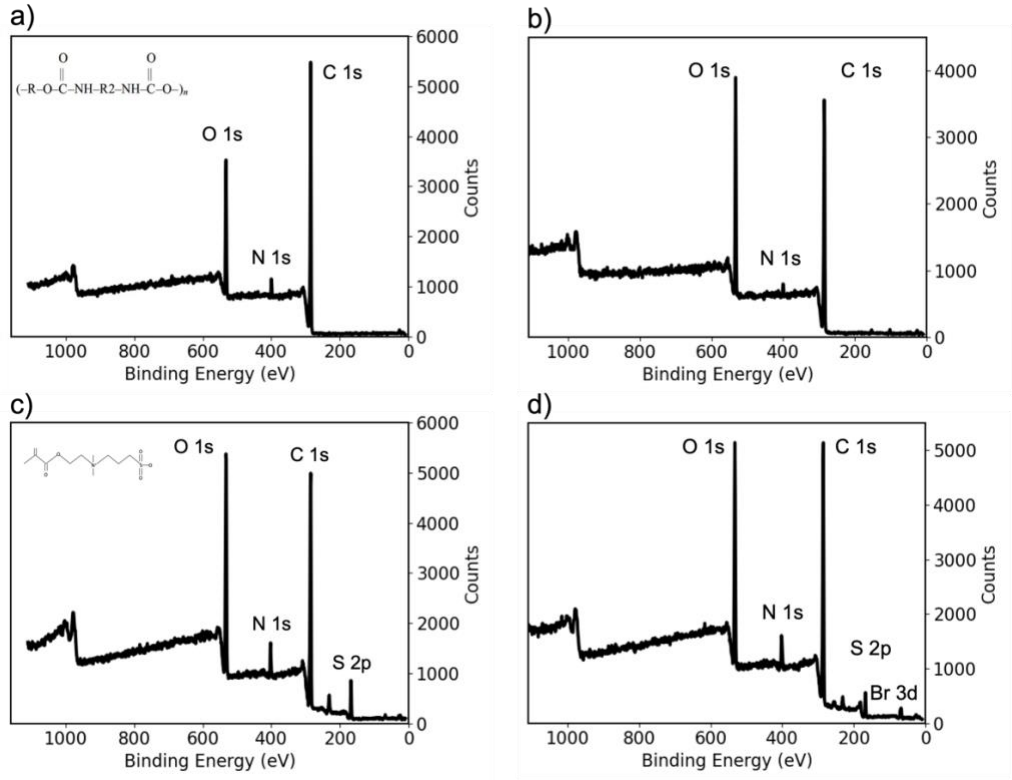

Figure 2.16. Representative XPS survey scans of bare RPU surfaces a) before and b) after EtO sterilization and of pSBMA-grafted surfaces c) before and d) after EtO sterilization. Major peaks are labeled in each scan.

Table 2.7. Summary of the representative surface composition results of RPU surfaces before and after EtO sterilization as obtained by high resolution C 1s and N 1s scans from XPS.

Sample	C 1s (%)			N 1s (%)	
	CH	CN, CO	COOR	N	N^+
RPU	62.4	31.6	6	100	-
RPU_Sterilized	58.6	33.7	7.7	100	-
RPU-HEMA-pSBMA	54.2	38.5	7.4	18.3	81.7
RPU-HEMA-pSBMA_Sterilized	51.4	41	7.6	7.4	92.6

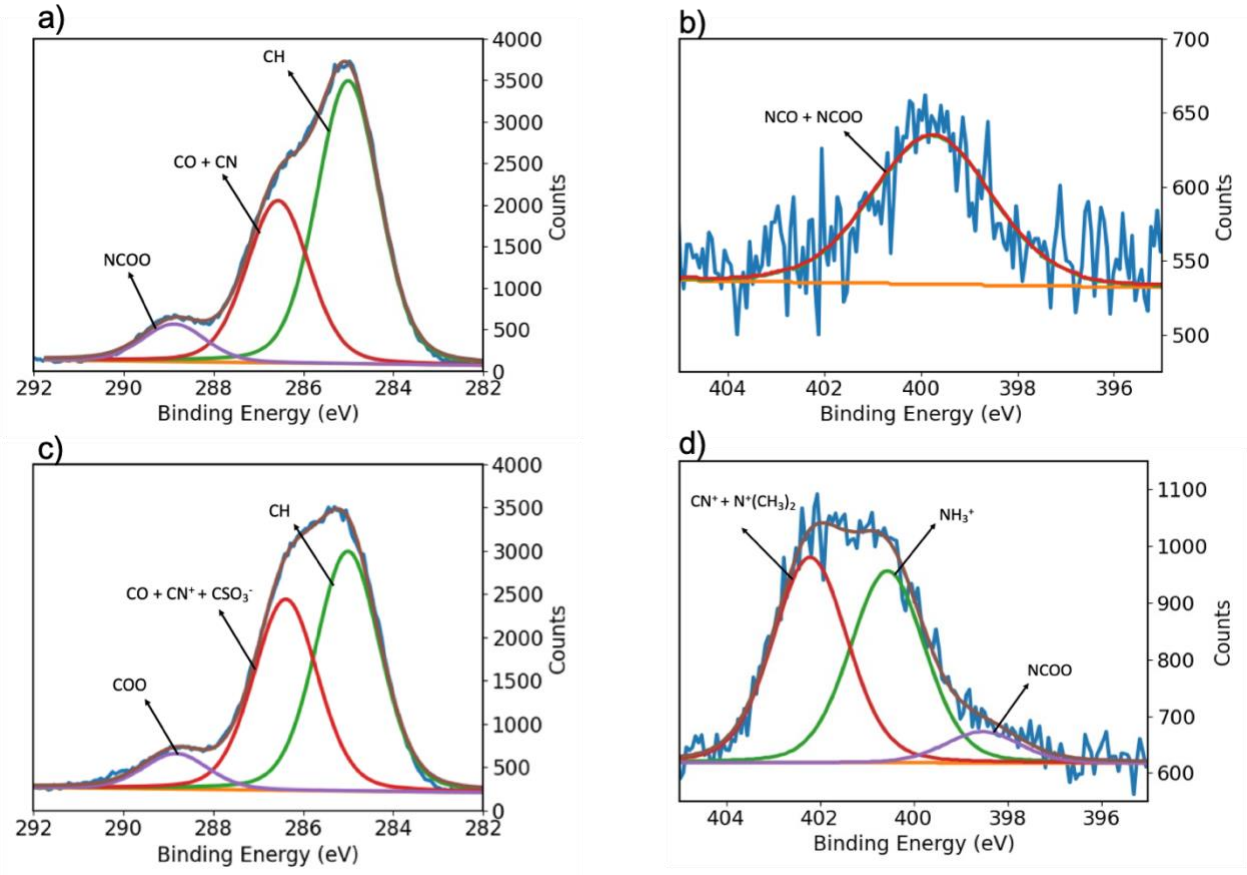

Figure 2.17. Representative high-resolution spectra of the a) C 1s peak and b) N 1s peak of bare RPU and c) C 1s peak and d) N 1s peak of pSBMA-grafted RPU after EtO sterilization. Fitted peaks are labeled to represent different bonding environments within each chemical structure.

2.4.2 SURFACE COATING THICKNESS MEASUREMENT USING PROFILOMETRY

Following the chemical confirmation of the synthesis of a stable and uniform pSBMA coating, the coating thickness was measured using a profilometer. All coating measurements were made on silicon wafer substrates since the profilometer requires a hard and flat surface. RPU is a plastic, and the 3-D printed discs contain grooves on the surface, making them unsuitable for use with the profilometer instrument. An unsuccessful attempt was also made to take these measurements on titanium. The thick and uneven oxide layer inherently present on the surface of titanium posed challenges to accurate thickness measurements on these surfaces. Silicon wafer was thus used as the substrate for these measurements.

The thickness measurements were taken after each functionalization step. The thickness of the HEMA layer reduced from 204 ± 3.4 nm to 71 ± 4.1 nm after soaking in water for 1 h. However, further soaking resulted in negligible changes in the HEMA coating thickness. This decrease can be attributed to the removal of unreacted or loosely attached HEMA monomer. After immobilizing the BIBB initiator, the measured thickness increased to 86 ± 1.8 nm, indicating the addition of the subsequent layer. Upon grafting the pSBMA coating, the thickness further increased to 116 ± 1.9 nm, indicating successful addition of the non-fouling coating on the HEMA activated surfaces. These results are summarized in Figure 2.18 and Figure 2.19.

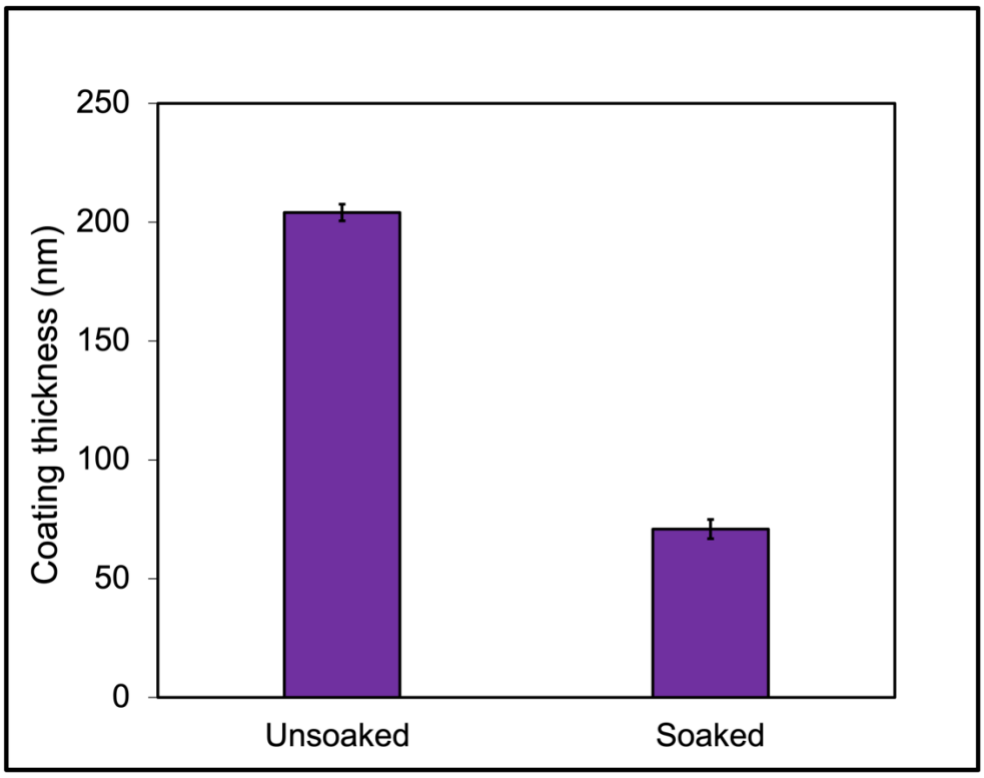

Figure 2.18. Change in thickness of the HEMA coating after soaking in water for 1 h, measured using a profilometer (n=5).

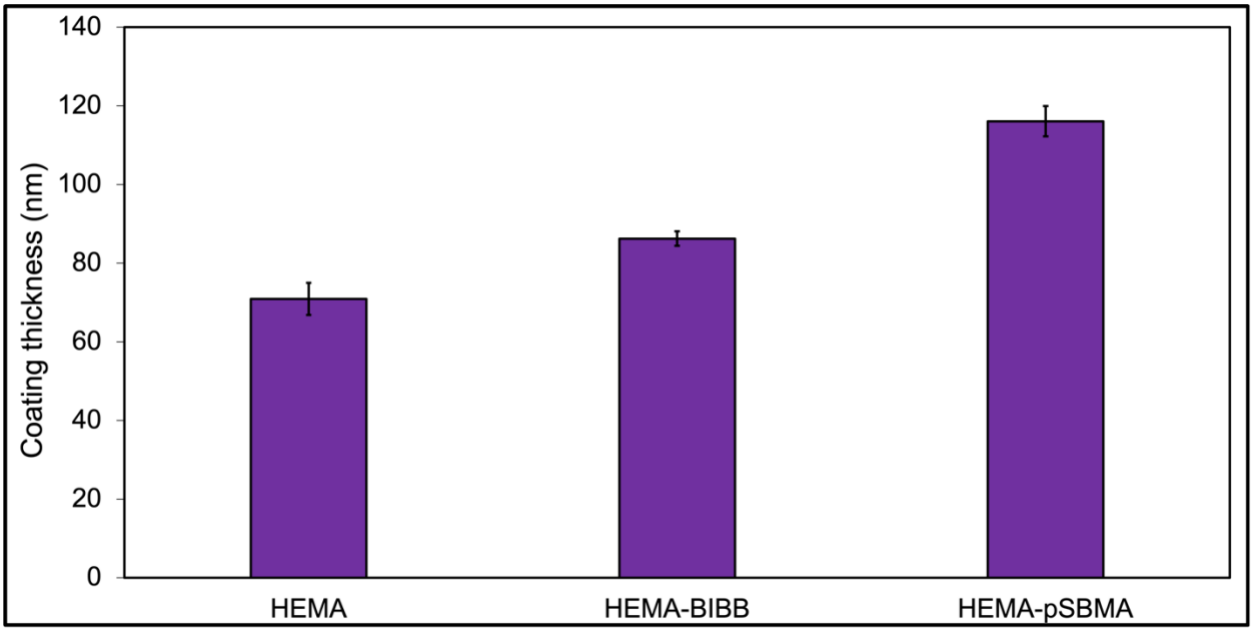

Figure 2.19. Thickness of the pSBMA coatings, measured using a profilometer (n=5).

Thickness measurements were also made after soaking the samples in 0.9% saline solution at 37°C for 10 days, to check for any delamination. As depicted in Figure 2.20, no significant changes were observed in the thickness of pSBMA coating after a 10-day soak indicating robust coatings that are resistant to delamination. These observations are in line with the surface composition results depicted in Table 2.5.

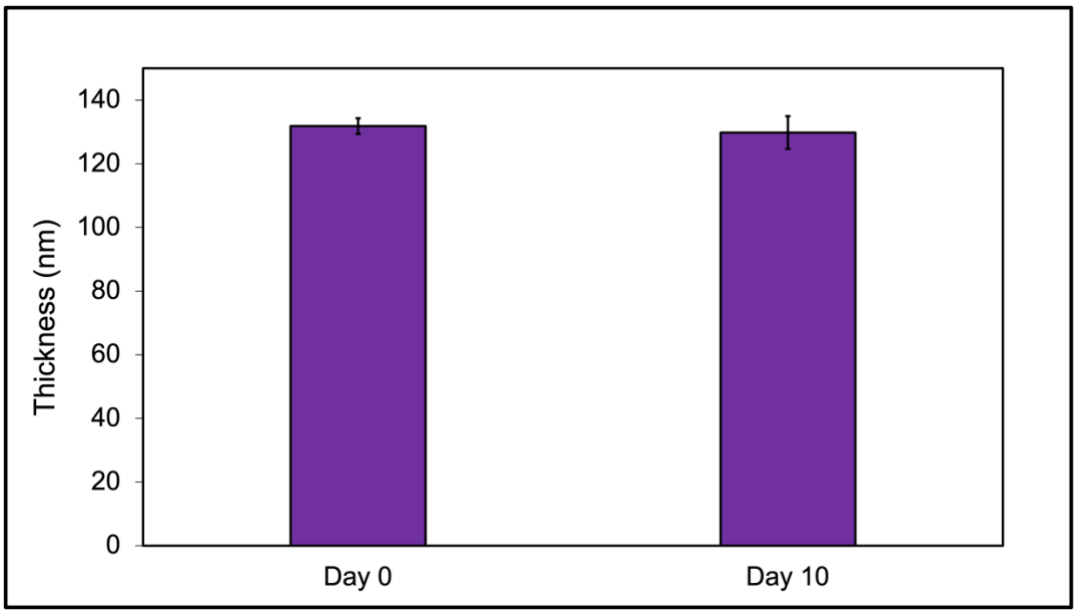

Figure 2.20. Thickness of the pSBMA coatings after a 10-day soak in 0.9% saline solution, measured using a profilometer (n=5).

2.4.3 SURFACE WETTABILITY MEASUREMENT USING GONIOMETER

The contact angle was measured on titanium substrates before and after grafting the pSBMA coating to quantify changes in surface wettability from the introduction of the hydrophilic zwitterionic species. The contact angle of bare titanium surface was measured to be 84° which reduced by 86% to 13° upon introduction of the pSBMA coating, indicating a significant increase in surface wettability (Figure 2.21). These values are in agreement with previously reported values in the literature for chemically similar surfaces.[60–62] The high contact angle of the bare titanium

surface can be attributed to the thick oxide layer inherently present on the titanium surface. The significant reduction in the contact angle after pSBMA grafting can be explained based on the super hydrophilic nature of pSBMA molecules, which tend to form strong and stable hydration layers on the surface.

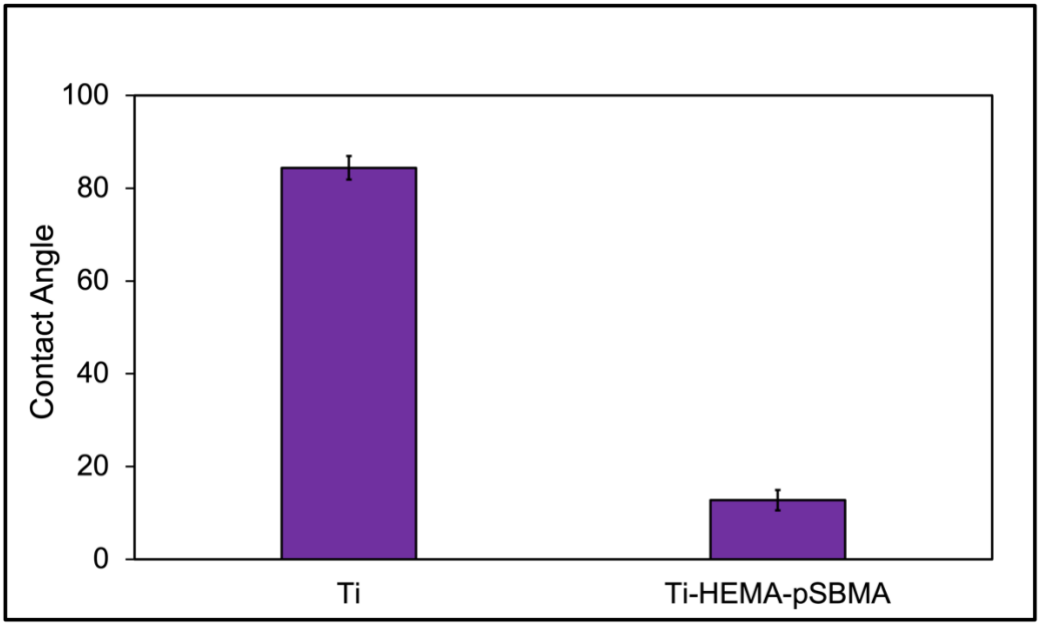

Figure 2.21. Contact angle measurements on titanium substrates, measured before and after pSBMA grafting (n=6).

2.4.4 PROTEIN ADSORPTION MEASUREMENT USING RADIOLABELED HSA

Limiting non-specific protein adsorption on the implant surfaces is arguably the most critical aspect of minimizing FBR and is the chief objective of the work described in this chapter.[32,63] For substrates grafted with pSBMA, amount of albumin adsorbed was 93% lower than that for bare substrates (Figure 2.22). This significant reduction in the amount of protein adsorbed can be explained based on the super-hydrophilic nature of SBMA molecules, due to their ability to form interfacial hydration layers *via* electrostatic interactions and hydrogen bonding. The "ice-like" structured hydration layer limits non-specific protein adsorption, thus inhibiting foreign body

response.[64,65] In addition, a 70% reduction in protein adsorption was observed for surfaces deposited with only HEMA coating. This is a reasonable observation given the hydrophilic nature of HEMA molecules and their ability to form hydration layers at the surface, although unlike pSBMA brushes this is primarily *via* hydrogen bonding.[66] The structured electrostatic forces in case of pSBMA provide a full-coverage hydration layer that is strongly adhered to the surface, further reducing the extent of protein adsorption.

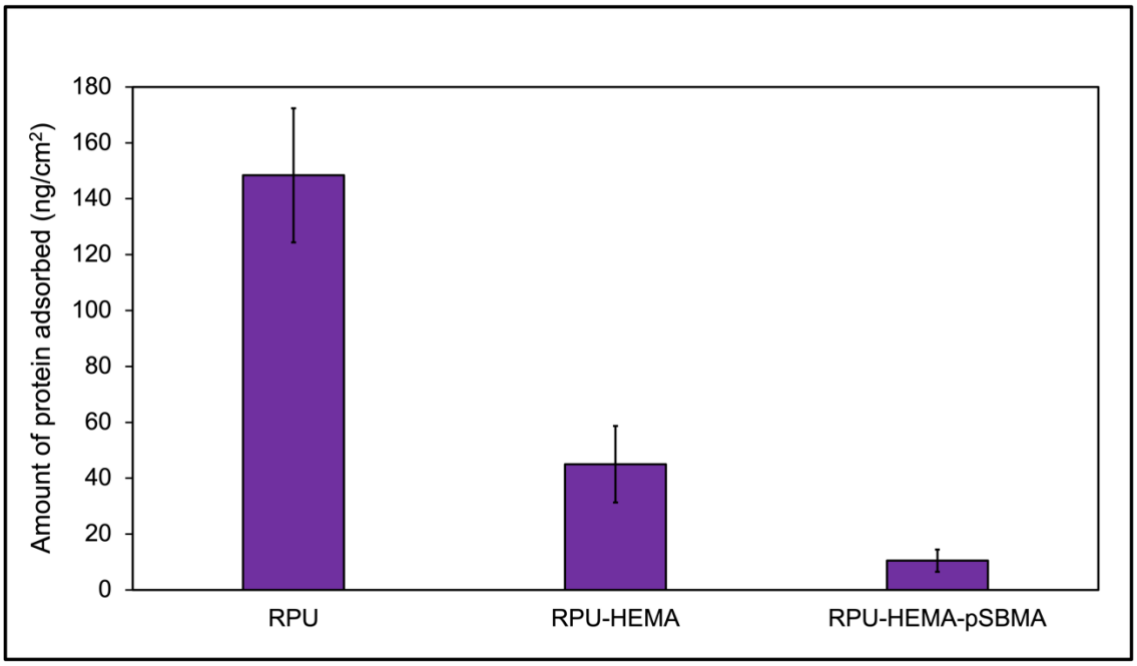

Figure 2.22. Amount of protein adsorption on various RPU surfaces, measured using radiolabeled human serum albumin (n=4).

Zhang et.al. have previously demonstrated that gold surfaces covered with similar pSBMA coatings can achieve protein adsorption values of less than 0.3 ng/cm^2 of fibrinogen.[23] Based on past studies, protein adsorption metrics below 3-5 ng/cm^2 have been demonstrated to significantly reduce FBR.[63,67] While the values reported in this work are somewhat higher than the 3-5 mg/cm^2 range, the coatings prepared in this work do dramatically limit protein attachment. For RPU

surfaces, protein adsorption values as low as 10.5 ng/cm^2 were achieved for pSBMA grafted surfaces in comparison to 148 ng/cm^2 for bare substrates. These observations suggest that with only minor optimizations of the protocols used, the pSBMA coating synthesis methods can also achieve protein adsorption metrics below the 5 ng/cm^2 threshold. These considerations thus illustrate the potential of these methodologies to develop robust and uniform surfaces that exhibit ultra-low fouling and protein resistant properties.

2.4.5 CYTOTOXICITY ASSESSMENT USING NIH-3T3 FIBROBLASTS

Cytotoxicity of the pSBMA grafted surfaces was assessed as discussed in section 2.3.2.6. Visual microscopic inspection and reactivity grading did not indicate a cytotoxic response to extracts from RPU-HEMA-pSBMA and Ti-HEMA-pSBMA samples relative to latex controls.

2.4.6 *IN VIVO* TESTING IN MICE AND CHICKENS

All the results discussed thus far indicate robustness, delamination resistance, sterilization stability, non-cytotoxicity and significant resistance to protein adsorption, indicating substantially enhanced biocompatibility compared to bare substrates. To test *in vivo* performance of the prepared coatings, RPU samples coated with pSBMA were implanted in mice and chickens based on the methods described in the section 2.3.3. Mice studies were conducted at the University of Washington and the implants were tested in the form of 8 mm RPU discs. All samples were implanted subcutaneously. The chicken studies were conducted at Oregon State University (OSU) and the devices implanted were in the form of 3-D-printed implants designed by Balasubramanian et.al.

Representative images for sections from coated and uncoated samples implanted in mice are shown in Figure 2.23. All the images were taken at 4x magnification. RPU-70 proved a difficult

material to section due to large differences between the material properties of RPU and the embedded tissue. RPU sections were found to be displaced from their actual position, creating voids observable in the images. These images are representative of a qualitative histological analysis. Due to the complexity of the biological environment and presence of artifacts, there are a number of factors that can affect the density of the capsule around the implant. The samples were evaluated based on thickness, density and coverage of the capsule around the implant or the void. Significantly reduced thickness and coverage of foreign body capsule was observed for the pSBMA coated samples in comparison to bare samples.

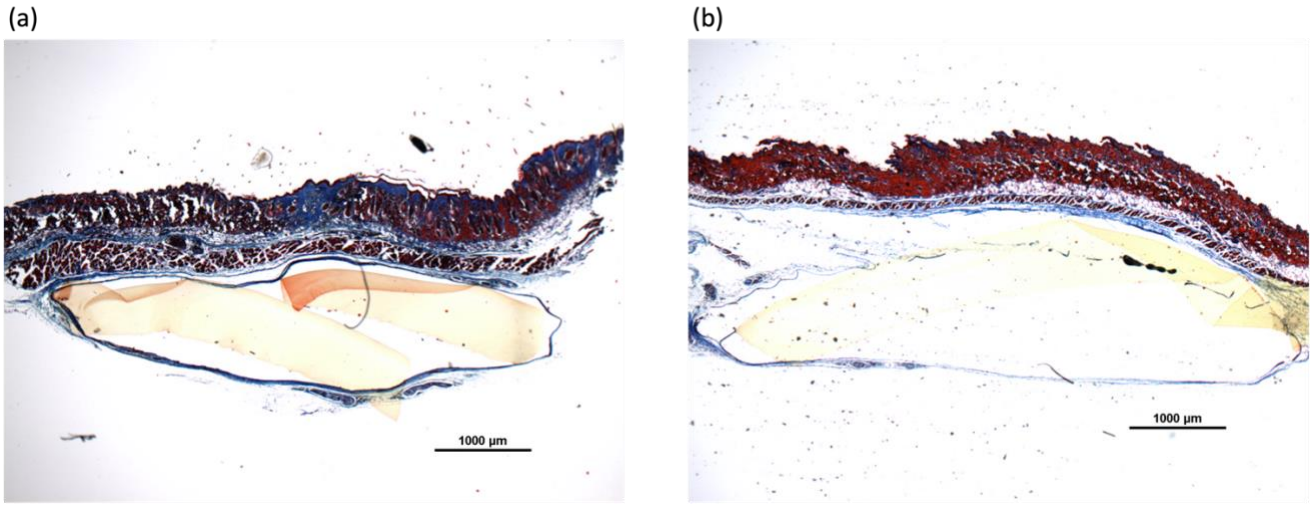

Figure 2.23. Representative images of sections from a) uncoated and b) coated RPU discs implanted in mice.

For chicken studies, all chickens were implanted for 12 weeks. Representative images of uncoated and coated samples, annotated with histopathologist notes are depicted in Figure 2.24. Severe fibrosis was observed around the tendon surrounding the device in case of uncoated devices. The histopathologist notes indicated significantly reduced fibrosis around the implants coated with pSBMA as compared to the untreated devices. It is noteworthy that little reactivity

was observed towards the implant material in contact with the surrounding tissue and tendon, indicating significantly enhanced biocompatibility of pSBMA-coated surfaces.

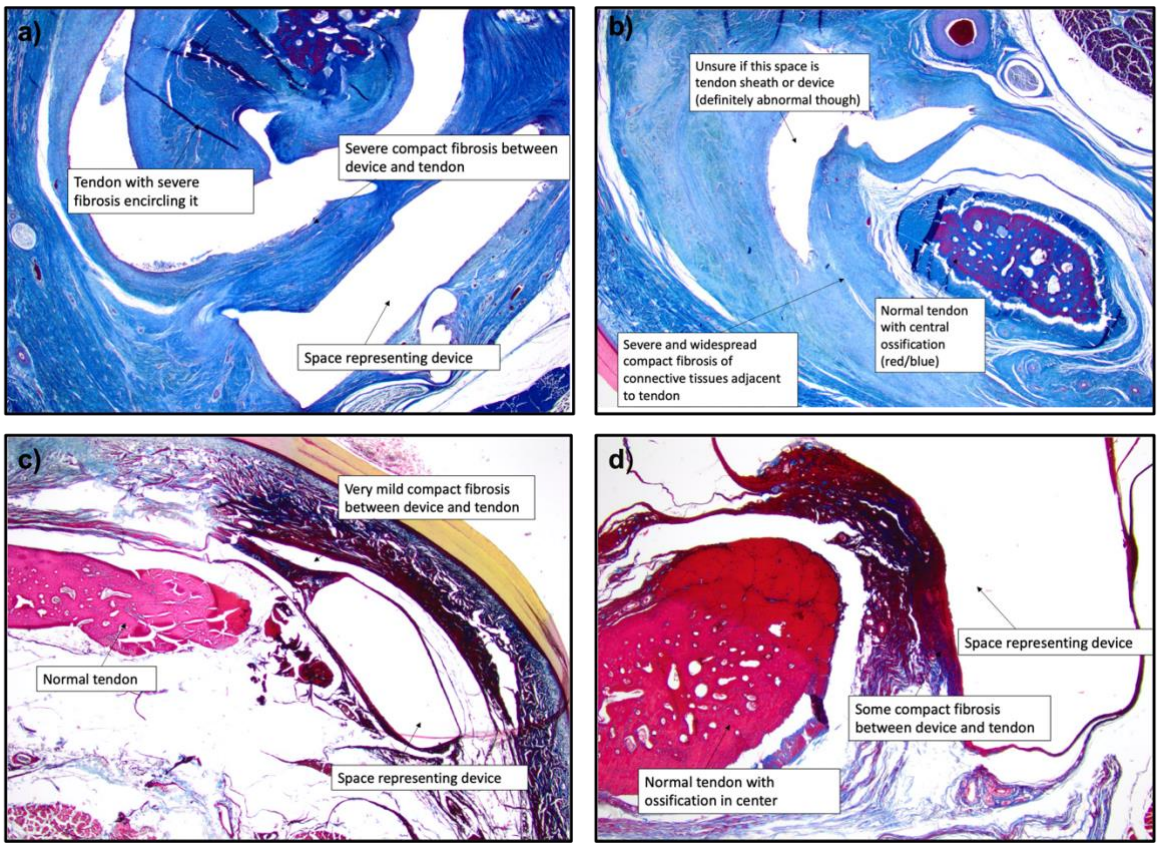

Figure 2.24. Representative images of sections of 3-D printed devices implanted in chicken feet. All sections are stained with mason's trichrome stain: a) and b) represent sections of uncoated implants and c) and d) are sections of coated implants.

2.5 SUMMARY AND CONCLUSIONS

The continued progress of the medical device industry, particularly the development of biomedical implants, greatly hinges on the development of surface modification methods that can create uniform and robust non-fouling surface coatings and improve biocompatibility of a diverse range of materials. Non-specific protein adsorption on the implant surface can initiate FBR, which eventually renders the device futile. This research thus successfully demonstrated robust and

versatile surface coating methodologies for orthopedic implants being designed by collaborators.[68,69] A variety of polymeric and metallic materials were tested for 3-D printing the implant design with high design resolution of features. The developed coating methodology was demonstrated on polymeric polyurethane (RPU) and metallic titanium implants, indicating wide applicability for implants with different surface chemistries.

To achieve the desired non-fouling surface treatments, RFGD plasma and ARGET ATRP techniques were applied and integrated in this work, with sulfobetaine methacrylate (SBMA) chosen as the candidate super-hydrophilic molecule. The combined use of these technologies resulted in uniform and delamination resistant surface coatings of pSBMA robust to vigorous chemical exposure and stable *in vitro.* The coatings are non-toxic and exhibit protein adsorption as low as 10.5 ng/cm^2 on polyurethane substrates. In addition, even the intermediate stage of RFGD plasma-deposited HEMA surfaces exhibited low fouling and non-toxic properties, resulting in a 70% reduction in protein adsorption in comparison to bare substrates. RPU implants coated with non-fouling pSBMA coatings also exhibited reasonable stability *in vivo* in mice and chicken models, indicating enhanced biocompatibility. Due to the versatility of RFGD plasma, and the ability of ARGET ATRP to be performed under ambient conditions sans any specialized equipment, we envisage this methodology to be scalable and applicable to a variety of polymeric, ceramic and metallic materials of varied surface chemistry and geometry.

Generally, the threshold protein adsorption metric for a material to be considered non-fouling is <5 ng/cm^2.[63,67] Although the protein adsorption values achieved in this work are somewhat higher, they still represent over an order-of-magnitude reduction with significant scope for further improvement with minor protocol modifications. In addition, the *in vitro* and *in vivo* results show promise. One strategy to achieve even further improvements is the tuning of coating

thickness and density. Exploring different macroinitiators and initiator immobilization methods can also result in increased initiator density, which in turn increases the grafting density of the polymer brushes, resulting in stronger hydration layers with better coverage. Another parameter to explore could be the effect of temperature on the effectiveness of the ARGET ATRP polymerization and coating stability. Using a different zwitterionic monomer such as CBMA, which are known to be more hydrophilic because of their chemical design, can also help improve results and is a logical extension of this work. The next chapter now attempts to improve the methodology by studying one of these refinements, namely alternative ARGET ATRP initiators and immobilization methods.

2.6 REFERENCES

(1) Teo, A. J. T.; Mishra, A.; Park, I.; Kim, Y. J.; Park, W. T.; Yoon, Y. J. Polymeric Biomaterials for Medical Implants and Devices. ACS Biomater Sci Eng 2016, 2 (4), 454–472. https://doi.org/10.1021/acsbiomaterials.5b00429.

(2) Sastri, V. R. Plastics in Medical Devices: Properties, Requirements, and Applications: Second Edition; 2013. https://doi.org/10.1016/C2012-0-05946-7.

(3) Williams, D. F. On the Mechanisms of Biocompatibility. Biomaterials 2008, 29 (20). https://doi.org/10.1016/j.biomaterials.2008.04.023.

(4) Bazaka, K.; Jacob, M. v. Implantable Devices: Issues and Challenges. Electronics (Switzerland). 2012. https://doi.org/10.3390/electronics2010001.

(5) Onuki, Y.; Bhardwaj, U.; Papadimitrakopoulos, F.; Burgess, D. J. A Review of the Biocompatibility of Implantable Devices: Current Challenges to Overcome Foreign Body Response. J Diabetes Sci Technol 2008, 2 (6), 1003–1015. https://doi.org/10.1177/193229680800200610.

(6) Kammula, R. G.; Morris, J. M. Considerations for the Biocompatibility Evaluation of Medical Devices. Medical Device and Diagnostic Industry 2001, 23 (5).

(7) Biological Evaluation of Medical Devices. Biomedical Safety & Standards 1996, 26 (7). https://doi.org/10.1097/00149078-199604150-00011.

(8) Zheng, S.; Bawazir, M.; Dhall, A.; Kim, H. E.; He, L.; Heo, J.; Hwang, G. Implication of Surface Properties, Bacterial Motility, and Hydrodynamic Conditions on Bacterial Surface Sensing and Their Initial Adhesion. Front Bioeng Biotechnol 2021, 9 (February), 1–22. https://doi.org/10.3389/fbioe.2021.643722.

(9) Anderson, J. M.; Rodriguez, A.; Chang, D. T. Foreign Body Reaction to Biomaterials. Seminars in Immunology. 2008. https://doi.org/10.1016/j.smim.2007.11.004.

(10) Ngo, B. K. D.; Grunlan, M. A. Protein Resistant Polymeric Biomaterials. ACS Macro Lett 2017, 6 (9), 992–1000. https://doi.org/10.1021/acsmacrolett.7b00448.

(11) Rosales-Leal, J. I.; Rodríguez-Valverde, M. A.; Mazzaglia, G.; Ramón-Torregrosa, P. J.; Díaz-Rodríguez, L.; García-Martínez, O.; Vallecillo-Capilla, M.; Ruiz, C.; Cabrerizo-Vílchez, M. A. Effect of Roughness, Wettability and Morphology of Engineered Titanium Surfaces on Osteoblast-like Cell Adhesion. Colloids Surf A Physicochem Eng Asp 2010, 365 (1–3). https://doi.org/10.1016/j.colsurfa.2009.12.017.

(12) Sin, M. C.; Sun, Y. M.; Chang, Y. Zwitterionic-Based Stainless Steel with Well-Defined Polysulfobetaine Brushes for General Bioadhesive Control. ACS Appl Mater Interfaces 2014, 6 (2). https://doi.org/10.1021/am4041256.

(13) Riveiro, A.; Soto, R.; Del Val, J.; Comesaña, R.; Boutinguiza, M.; Quintero, F.; Lusquiños, F.; Pou, J. Laser Surface Modification of Ultra-High-Molecular-Weight Polyethylene (UHMWPE) for Biomedical Applications. In Applied Surface Science; 2014; Vol. 302. https://doi.org/10.1016/j.apsusc.2014.02.130.

(14) Xia, N.; Hu, Y.; Grainger, D. W.; Castner, D. G. Functionalized Poly (Ethylene Glycol)-Grafted Polysiloxane Monolayers for Control of Protein Binding. Langmuir 2002, 18 (8), 3255–3256. https://doi.org/10.1021/la011423x.

(15) Garay, R. P. Immunogenicity of Polyethylene Glycol (PEG). Open Conf Proc J 2011, 2 (1), 104–107. https://doi.org/10.2174/2210289201102010104.

(16) Garay, R. P.; El-Gewely, R.; Armstrong, J. K.; Garratty, G.; Richette, P. Antibodies against Polyethylene Glycol in Healthy Subjects and in Patients Treated with PEG-Conjugated Agents. Expert Opin Drug Deliv 2012, 9 (11), 1319–1323. https://doi.org/10.1517/17425247.2012.720969.

(17) Thanh, T.; Thi, H.; Pilkington, E. H.; Nguyen, D. H.; Lee, J. S. The Importance of Poly (Ethylene Glycol) Alternatives for Overcoming PEG Immunogenicity in Drug. Polymers (Basel) 2020, 12 (2), 298.

(18) Chen, B. M.; Cheng, T. L.; Roffler, S. R. Polyethylene Glycol Immunogenicity: Theoretical, Clinical, and Practical Aspects of Anti-Polyethylene Glycol Antibodies. ACS Nano 2021, 15, 14022–14048. https://doi.org/10.1021/acsnano.1c05922.

(19) Yuan, J.; Chen, L.; Jiang, X.; Shen, J.; Lin, S. Chemical Graft Polymerization of Sulfobetaine Monomer on Polyurethane Surface for Reduction in Platelet Adhesion. Colloids Surf B Biointerfaces 2004, 39 (1–2), 87–94. https://doi.org/10.1016/j.colsurfb.2004.08.019.

(20) Akamatsu, K.; Noto, W.; Fukuzawa, H.; Hara, A.; Nakao, S. ichi. Grafting of Carboxybetaine Polymers to Polyethylene Membranes via Plasma Graft Polymerization to Improve Low-Fouling Properties and to Tune the Molecular Weight Cut-Off. Sep Purif Technol 2018, 204, 298–303. https://doi.org/10.1016/j.seppur.2018.05.004.

(21) Moro, T.; Takatori, Y.; Ishihara, K.; Konno, T.; Takigawa, Y.; Matsushita, T.; Chung, U. I. L.; Nakamura, K.; Kawaguchi, H. Surface Grafting of Artificial Joints with a Biocompatible Polymer for Preventing Periprosthetic Osteolysis. Nat Mater 2004, 3 (11), 829–836. https://doi.org/10.1038/nmat1233.

(22) Cao, Z.; Zhang, L.; Jiang, S. Superhydrophilic Zwitterionic Polymers Stabilize Liposomes. Langmuir 2012, 28 (31), 11625–11632. https://doi.org/10.1021/la302433a.

(23) Zhang, Z.; Chen, S.; Chang, Y.; Jiang, S. Surface Grafted Sulfobetaine Polymers via Atom Transfer Radical Polymerization as Superlow Fouling Coatings. Journal of Physical Chemistry B 2006, 110 (22), 10799–10804. https://doi.org/10.1021/jp057266i.

(24) Schlenoff, J. B. Zwitteration: Coating Surfaces with Zwitterionic Functionality to Reduce Nonspecific Adsorption. Langmuir 2014, 30 (32), 9625–9636. https://doi.org/10.1021/la500057j.

(25) Li, G.; Cheng, G.; Xue, H.; Chen, S.; Zhang, F.; Jiang, S. Ultra Low Fouling Zwitterionic Polymers with a Biomimetic Adhesive Group. Biomaterials 2008, 29 (35), 4592–4597. https://doi.org/10.1016/j.biomaterials.2008.08.021.

(26) Chen, S.; Li, L.; Zhao, C.; Zheng, J. Surface Hydration: Principles and Applications toward Low-Fouling/Nonfouling Biomaterials. Polymer (Guildf) 2010, 51 (23), 5283–5293. https://doi.org/10.1016/j.polymer.2010.08.022.

(27) Leigh, B. L.; Cheng, E.; Xu, L.; Derk, A.; Hansen, M. R.; Guymon, C. A. Antifouling Photograftable Zwitterionic Coatings on PDMS Substrates. Langmuir 2019, 35 (5), 1100–1110. https://doi.org/10.1021/acs.langmuir.8b00838.

(28) Wu, J.; Lin, W.; Wang, Z.; Chen, S. Investigation of the Hydration of Nonfouling Material Poly (Sulfobetaine Methacrylate) by Low-Field Nuclear Magnetic Resonance. Langmuir 2012, 28 (4), 2137–2144. https://doi.org/10.1021/la203827h.

(29) Leng, C.; Hung, H. C.; Sun, S.; Wang, D.; Li, Y.; Jiang, S.; Chen, Z. Probing the Surface Hydration of Nonfouling Zwitterionic and PEG Materials in Contact with Proteins. ACS Appl Mater Interfaces 2015, 7 (30), 16881–16888. https://doi.org/10.1021/acsami.5b05627.

(30) Zhang, Y.; Liu, Y.; Ren, B.; Zhang, D.; Xie, S.; Chang, Y.; Yang, J.; Wu, J.; Xu, L.; Zheng, J. Fundamentals and Applications of Zwitterionic Antifouling Polymers. J Phys D Appl Phys 2019, 52 (40), 403001. https://doi.org/10.1088/1361-6463/ab2cbc.

(31) Golabchi, A.; Wu, B.; Cao, B.; Bettinger, C. J.; Cui, X. T. Zwitterionic Polymer/Polydopamine Coating Reduce Acute Inflammatory Tissue Responses to Neural Implants. Biomaterials 2019, 225 (September), 119519. https://doi.org/10.1016/j.biomaterials.2019.119519.

(32) Zhang, L.; Cao, Z.; Bai, T.; Carr, L.; Ella-Menye, J. R.; Irvin, C.; Ratner, B. D.; Jiang, S. Zwitterionic Hydrogels Implanted in Mice Resist the Foreign-Body Reaction. Nat Biotechnol 2013, 31 (6), 553–556. https://doi.org/10.1038/nbt.2580.

(33) Sin, M. C.; Chen, S. H.; Chang, Y. Hemocompatibility of Zwitterionic Interfaces and Membranes. Polym J 2014, 46 (8), 436–443. https://doi.org/10.1038/pj.2014.46.

(34) Zhang, Z.; Finlay, J. A.; Wang, L.; Gao, Y.; Callow, J. A.; Callow, M. E.; Jiang, S. Polysulfobetaine-Grafted Surfaces as Environmentally Benign Ultralow Fouling Marine Coatings. Langmuir 2009, 25 (23), 13516–13521. https://doi.org/10.1021/la901957k.

(35) Zhang, Z.; Zhang, M.; Chen, S.; Horbett, T. A.; Ratner, B. D.; Jiang, S. Blood Compatibility of Surfaces with Superlow Protein Adsorption. Biomaterials 2008, 29 (32), 4285–4291. https://doi.org/10.1016/j.biomaterials.2008.07.039.

(36) Ding, Z.; Chen, C.; Yu, Y.; de Beer, S. Synthetic Strategies to Enhance the Long-Term Stability of Polymer Brush Coatings. J Mater Chem B 2022, 10 (14), 2430–2443. https://doi.org/10.1039/d1tb02605d.

(37) Khabibullin, A.; Mastan, E.; Matyjaszewski, K.; Zhu, S. Surface-Initiated Atom Transfer Radical Polymerization. In Controlled Radical Polymerization at and from Solid Surfaces; 2016; pp 29–76.

(38) Yu, Y. Switchable Adhesion and Friction by Stimulus Responsive Polymer Brushes, 2017.

(39) Kocak, G.; Butun, V.; Tuncer, C. PH-Responsive Polymers. Polym Chem 2017, 8, 144–176.

(40) Kim, M.; Schmitt, S. K.; Krutty, J. D.; Gopalan, P. From Self-Assembled Monolayers to Coatings: Advances in the Synthesis and Nanobio Applications of Polymer Brushes. Polymers (Basel) 2015, 7 (7), 1346–1378.

(41) He, R. X.; Zhang, M.; Tan, F.; Leung, P. H. M.; Zhao, X. Z.; Chan, H. L. W.; Yang, M.; Yan, F. Detection of Bacteria with Organic Electrochemical Transistors. J Mater Chem 2012, 22 (41), 22072–22076. https://doi.org/10.1039/c2jm33667g.

(42) Welch, M. E.; Xu, Y.; Chen, H.; Smith, N.; Tague, M. E.; Abruña, H. D.; Baird, B.; Ober, C. K. Polymer Brushes as Functional, Patterned Surfaces for Nanobiotechnology. Journal of Photopolymer Science and Technology 2012, 25 (1), 53–56.

(43) Hoffman, A. S. Ionizing Radiation and Gas Plasma (or Glow) Discharge Treatments for Preparation of Novel Polymeric Biomaterials. In Polymers in Medicine; 1984; pp 141–157. https://doi.org/10.1007/3-540-12796-8_12.

(44) Yasuda, H. Glow Discharge Polymerization. Journal of Polymer Science: Macromolecular Reviews 1981, 16, 199–293.

(45) Biederman, H.; Slavínská, D. Plasma Polymer Films and Their Future Prospects. Surf Coat Technol 2000, 125 (1–3), 371–376. https://doi.org/10.1016/S0257-8972(99)00578-2.

(46) Mecwan, M. M.; Dong, X.; Shi, G. H.; Ratner, B. D. Plasma Polymerized HMDSO Coatings For Syringes To Minimize Protein Adsorption. J Pharm Sci 2021, 110 (4), 1710–1717. https://doi.org/10.1016/j.xphs.2020.10.057.

(47) Matyjaszewski, K.; Patten, T. E.; Xia, J. Controlled/'living' Radical Polymerization. Kinetics of the Homogeneous Atom Transfer Radical Polymerization of Styrene. J Am Chem Soc 1997, 119 (4), 674–680. https://doi.org/10.1021/ja963361g.

(48) Matyjaszewski, K.; Hongchen, D.; Jakubowski, W.; Pietrasik, J.; Kusumo, A. Grafting from Surfaces for “Everyone”: ARGET ATRP in the Presence of Air. Langmuir 2007, 23 (8), 4528–4531. https://doi.org/10.1021/la063402e.

(49) Simakova, A.; Averick, S. E.; Konkolewicz, D.; Matyjaszewski, K. Aqueous ARGET ATRP. Macromolecules 2012, 45 (16), 6371–6379. https://doi.org/10.1021/ma301303b.

(50) Hong, D.; Hung, H. C.; Wu, K.; Lin, X.; Sun, F.; Zhang, P.; Liu, S.; Cook, K. E.; Jiang, S. Achieving Ultralow Fouling under Ambient Conditions via Surface-Initiated ARGET ATRP of Carboxybetaine. ACS Appl Mater Interfaces 2017, 9 (11), 9255–9259. https://doi.org/10.1021/acsami.7b01530.

(51) Kaßel, M.; Gerke, J.; Ley, A.; Vana, P. Surface Modification of Wood Flour via ARGET ATRP and Its Application as Filler in Thermoplastics. Polymers (Basel) 2018, 10 (4), 1–16. https://doi.org/10.3390/polym10040354.

(52) Löpez, G. P.; Ratner, B. D.; Tidwell, C. D.; Haycox, C. L.; Rapoza, R. J.; Horbett, T. A. Glow Discharge Plasma Deposition of Tetraethylene Glycol Dimethyl Ether for Fouling-resistant Biomaterial Surfaces. J Biomed Mater Res 1992, 26 (4), 415–439. https://doi.org/10.1002/jbm.820260402.

(53) Kim, D. D.; Takeno, M. M.; Ratner, B. D.; Horbett, T. A. Glow Discharge Plasma Deposition (GDPD) Technique for the Local Controlled Delivery of Hirudin from Biomaterials. Pharmaceutical Research. 1998, pp 783–786. https://doi.org/10.1023/A:1011987423502.

(54) Mecwan, M. M.; Taylor, M. J.; Graham, D. J.; Ratner, B. D. Highly-Reactive Haloester Surface Initiators for ARGET ATRP Readily Prepared by Radio Frequency Glow Discharge Plasma. Biointerphases 2019, 14 (4), 041006. https://doi.org/10.1116/1.5110163.

(55) Chen, J. Y.; Tian, R. L.; Leng, Y. X.; Yang, P.; Wang, J.; Wan, G. J.; Zhao, A. S.; Sun, H.; Huang, N. Effect of Ar Plasma Etching of Ti-O Film Surfaces on Biological Behavior of Endothelial Cell. Surf Coat Technol 2007, 201 (15), 6901–6905. https://doi.org/10.1016/j.surfcoat.2006.09.110.

(56) Ko, Y. C.; Ratner, B. D.; Hoffman, A. S. Characterization of Hydrophilic-Hydrophobic Polymeric Surfaces by Contact Angle Measurements. J Colloid Interface Sci 1981, 82 (1), 25–37.

(57) Horbett, T. A. Adsorption of Proteins from Plasma to a Series of Hydrophilic-Hydrophobic Copolymers. II. Compositional Analysis with the Prelabeled Protein Technique. J Biomed Mater Res 1981, 15 (5), 673–695. https://doi.org/https://doi.org/10.1002/jbm.820150506.

(58) Kuo, T. Y.; Chung, Y. C. Surface-Initiated Polymerization of Mussel-Inspired Dopamine for Hydrophilic Coatings. Mater Adv 2021, 2 (17), 5686–5690. https://doi.org/10.1039/d0ma00908c.

(59) Fontes, C. M.; Achar, R. K.; Joh, D. Y.; Ozer, I.; Bhattacharjee, S.; Hucknall, A.; Chilkoti, A. Engineering the Surface Properties of a Zwitterionic Polymer Brush to Enable the Simple Fabrication of Inkjet-Printed Point-of-Care Immunoassays. Langmuir 2019, 35 (5), 1379–1390. https://doi.org/10.1021/acs.langmuir.8b01597.

(60) Cheng, C. H.; Liu, H. C.; Lin, J. C. Surface Modification of Polyurethane Membrane with Various Hydrophilic Monomers and N-Halamine: Surface Characterization and Antimicrobial Properties Evaluation. Polymers (Basel) 2021, 13 (14). https://doi.org/10.3390/polym13142321.

(61) Dugan, J. M.; Colominas, C.; Garcia-Granada, A. A.; Claeyssens, F. Spatial Control of Neuronal Adhesion on Diamond-Like Carbon. Front Mater 2021, 8. https://doi.org/10.3389/fmats.2021.756055.

(62) Čolović, B.; Kisić, D.; Jokanović, B.; Rakočević, Z.; Nasov, I.; Petkoska, A. T.; Jokanović, V. Wetting Properties of Titanium Oxides, Oxynitrides and Nitrides Obtained by DC and Pulsed Magnetron Sputtering and Cathodic Arc Evaporation. Materials Science- Poland 2019, 37 (2), 173–181. https://doi.org/10.2478/msp-2019-0031.

(63) Lin, X.; Jain, P.; Wu, K.; Hong, D.; Hung, H. C.; O'Kelly, M. B.; Li, B.; Zhang, P.; Yuan, Z.; Jiang, S. Ultralow Fouling and Functionalizable Surface Chemistry Based on Zwitterionic Carboxybetaine Random Copolymers. Langmuir 2019, 35 (5), 1544–1551. https://doi.org/10.1021/acs.langmuir.8b02540.

(64) Vogler, E. A. Protein Adsorption in Three Dimensions. Biomaterials 2012, 33 (5), 1201–1237. https://doi.org/10.1016/j.biomaterials.2011.10.059.

(65) Sengupta, T.; Razumovsky, L.; Damodaran, S. Energetics of Protein-Interface Interactions and Its Effect on Protein Adsorption. Langmuir 1999, 15 (20), 6991–7001. https://doi.org/10.1021/la990235s.

(66) Samavedi, S.; Poindexter, L. K.; van Dyke, M.; Goldstein, A. S. Synthetic Biomaterials for Regenerative Medicine Applications. In Regenerative Medicine Applications in Organ Transplantation,; Orlando, G., Lerut, J., Soker, S., Stratta, R. J., Eds.; Academic Press, 2014; pp 81–99.

(67) Horbett, T. A. Protein Adsorption on Biomaterials. In Biomaterials: Interfacial Phenomena and Applications; Cooper et al., Ed.; American Chemical Society: Washington, D.C., 1982; pp 233–244.

(68) Le, A. J.; Casebier, J.; Mandich, J.; Larson, M. K.; Warnock, J.; Sweeney, J.; Balasubramanian, R. Evaluation of Postoperative Healing for Novel Tendon-Transfer Surgery Using an Implantable Passive Mechanism: A Pilot In Vivo Study. In Proceedings of the Veterinary Orthopedics Society; 2017.

(69) Mandich, J.; Casebier, J.; Francis, J.; Chandramouli, S.; Balasubramanian, R.; Warnock, J. Implantable Mechanisms for Orthopedic Surgery: Validation Using Biomechanical Simulation and Cadaver Study in Chicken Foot. In Proceedings of the Veterinary Orthopedics Society; 2017.

Chapter 3. GRAFTING pSBMA COATINGS USING RFGD PLASMA DEPOSITED HALOESTERS AS SOLVENT-FREE INITIATORS FOR ARGET ATRP

Abstract: Surface modification techniques involving grafting of hydrophilic polymer brush coatings using ARGET ATRP are a promising method for developing protein resistant surfaces, thus improving the biocompatibility and lifetime of medical implants. However, typical methodologies involve the covalent attachment of a halogen based macroinitiator using harsh solvents such as methylene chloride, which are incompatible with certain polymeric substrates such as polyurethanes, resulting in mechanical degradation. There thus exists scope for simplification by way of alternative initiator immobilization techniques. The radio frequency glow discharge (RFGD) plasma deposition of highly reactive haloesters has been shown to be a promising solvent-free alternative in this regard. This work thus adapts RFGD plasma-based initiator deposition methods for a simple, one-step immobilization of a bromo haloester methyl 3-bromopropionate (M3BP) on various substrates, and uses the attached bromine for initiating the subsequent ARGET ATRP reaction. Following the M3BP deposition, pSBMA brushes are synthesized on the substrate surface using ARGET ATRP. The initiator layers prepared using this approach are shown to be chemically robust and resistant to delamination, while the pSBMA coated surfaces are non-toxic, exhibit *in vitro stability,* and an 87% reduction in protein adsorption over pristine surfaces. These metrics are comparable to surfaces prepared using protocols discussed in Chapter 2. Thus, this work presents the design and investigation of a solvent-free approach, that offers one step initiator immobilization via RFGD plasma. This technique is applicable to a variety of substrate chemistries and geometries, resulting in a substantially simplified surface modification protocol amenable for use at scale.

3.1 INTRODUCTION

Chapter 2 discussed the development of a surface modification methodology to introduce hydrophilic coatings combining RFGD plasma deposition and surface-initiated polymerization using ARGET ATRP.[1–9] The substrate surface is first functionalized with hydroxyl groups by the RFGD plasma deposition of 2-hydroxyethyl methacrylate (HEMA). A bromine-based macroinitiator, α-bromoisobutyryl bromide (BIBB) is then covalently introduced on the activated substrate, which in turn serves as initiator for ARGET ATRP for grafting poly (sulfobetaine methacrylate) (pSBMA) coatings. This chapter now introduces improvements to this methodology based on the use of an alternative solvent-free initiator immobilization method. In this modified methodology, RFGD plasma is used for the deposition of highly reactive bromoesters that are then used as initiators for ARGET ATRP.[10] The concept, experimental methodology, and performance of this alternative protocol is described in detail, with the performance of the hydrophilic surfaces prepared using this method evaluated in a manner similar to Chapter 2.

Despite the versatility of the surface modification techniques discussed in previous chapters, they suffer from limitations that can have a deleterious effect on the mechanical properties of the plastic materials used in medical devices. The step involving the immobilization of BIBB requires organic solvents such as methylene chloride, which are not compatible with plastics like polyurethanes and acrylates and can cause them to swell and distort, compromising their mechanical integrity and negatively affecting device performance. Plastic based materials like polyurethanes are widely used in medical implants given their desirable mechanical properties and are also of salience in this work. This motivates the search for alternative protocols which avoid the use of harsh solvent systems. In this chapter, we discuss the use of an RFGD plasma deposited bromoester, methyl 3-bromopropionate (M3BP), as an alternative initiator for ARGET

ATRP for synthesizing non-fouling pSBMA coatings on materials with varied surface chemistries and geometries. In this work, we covalently surface-localized a polymerization initiator using RFGD plasma deposition and utilized the introduced bromine molecules to achieve uniform, tunable and delamination resistant surface functionalization.

Recently, our group developed an RFGD plasma-based technique for the deposition of highly reactive haloesters to serve as initiators for ARGET ATRP for grafting poly (hydroxyethyl methacrylate).[10] This work in turn was based on the application of previously introduced plasma deposition approaches for various applications.[11,12] Of the various candidate molecules evaluated as ARGET ATRP initiators, M3BP was found to yield abundant initiator density, as determined by XPS studies. In addition, XPS analysis also revealed negligible changes in bromine content even after sustained and vigorous wash steps.[11,12] This method allows for tunable initiator density by way of variation of the plasma process parameters. In addition, it is noteworthy that with plasma deposited M3BP as initiator, ARGET-ATRP was able to grow pHEMA brushes in only 15 min, illustrating high reactivity of the introduced bromine groups and the potential scalability for industrial applications.[10] In particular, the simplicity of the protocol is illustrated by the fact that it only a two-step process of synthesizing polymer coatings in comparison to the three-step process discussed in Chapter 2. A higher initiator density is also likely to result in improved grafting density of polymer brushes, which is a critical aspect of ensuring adequate non-fouling and lubrication properties, as discussed in detail in Chapter 1.[8,13–16]

The above considerations thus motivate the adaptation of this technique for pSBMA grafting on a wide range of substrates relevant to this work, for developing hydrophilic and protein resistant surfaces. Polyurethanes, acrylates and titanium are some of the substrates investigated herein. RFGD plasma deposition was used to first immobilize the M3BP initiator on the surface

of the substrate. This resulted in relatively uniform, delamination-resistant initiator layers. An optimized version of the ARGET ATRP protocol of Chapter 2 was then repeated for the synthesis of pSBMA brushes. The efficacy of the immobilization was evaluated by quantification of the surface bromine content using XPS and was found to agree with expectations from theory. In addition, the chemical stability of the layers was established by surface characterization before and after vigorous wash steps. The final, pSBMA-coated surfaces were evaluated based on surface characterization and protein adsorption steps similar to that of Chapter 2. The pSBMA-coated surfaces prepared using this methodology showed an 87% reduction in protein adsorption levels over bare surfaces, which is comparable to the values in Chapter 2 while providing a simplified, solvent-free alternative for initiator immobilization applicable to industrially relevant substrates. A schematic of the two-step methodology used in this study is shown in Figure 3.1.

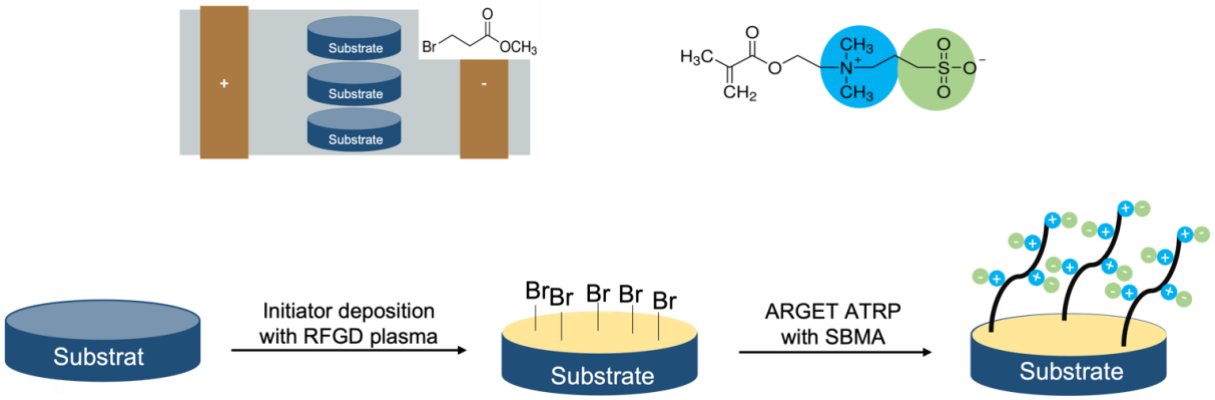

Figure 3.1. Schematic of the general coating process. In step 1, a clean, bare substrate of the given implant material is functionalized with bromine by means of RFGD plasma deposition of M3BP. In step 2, the non-fouling pSBMA coating is grafted via ARGET ATRP.

3.2 MATERIALS

Methyl 3-bromopropionate (M3BP, CAS No.: 3395-91-3), copper (II) bromide ($CuBr_2$, CAS No.: 7789-45-9), 2,2-bipyridyl (bpy, CAS No.: 366-18-7), L-ascorbic acid (CAS No.: 50-81-7), 2-(methacryloyloxy)ethyl]dimethyl-(3-sulfopropyl) ammonium hydroxide (SBMA, CAS No.: 3637-26-1), human serum albumin (HSA, ≥99%, CAS No.:70024-90-7), sodium azide (CAS No.: 26628-22-8), and sodium iodide (CAS No.: 7681-82-5) were purchased from Sigma-Aldrich and used as received. Sodium chloride (CAS No.: 7647-14-5) was purchased from EMD Millipore. Citric acid monohydrate (CAS No.: 5949-29-1) was purchased from J.T. Baker. Iodine-125 radionuclide (Specific Activity: ~17Ci/mg) was purchased from Perkin Elmer. Chromatography columns (10DG Desalting Columns, CAS No.: 7322010) were purchased from Bio-Rad. Sodium phosphate monobasic monohydrate (CAS No.:10049-21-5), and boric acid (CAS No.:10045-35-3), were purchased from Fisher Scientific. All organic solvents were also purchased from Fisher Scientific and used as received without further purification. 3D-printed 8 mm RPU-70 discs were received from Dependable Plastics (Fairfield, CA). Titanium sheets were purchased from McMaster-Carr.

3.3 EXPERIMENTAL METHODS

3.3.1 SAMPLE PREPARATION

3.3.1.1 Substrate preparation and cleaning

Titanium sheets were first cut into 0.5-inch squares. To remove any surface impurities, the samples were thoroughly washed by sonication in n-hexane, methylene chloride, acetone and methanol for 15 min each. The cycle was repeated three times. The solvents were changed after every cycle. RPU-70 discs were washed by sonicating only in n-hexane for 15 min, repeating the

cycle three times. All samples were then dried under vacuum and stored in a desiccator until further use.

3.3.1.2 Initiator immobilization using plasma deposited M3BP

A layer of M3BP was deposited on the substrates using RFGD plasma. A custom-built plasma reactor based on the design reported by Lopez et. al. was used for all plasma-based experiments in this study (Figure 3.2).[17] The plasma reactor parameters used for RPU-70 were slightly different from those used for titanium substrates. This was due to the presence of a thick oxide layer on the titanium surfaces, which can lead to easy delamination of coatings. The process parameters thus required optimization.

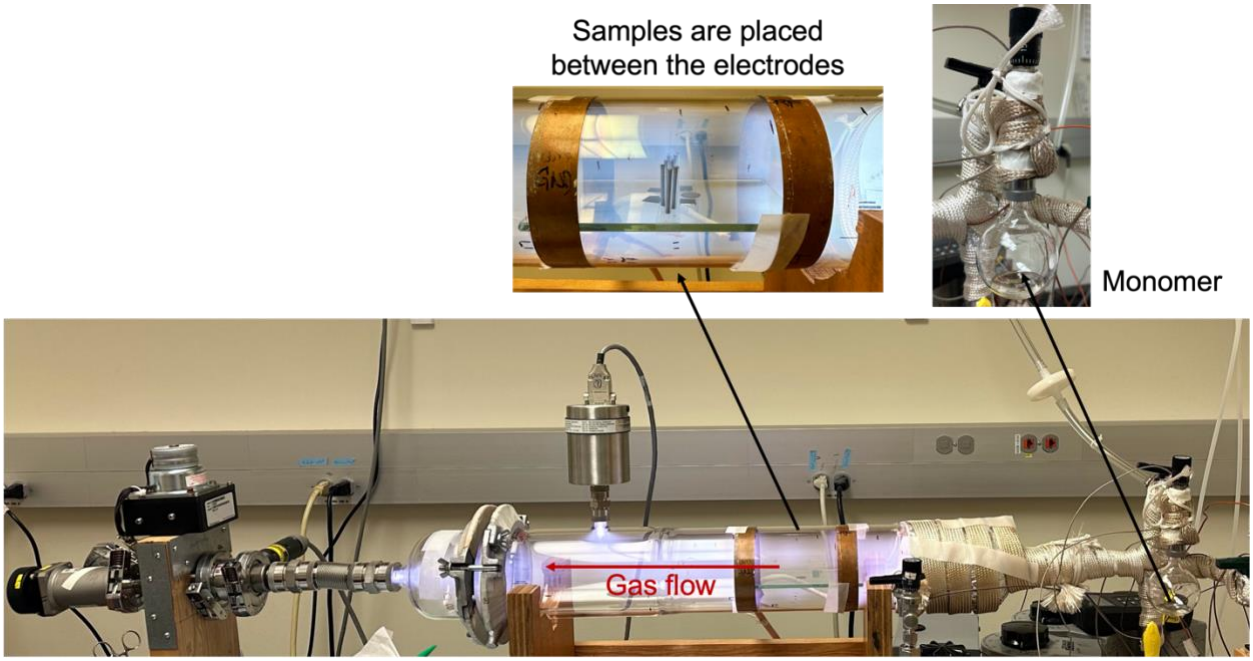

Figure 3.2. Image of the RFGD plasma setup.

After thorough cleaning, the substrates were loaded in the plasma reactor and placed between the two electrodes (powered and grounded) positioned 100 mm apart. An automatic impedance matching network and a 13.57 MHz radio frequency power source were connected to the powered electrode. A mechanical pump was used to pump down the reactor to a base pressure

of 6-7 mTorr. A cold trap cooled using liquid nitrogen was installed between the mechanical pump and the reactor to condense any waste organic vapors.

For RPU-70, after the reactor attained the base pressure, the samples were first argon-etched for 5 min at 60 W while maintaining a pressure of 250 mTorr. This was done to clean the sample surfaces of any organic impurities. After this step, methane gas was bled into the chamber and a methane layer was plasma deposited at 80 W for 5 min, while maintaining a stable pressure of 140 mTorr. The methane layer enables strong adhesion of subsequent plasma coatings to the substrates, thus preventing delamination. After the deposition of the methane layer, the reactor was again pumped down to base pressure. M3BP was then introduced into the reactor from a glass flask attached to the system through a caliper valve and allowed to reach a stable pressure of 150 mTorr. An initial adhesion layer was first formed by plasma depositing the M3BP at 100 W for 1 min, after which the power was reduced to 6 W for 4 min, while maintaining a stable pressure of 150 mTorr. The plasma generator was then turned off and the samples were quenched in the vapors for 5 min at a pressure of 150 mTorr. This was done to achieve complete utilization of the free radicals generated by the plasma. The chamber was then pumped down to base pressure and flushed with argon thrice, to prevent any organic vapors from escaping into the atmosphere upon opening the reactor. The plasma-deposited samples were retrieved under argon and stored in vacuum overnight to lessen surface chemical reactivity.

For titanium substrates, the above procedure was applied albeit with minor modifications for the durations of argon etching and adhesion layer deposition. For titanium, the samples were argon etched for 15 min at 60 W, while maintaining a stable pressure of 250 mTorr. After this, a layer of methane was plasma deposited for 8 min at 80 W and a pressure of 140 mTorr. M3BP was then plasma deposited for 2 min at 100 W and 4 min at 6 W, at a stable pressure of 150 mTorr,

and quenched for 5 min before collecting under argon. The Argon etching was performed for a longer duration for titanium to reduce the thickness of the surface oxide layer and thus minimize surface roughness.[18] The longer duration for methane deposition and M3BP deposition at 100 W is expected to aid the adhesion of subsequent layers.

Following plasma deposition, the M3BP coated samples (hereafter denoted as RPU-M3BP for RPU-70 and Ti-M3BP for titanium) were first soaked in a 1:1 mixture of methanol and water for 1 h to remove any unreacted agglomerates of bromine from the surface. The samples were then dried overnight under vacuum before further use in experiments.

3.3.1.3 Surface-initiated ARGET ATRP of SBMA

A schematic of ARGET ATRP is shown in Figure 3.3. The polymerization was performed in air under ambient conditions. Glass vials and round bottomed flasks were used for conducting these experiments. Since SBMA is a polar molecule, a mixture of water and methanol was used as the solvent mixture. To prepare the reaction mixture, a predetermined amount of SBMA (0.72 mmol) and L-ascorbic acid (0.04 mmol) were first dissolved in DI water and $CuBr_2$ (0.001 mmol) and bpy (0.005 mmol) were dissolved in methanol. The denser aqueous mixture was then added to the methanolic mixture, and the solution was degassed with nitrogen for 1 h under constant stirring. The reaction mixture was then added to glass vials containing the initiator-immobilized substrates and kept on a slow shaker at room temperature. The reaction was allowed to run for 2.5 h. Deionized water and methanol were used in a 60:40 ratio as the solvent mixture for this reaction. 3 ml of the prepared solution was used for each sample. At the end of the reaction time, the samples were removed from the vials and washed with a 1:1 mixture of methanol and water at least six times. pSBMA grafted samples (Ti-M3BP-pSBMA and RPU-M3BP-pSBMA) were then dried under vacuum and stored in a desiccator until further analysis.

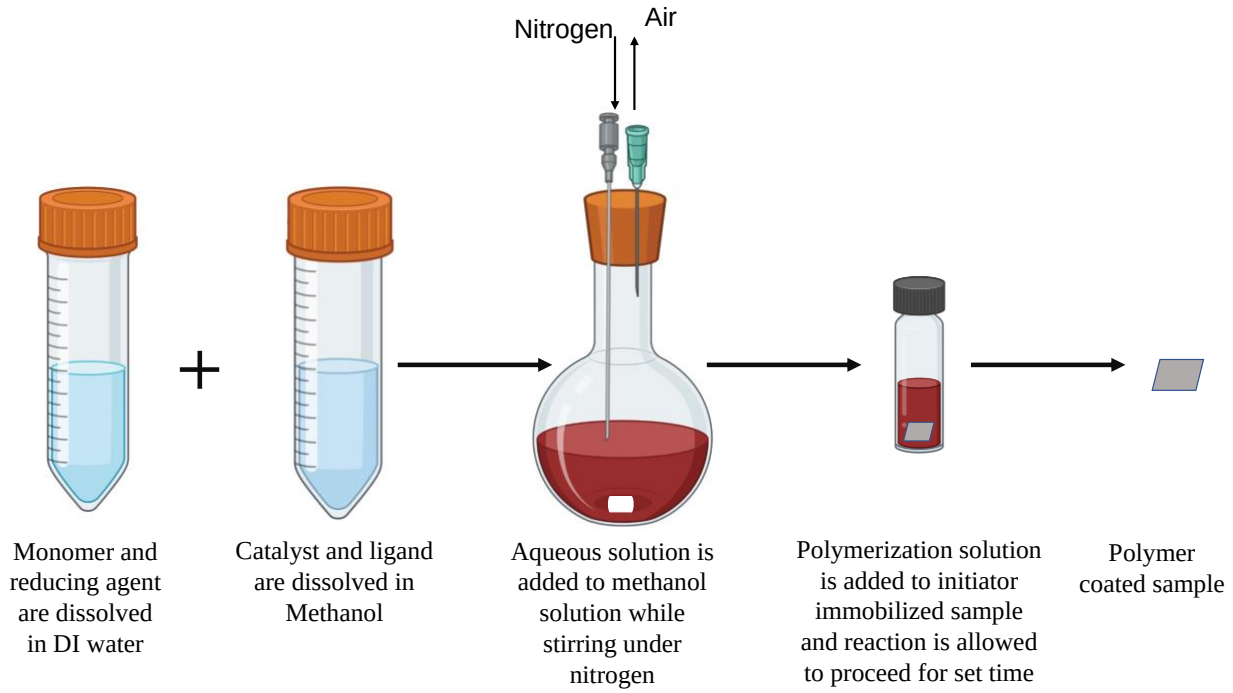

Figure 3.3. Schematic of ARGET ATRP.

3.3.2 SAMPLE ANALYSIS METHODS

3.3.2.1 X-ray photoelectron spectroscopy (XPS)

All XPS spectra were collected on a Kratos Axis-Ultra DLD spectrometer equipped with a monochromatized Al Kα X-ray source operated at 10 mA emission current and 12 kV anode potential. Charge neutralization was done using a low energy electron flood gun. The X-ray analysis area for all acquisitions was set at 700 x 300 μm. During the spectral acquisition the pressure in the analytical chamber was maintained at a value less than 5 x 10^{-9} Torr. The take-off angle, i.e. the angle between the sample normal and the input axis of the energy analyzer was set to 0°, which allows for a sampling depth of ~ 100 Å. Low resolution survey scans were obtained in the energy range of 0 to 1100 eV with a step size of 1 eV and a pass energy of 80 eV. High resolution C 1s scans were obtained from 270 to 290 eV, N 1s scans from 390 eV to 410 eV, and S 2p scans were obtained from 160 eV to 180 eV, all at a pass energy of 20 eV. The Kratos Vision

2 software was used to determine peak areas for calculating the elemental composition. Casa XPS software was used for peak fitting of the high-resolution spectra. All binding energies were referenced to the aliphatic carbon (C 1s) at 285 eV. All high-resolution spectra were fitted with a Shirley background.

3.3.2.2 Profilometry

The thickness of the prepared surface coatings was measured using a Bruker-DektakXT Profilometer with a 2 μm radius diamond stylus. Thickness was measured for dry samples using the hill-and-valley profile acquisition setting across a scratch made on the surface with a razor blade. All thickness measurements were performed on silicon substrates.

3.3.2.3 Contact angle

The contact angle of the prepared surfaces was measured in air using an NRL contact angle goniometer (Model A-100, Rame-Hart, Inc.). Water droplets were transferred to the sample surfaces using a pipette. The contact angle measurements were repeated n=6 times for each sample group.[18]

3.3.2.4 Radiolabeling of human serum albumin using ICl method

Human serum albumin (HSA) was radiolabeled by tagging with iodine-125 (I-125) using the iodine monochloride (ICl) method, based on protocols previously established in our lab and described by Horbett et.al. and Mecwan et. al.[4,19] Briefly, to tag the HSA with I-125, 1 mCi of I-125 radionuclide was added to 0.5 ml of 2X borate buffer which was immediately added to 0.5 ml of a 3:1 mixture of ICl/NaCl. This mixture was then finally added to 0.5 ml of 10 mg/ml HSA solution prepared in 1X borate. The mixture was placed on ice for 20 min for the tagging reaction to occur. The solution was then passed through a chromatography column for purification. 40

fractions of the purified tagged protein were collected, and the activity measured using a Perkin Elmer 2470 WIZARD 2 gamma counter. This was done to capture the free iodine peaks and evaluate the efficiency of iodination. The three or four fractions with the highest activity were collected, pooled together, and run through a second chromatography column for further purification followed by a second fraction collection and activity measurement for peak identification. The three or four fractions with the highest activity were again collected and pooled together. The purified radiolabeled protein was placed in a lead pig and stored at -80°C until further use.

3.3.2.5 I-125 radiolabeled HSA adsorption

Non-specific protein adsorption was measured for the coated surfaces using bare substrates as negative controls. Human serum albumin was used as the model protein for this study. A sample set of n=4 was used for all studies. First, all samples were incubated in 0.75 ml of degassed citrate phosphate buffer saline with sodium azide (cPBSzI) for 2 h at 37°C in 2 ml cups. This was performed to equilibrate the surfaces. The radiolabeled albumin was then thawed and added to a 0.6 mg/ml stock solution of HSA in degassed cPBSzI, to prepare the "hot" protein solution. The activity of the hot solution (HSA containing radiolabeled protein) was measured to obtain a minimum 2:1 signal-to-noise ratio, with an activity of ~ 100 CPM/ng. After the 2 h incubation period, 0.75 ml of the hot protein solution was added to each sample and incubated for another 2 h at 37°C. After this step, the samples were thoroughly washed with cPBSzI using a rinsing setup to remove any excess non-adsorbed protein from the sample surface. The samples were then transferred to gamma counter tubes and carefully capped. The radioactivity of each sample was measured for 1 min using the gamma counter. The amount of the protein adsorbed was measured

based on the activity of the hot protein solution and surface area of the samples and was calculated in ng/cm^2.

3.3.2.6 Cytotoxicity studies

NIH-3T3 mouse fibroblasts were used to determine the toxicity of the coated samples. RPU and titanium samples grafted with pSBMA (n=3) were first sterilized by soaking in 70% ethanol for 1 h. The sterilized samples were then aseptically placed in 12-well plates along with 1 ml of complete growth medium (DMEM-high glucose + 1 v% L-glutamine + 1 v% antibiotic/antimycotic + 10 v% fetal bovine serum) and allowed to elute for 24 h by incubation at 37°C. After elution, 1 ml eluates were transferred from the samples to another 12-well plate with the sub-confluent cultured cells. The samples were again incubated at 37°C for an additional 72 h and removed for microscopic examination at 24, 48 and 72 h time points. The well plates were periodically swirled during the incubation period. Blank wells of a tissue culture polystyrene (TCPS) plate incubated in normal media were used as negative control while latex was used as positive control. The cells were observed for visible signs of toxicity as indicated by changes in cell morphology by way of comparison with the negative control cells. The samples were rated on a reactivity grade from 0 to 4 using guidelines developed by the US Pharmacopeia (USP) or ISO 10993-5, with 0 denoting no reactivity and 4 indicating severe reactivity.

3.4 RESULTS AND DISCUSSION

This section now analyzes the proposed protocol for grafting of zwitterionic pSBMA coatings incorporating solvent-free RFGD plasma deposition of reactive bromoesters as initiator for ARGET ATRP. The surfaces were first deposited with a layer of M3BP using RFGD plasma. The attached bromine from M3BP was then used for the synthesis of the pSBMA coatings using

ARGET ATRP. M3BP was chosen as the haloester for this study given the successful application of plasma deposited M3BP for grafting poly (hydroxyethyl methacrylate) coatings on glass surfaces in recent studies from our lab.[10] A schematic of this methodology is shown in Figure 3.1. For the evaluation of this functionalization approach, 3-D printed acrylate was also initially tested as a candidate implant material. However, as with polypropylene in Chapter 2, it was superseded in favor of RPU with its improved mechanical properties and 3-D printability. Titanium substrates were also investigated as in Chapter 2 due to their wide use and the relative ease of obtaining regulatory approvals for Ti-based devices. The protein adsorption results for acrylate-based substrates are summarized in Appendix B. The results for RPU and titanium substrates are now discussed.

3.4.1 SURFACE CHARACTERIZATION USING XPS

To begin with, a layer of M3BP was plasma deposited on the substrates to introduce bromine molecules on the surface (RPU-M3BP, Ti-M3BP). The introduced bromine was used as initiator for ARGET ATRP for grafting pSBMA coatings (RPU-M3BP-pSBMA, Ti-M3BP-pSBMA). A stable and dense layer of initiator is crucial for grafting a thick and stable layer of polymer brushes given the strong dependence of grafting density and robustness on initiator density and stability.[8,16] XPS was used to analyze the surface composition after each modification step to verify the success of surface modification. Most importantly, the stability of the deposited M3BP layer was first confirmed. M3BP coated samples were soaked in a 1:1 mixture of methanol and water for 1 h. The solution was refreshed every 20 min. Surface composition of the samples was measured using XPS before and after the soaking step. The atomic compositions of M3BP coated surfaces before and after the wash are summarized in Table 3.1.

Table 3.1. Summary of the surface composition of M3BP coated surfaces before and after soaking in methanol water solution, as obtained by survey scans from XPS (n=3).

Sample	Elemental composition (%)		
	C 1s	O 1s	Br 3d
RPU-M3BP_unsoaked	59.6 ± 0.3	11 ± 0.4	29.4 ± 0.2
RPU-M3BP_soaked	70.9 ± 1	12 ± 0.4	17.1 ± 1.4
Ti-M3BP_unsoaked	61.7 ± 0.6	7.4 ± 0.2	31 ± 0.9
Ti-M3BP_soaked	71.7 ± 1	12.6 ± 1	15.6 ± 0.3

The amount of bromine reduces by approximately 42% for RPU and 55% for titanium samples after soaking in the methanol-water mixture. This decrease in bromine content can be attributed to the weakly bound polybromine agglomerates that get washed away upon soaking.[10] No further decrease was observed in the bromine concentration upon further washing, indicating a stable and delamination resistant M3BP layer. Even after the removal of loosely bound bromines, >14% bromine was observed on both substrates, values comparable to the 14.3% bromine concentration theoretically expected from the M3BP molecular structure and reaction stoichiometry. High resolution C 1s spectra were also collected for titanium samples to gain further insight into the bonding environment of the plasma deposited M3BP (Figure 3.4). The observed contributions of the chemical states of carbon and bromine were similar to values previously reported in literature.[10] As depicted in Figure 3.4 the C 1s spectra was fitted with three peaks corresponding to the three bonding environments for carbon. It can be observed that nearly 43%

of the total signal comes from the overlapping peaks of CO and CBr (286.5 eV), indicating that the plasma deposited M3BP coatings are rich in CBr_x species.

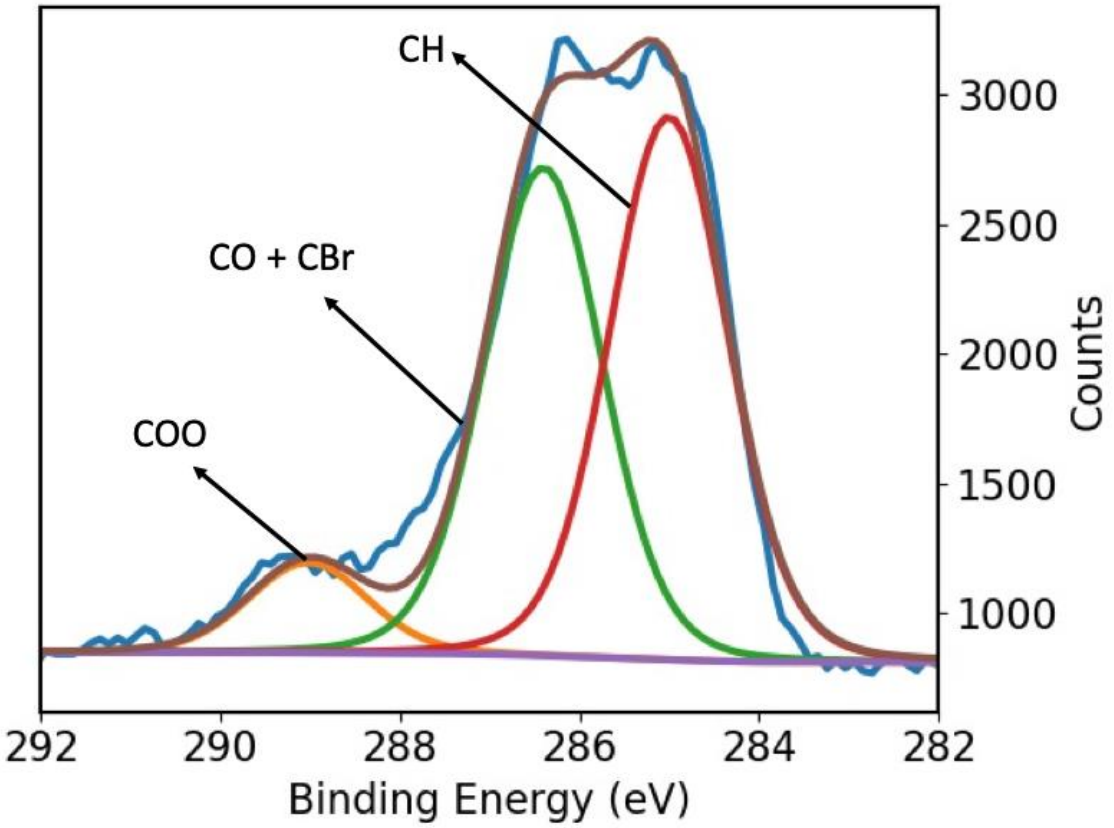

Figure 3.4. Representative high-resolution spectrum of the C1s peak on M3BP coated titanium surface. Fitted peaks are labeled to represent different bonding environments within each chemical structure.

Following the successful confirmation of a stable M3BP layer, a non-fouling pSBMA coating was synthesized on the substrates using ARGET ATRP using procedures described in section 3.3.1.3. The atomic compositions of various surfaces as measured before and after surface functionalization are summarized in Table 3.2 and Table 3.3. XPS survey scans are depicted in Figure 3.5 and Figure 3.6. For clean bare RPU, only carbon (C), oxygen (O) and nitrogen (N) were observed on the surface, as expected for a clean polyurethane surface. After the introduction of M3BP, clear signals are observed for C, O, and bromine (Br) species. For titanium, only C, O and

Ti were observed on the surface of a clean bare titanium sample. After the introduction of M3BP, the titanium was no longer observed and high amounts of bromine was observed on the surface in addition to C and O, as expected for M3BP. No nitrogen or sulfur species were observed after M3BP deposition on either of the substrates.

The pSBMA surfaces synthesized using ARGET ATRP are now studied. A surface grafted with a uniform pSBMA coating should contain 5.6 % (atom percentage) of both N and S as stoichiometrically expected from the structure of SBMA. The close agreement of the values measured for pSBMA-grafted RPU and titanium surfaces with the theoretical values confirm the successful grafting of pSBMA brush coatings. In addition, no more bromine was detected on titanium surfaces after pSBMA grafting, suggesting complete utilization of the bromine species and the presence of a dense pSBMA coating with thickness greater than 100 Å, overlaying the unreacted surface bromine from the initiator. Trace amounts of bromine can be observed on the RPU-M3BP-pSBMA sample, but these values are well within the margin of error for XPS measurements. Additionally, the absence of any unexpected contamination further confirms the presence and quality of the pSBMA coating on the surfaces.

Table 3.2. Summary of the surface composition of bare and functionalized RPU surfaces as obtained by survey scans from XPS (n=3).

Sample	Elemental composition (%)				
	C 1s	O 1s	Br 3d	N 1s	S 2p
RPU	83 ± 0.5	13.9 ± 0.4	-	3.1 ± 0.2	-
RPU-M3BP	70.9 ± 1	12 ± 0.4	17.2 ± 1.4	-	-
RPU-M3BP-pSBMA	64.1 ± 1.3	25.9 ± 1.2	0.5 ± 0.2	5 ± 0.3	4.5 ± 0.2

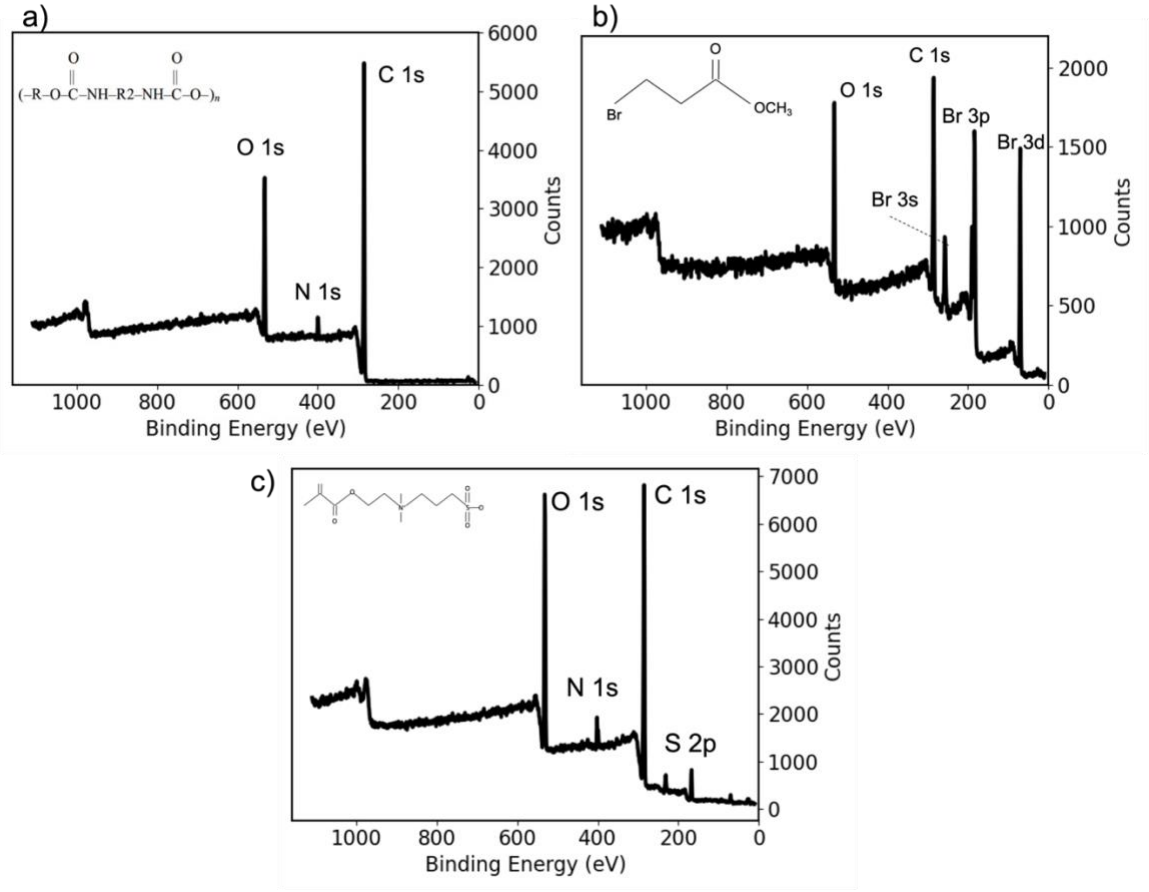

Figure 3.5. Representative XPS survey scans of RPU surfaces before and after functionalization. a) Bare RPU b) RPU-M3BP c) RPU-M3BP-pSBMA. Major peaks are labeled in each scan.

Table 3.3. Summary of the surface composition of bare and functionalized titanium surfaces as obtained by survey scans from XPS (n=3).

Sample	Elemental composition (%)					
	C 1s	O 1s	Br 3d	N 1s	S 2p	Ti 2p
Ti	34.7 ± 2.8	49.1 ± 1.6	-	-	-	16.2 ± 1.3
Ti-M3BP	71.7 ± 1	12.6 ± 1	15.6 ± 0.3	-	-	-
Ti-M3BP-pSBMA	66.5 ± 0.8	23.6 ± 0.5	-	5.9 ± 0.4	4.2 ± 0.1	-

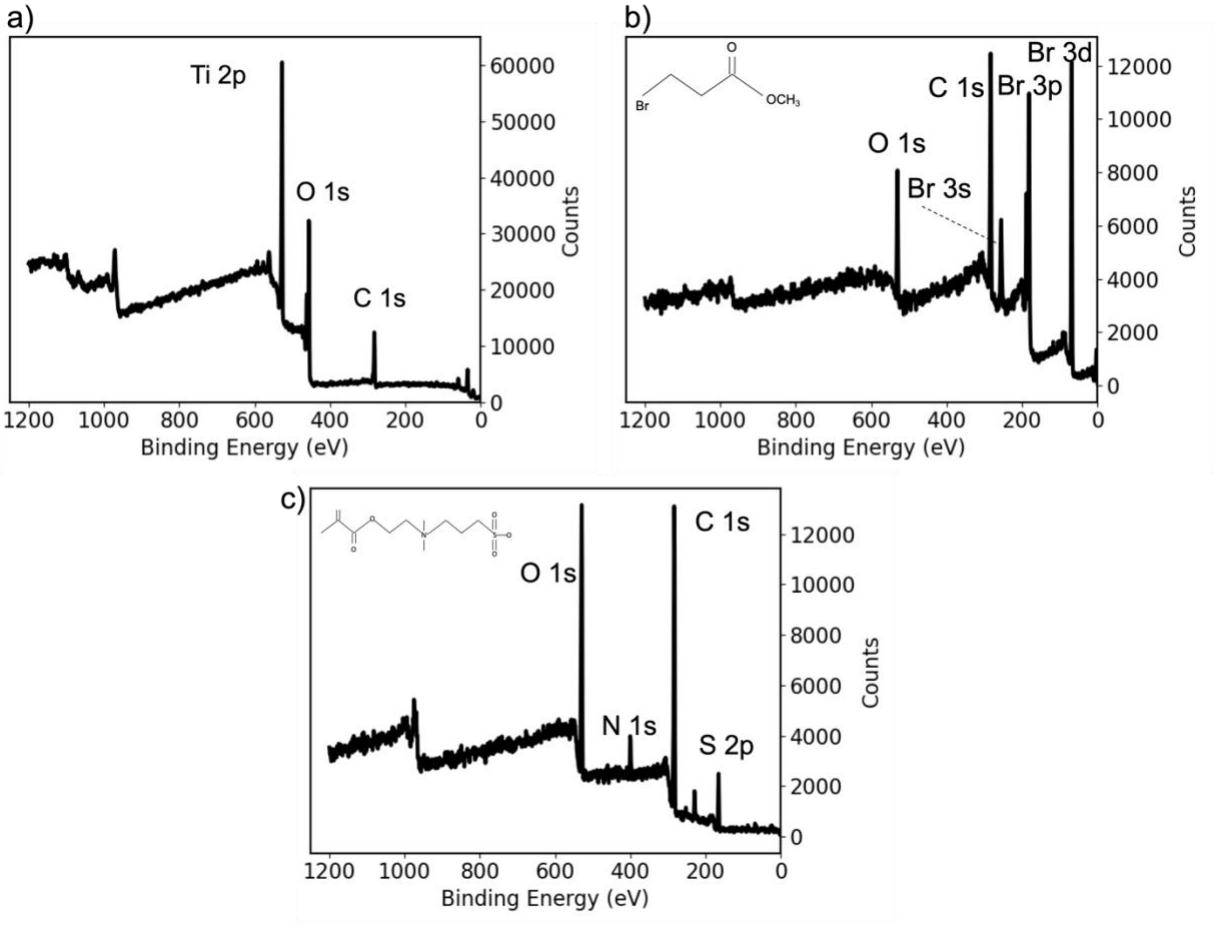

Figure 3.6. Representative XPS survey scans of RPU surfaces before and after functionalization. a) Bare RPU b) RPU-M3BP c) RPU-M3BP-pSBMA. Major peaks are labeled in each scan.

High resolution C 1s spectra for bare and functionalized RPU and titanium surfaces are now discussed. Characteristic shifts can be observed in carbon peaks for all samples, based on the chemical structure of the coating compound. The contributions of each chemical state of carbon on various titanium surfaces are summarized in Table 3.4. The shape and characteristics of high-resolution C 1s spectra of RPU and titanium surfaces before and after surface treatments are depicted in Figure 3.7 and Figure 3.8 respectively.

Table 3.4. Summary of the surface composition of bare and functionalized titanium surfaces as obtained by high-resolution C 1s scans from XPS (n=3).

Sample	**C 1s (%)**		
	CH	**CO**	**COOR**
Ti	76.3 ± 0.3	13.9 ± 1.3	9.8 ± 1
Ti-M3BP	49.2 ± 1	43.1 ± 0.8	8.2 ± 0.2
Ti-M3BP-pSBMA	53.4 ± 0.7	37.6 ± 0.3	9.5 ± 0.2

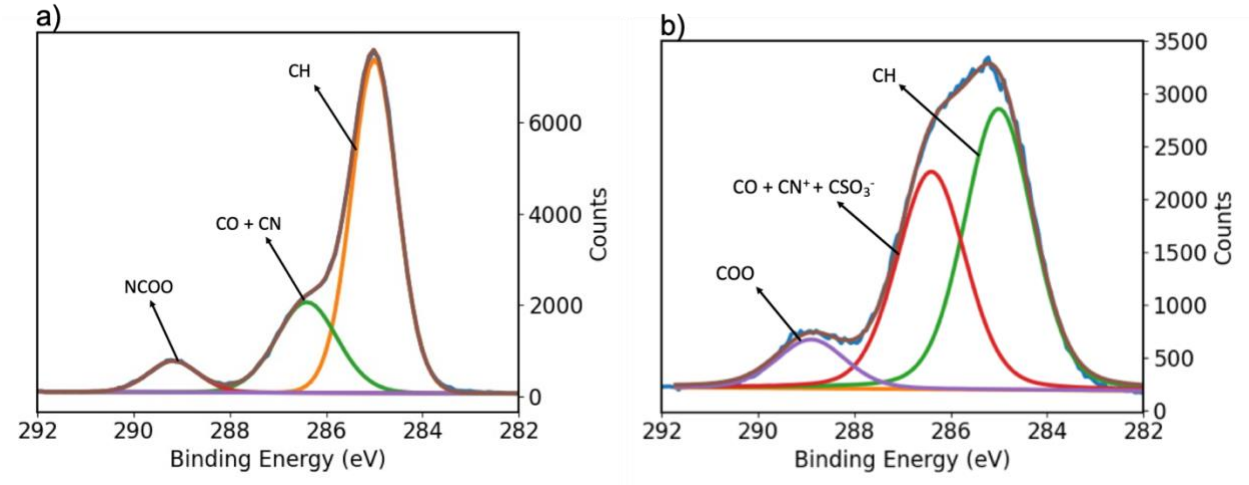

Figure 3.7. Representative high-resolution spectra of the C1s peak on various RPU surfaces. a) Bare RPU and b) RPU-M3BP-pSBMA. Fitted peaks are labeled to represent different bonding environments within each chemical structure.

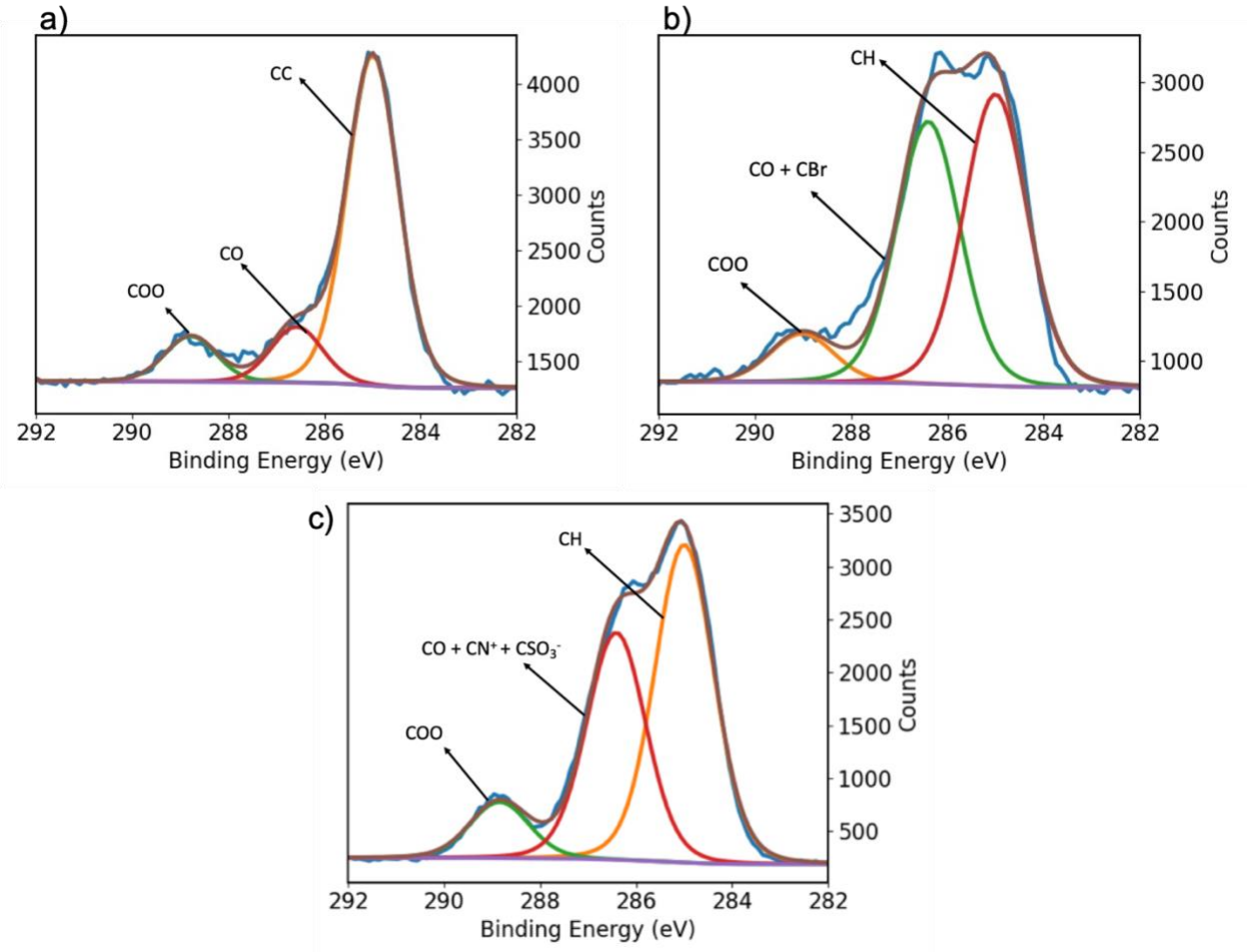

Figure 3.8. Representative high-resolution spectra of the C1s peak on various titanium surfaces. a) Bare titanium, b) Ti-M3BP and c) Ti M3BP-pSBMA. Fitted peaks are labeled to represent different bonding environments within each chemical structure.

All spectra were fitted with three peaks with constrained widths, each corresponding to different chemical states of carbon based on the chemistry of the surface coating. For bare surfaces, C-H or C-C was fitted at 285 eV, CO and CBr at 286.5 eV, and COO was fitted at 289 eV. For M3BP-immobilized surfaces, the peak at 286.5 eV represents overlapping CO and C-Br peaks. For pSBMA grafted surfaces, the peak at 286.5 eV represents an overlap of CO, CN^+, and CSO_3^-, confirming the presence of pSBMA on the surface. N 1s and S 2p high resolution spectra were also collected and analyzed for pSBMA-grafted titanium (Figure 3.9). A single peak was observed

in the nitrogen spectrum at around 400 eV. This peak could be assigned to the quarternary amine groups present in pSBMA. Similarly, 2 peaks, S $2p_{3/2}$ at 167.5 eV and S $2p_{1/2}$ at 168.5 eV were observed in the sulfur spectrum. Both the peaks represent the same bonding environment in the 2p orbital and can be assigned to the negatively charged sulfonate group present in the pSBMA molecule.[20,21] The composition of the chemical states of carbon, bromine, nitrogen and sulfur for bare and functionalized titanium surfaces are summarized in Table 3.5.

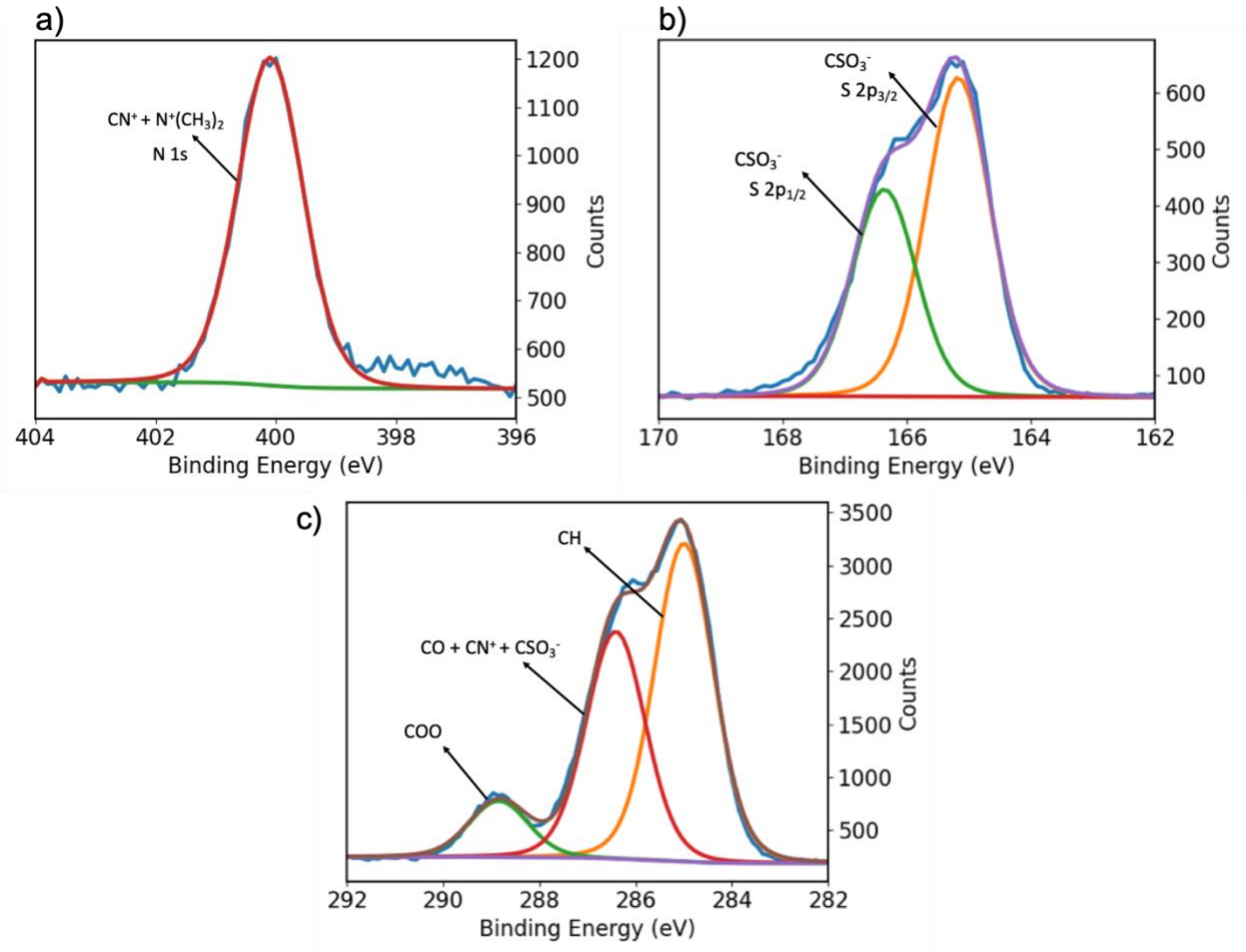

Figure 3.9. Representative high-resolution spectra of the pSBMA grafted titanium surface a) N 1s b) S 2p and c) C 1s. Fitted peaks are labeled to represent different bonding environments within each chemical structure.

Table 3.5. Summary of the surface composition of bare and functionalized titanium surfaces as obtained by high-resolution C 1s, N 1s and S 2p scans from XPS (n=3).

Sample	C 1s (%)			N 1s (%)		S 2p	
	CH	CO	COOR	N	N^+	S $2p_{3/2}$	S $2p_{1/2}$
Ti	76.3 ± 0.3	13.9 ± 1.3	9.8 ± 1	-	-	-	-
Ti-M3BP	49 ± 1	43 ± 0.8	8 ± 0.2	-	-	-	-
Ti-M3BP-pSBMA	53.4 ± 0.7	37.6 ± 0.3	9.5 ± 0.2	-	100	62.0 ± 1.9	37.7 ± 2.3

These observations further confirm the successful grafting of a uniform zwitterionic pSBMA coating on the substrate surfaces. After establishing the surface treatments, the *in vitro* stability of the synthesized coatings was evaluated on titanium surfaces. To study this, pSBMA grafted titanium samples were soaked in a 0.9% saline solution at 37°C for 10 days. Following this, the surface composition of the samples was evaluated using XPS. The elemental composition of bare and pSBMA grafted titanium surfaces before and after saline soak is summarized in Table 3.6.

It can be observed that the atomic percentage of titanium on a bare sample reduces to 5% after the saline soak, in comparison to the 16% for an unsoaked sample. In addition, the concentration of carbon increases by ~ 2x and that of oxygen decreases by ~ 2.5 x. Nitrogen, sodium and chlorine were also observed as new species on the samples. Similar changes were also observed for pSBMA grafted samples. There is a slight increase in the atomic percentage of nitrogen. In addition, sodium and chlorine were also observed in small amounts. These changes can be explained based on the deposition of a salt layer on the surface following a 10-day saline

soak, since the saline-soaked samples were not washed before analysis. This was done to avoid further processing of the samples following the saline soak. Since the increase in nitrogen is observed for both bare and pSBMA grafted samples after the saline soak, it could also be due to surface contamination during saline preparation or sample handling. Despite these minor changes, the presence of carbon, nitrogen and sulfur, in addition to carbon and oxygen, indicates the presence of a pSBMA coating on the surface even after wash. The absence of any titanium on the pSBMA surface also indicates that the coating remained intact even after the saline soak.

Table 3.6. Summary of the surface composition of titanium surfaces before and after soaking in 0.9% saline solution as obtained by survey scans from XPS (n=3).

Sample	**Elemental composition (%)**							
	C 1s	**O 1s**	**Br 3d**	**N 1s**	**S 2p**	**Ti 2p**	**Na 1s**	**Cl 2p**
Ti	34.7 ± 2.8	49.1 ± 1.6	-	-	-	16.2 ± 1.3	-	-
Ti_salt soaked	72.8 ± 1.3	18.4 ± 1.2	-	2.2 ± 0.8	-	5.1 ± 0.35	1.4 ± 0.42	0.3 ± 0.3
Ti-M3BP-pSBMA	66.5 ± 0.8	23.6 ± 0.5	-	5.9 ± 0.4	4.2 ± 0.1	-		-
Ti-M3BP-pSBMA_salt soaked	64.9 ± 0.2	22.1 ± 0.7	-	7.3 ± 0.7	2.8 ± 0.1	-	1.9 ± 0.1	1.7 ± 0.2

High-resolution C 1s scans were also collected for the bare and pSBMA grafted samples before and after the saline soak and are depicted in Figure 3.10 and Figure 3.11, respectively. Figure 3.11 also depicts the high-resolution N 1s and S 2p scans for the pSBMA grafted samples, before and after the saline soak. The composition of the various chemical states of C, N and S in the bare and pSBMA grafted samples before and after the salt soak are summarized in Table 3.7.

The differences in the contributions of various chemical states of C, and S for bare and pSBMA grafted samples before and after the saline soak are almost negligible. The only significant change is the presence of 2 peaks in the N 1s spectrum for the salt soaked pSBMA grafted sample in comparison to a single N 1s peak for the unsoaked sample. The major peak in the N 1s bonding environment is still primarily from the quaternary amine groups of pSBMA, as shown in Figure 3.9. It can be observed that 83% of the N 1s signal is from the quaternary amine group present in the pSBMA molecule. This observation along with the results of the C 1s and S 2p bonding environments suggests abundant presence of pSBMA species on the surface. These observations confirm the *in vitro* stability of the pSBMA grafted titanium surfaces.

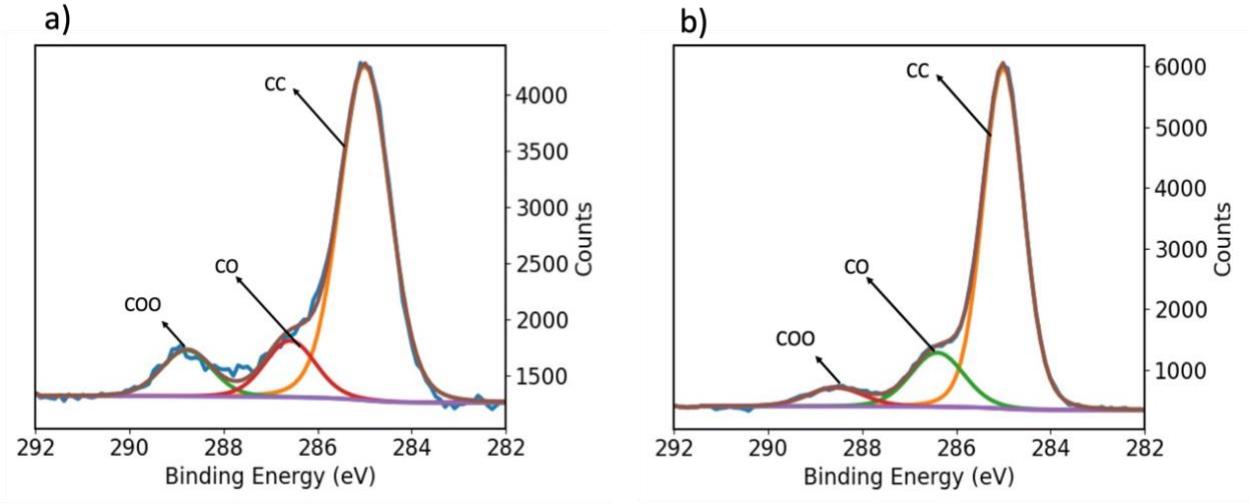

Figure 3.10. Representative high-resolution spectra of the C 1s peak on bare titanium a) before b) after soaking in 0.9 % saline solution. Fitted peaks are labeled to represent different bonding environments within each chemical structure.

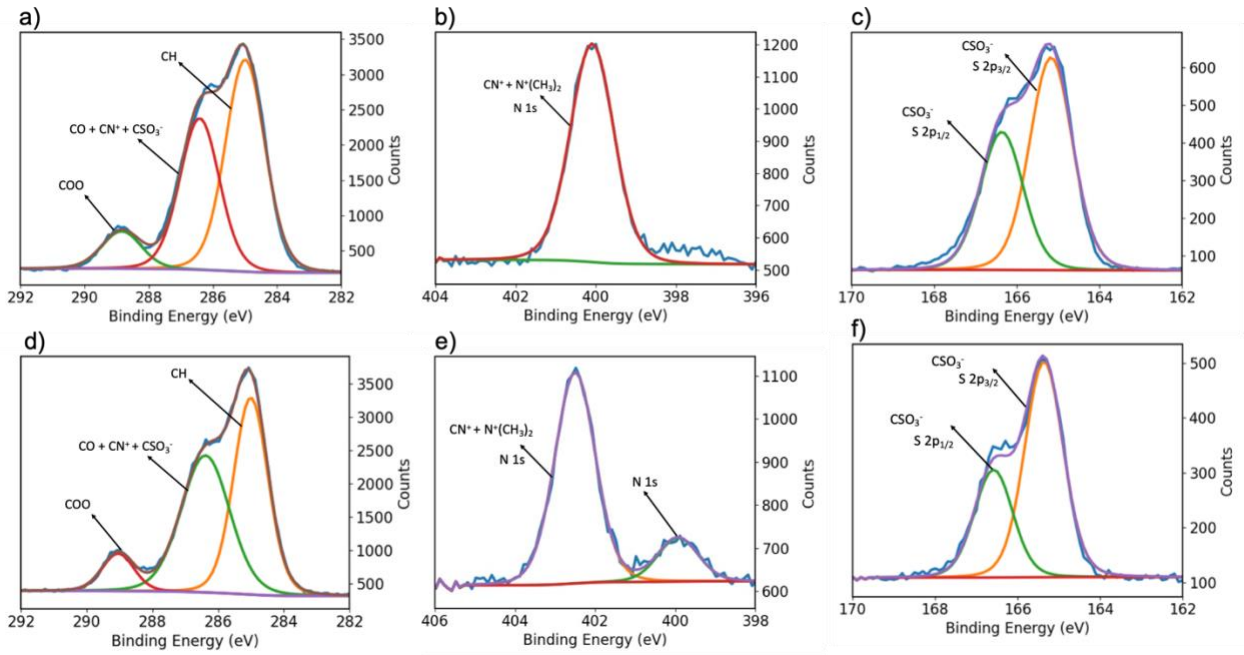

Figure 3.11. Representative a) N 1s b) S 2p and c) C 1s high-resolution spectra of the Ti-M3BP-pSBMA surfaces before the saline soak and d) N 1s e) S 2p and f) C 1s high-resolution spectra after the saline soak. Fitted peaks are labeled to represent different bonding environments within each chemical structure.

Table 3.7. Representative summary of the surface composition of bare and pSBMA grafted titanium surfaces before and after soaking in 0.9% saline solution as obtained by survey and high-resolution C 1s, N 1s and S 2p scans from XPS.

Sample	**C 1s (%)**			**N 1s (%)**		**S 2p**	
	CH	**CO**	**COOR**	**N**	**N^+**	**S 2p 3/2**	**S 2p 1/2**
Ti	76	14	10	-	-	-	-
Ti_salt soaked	78	16	6	-	-	-	-
Ti-M3BP-pSBMA	53	38	9	-	100	62	38
Ti-M3BP-pSBMA_salt soaked	56	36	8	17	83	66	34

3.4.2 SURFACE COATING THICKNESS USING PROFILOMETRY

Following confirmation of a stable, uniform and delamination resistant pSBMA coating, the thickness of the coatings was measured using a profilometer. Silicon wafer was used as the model substrate for these measurements since the profilometer requires a hard and flat surface for accurate measurements. The inherent presence of a thick and uneven oxide layer on the surface of titanium poses challenges to accurate thickness measurements. The RPU discs used in this study contain grooves from 3-D printing, making the surface uneven. Since RPU is a plastic, the relatively soft structure also makes it unsuitable for profilometer measurements.

The thickness measurements were taken both after M3BP deposition and after subsequent pSBMA grafting. The thickness of the M3BP layer reduced from 70 ± 3.8 nm to 43 ± 5.9 nm after soaking in a 1:1 methanol-water solution for 1 h (Figure 3.12). No noticeable change was measured in the M3BP coating thickness after further soaking. This decrease can be attributed to the removal of unreacted or loosely attached polybromine species. This observation also corroborates the XPS results discussed in Table 3.1 in section 3.4.1. After pSBMA grafting, the total thickness increased by almost 34 nm to 77 ± 6.3 nm, confirming the successful addition of the pSBMA coating on M3BP functionalized surfaces (Figure 3.13).

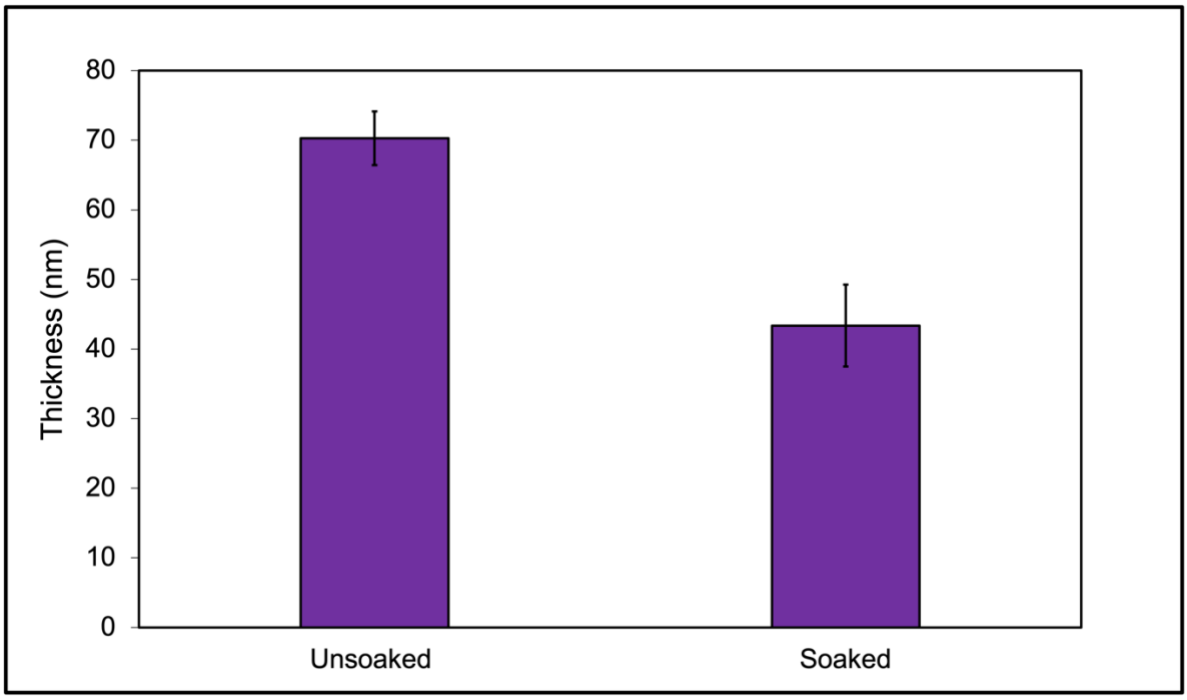

Figure 3.12. Change in thickness of the M3BP coating after soaking in 1:1 solution of methanol water for 1 h, measured using a profilometer (n=5).

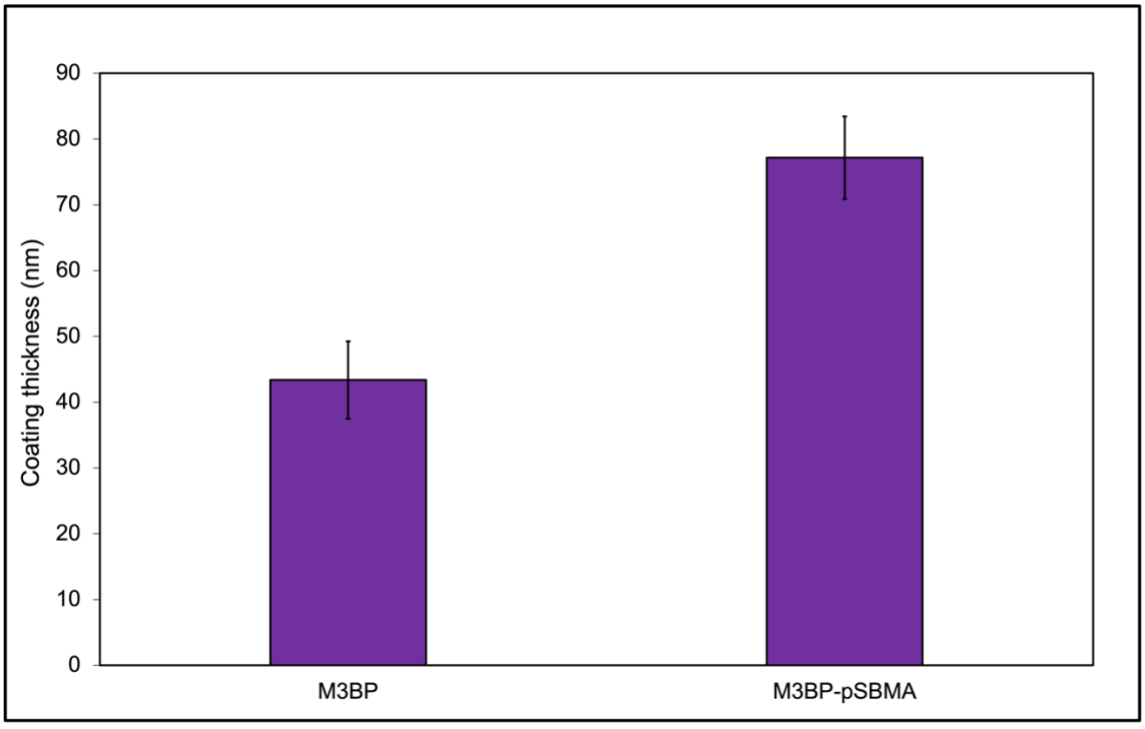

Figure 3.13. Thickness of the pSBMA coatings, measured using a profilometer (n=5).

To further confirm the *in vitro* stability, thickness of the pSBMA coating was also measured after incubating the samples in a 0.9% saline solution at 37°C for 10 days. The results are summarized in Figure 3.14. No notable change was observed in the coating thickness after the 10-day incubation, indicating the robustness and delamination resistance of the grafted non-fouling coatings. These results are also in line with the observations summarized in Table 3.6.

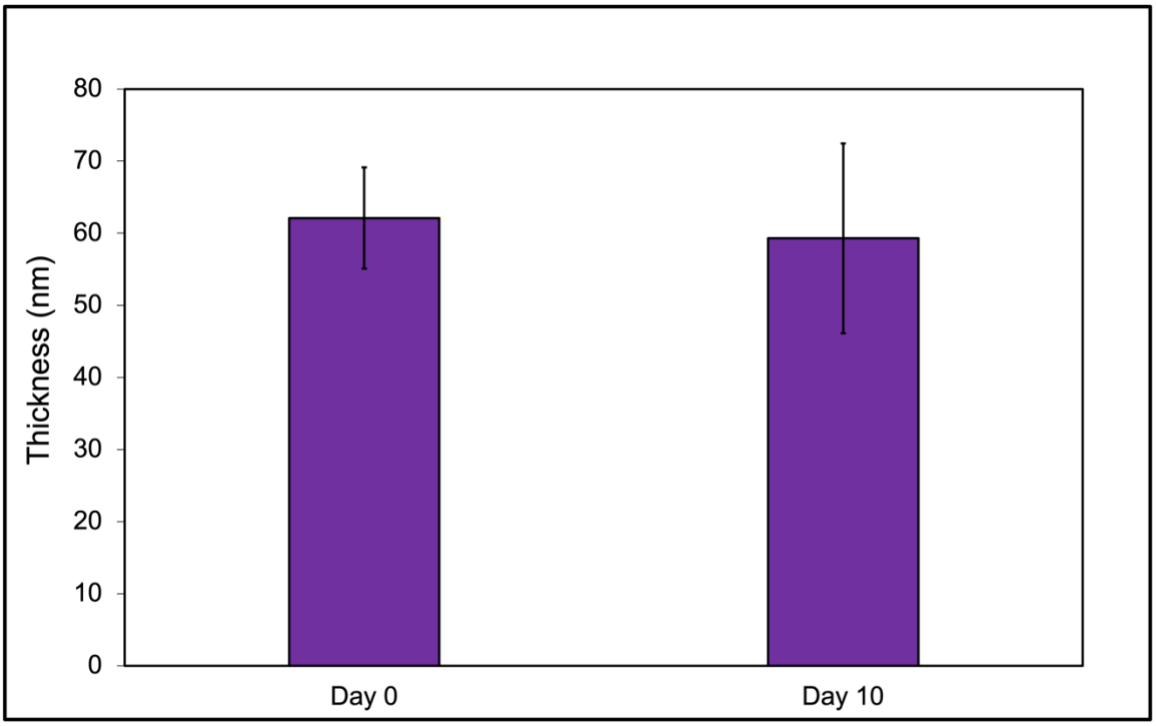

Figure 3.14. Thickness of the pSBMA coatings after a 10-day soak in 0.9% saline solution, measured using a profilometer (n=5).

3.4.3 SURFACE WETTABILITY MEASUREMENT USING GONIOMTER

Increase in the surface wettability of titanium from the introduction of the pSBMA coatings was quantified by measuring the contact angle before and after surface functionalization. The contact angle results are depicted in Figure 3.15. Upon grafting the pSBMA coating, the contact angle of titanium reduced from 84° to ~13°. These results indicate a significant increase in the surface wettability of titanium upon introduction of pSBMA coatings. These values are also in

agreement with previously reported values in the literature.[22–24] The presence of a thick oxide layer on the titanium surface explains the high contact angle (low surface wettability) of bare titanium surfaces. The increase in contact angle to ~88° upon the introduction of the M3BP layer can be attributed to the hydrophobic nature of bromine molecules. The ~85% reduction in the contact angle after pSBMA grafting can be explained by the super-hydrophilic nature of zwitterionic pSBMA molecules and their ability to form full-coverage, strong and stable surface hydration layers via electrostatic forces and hydrogen bonding.[22]

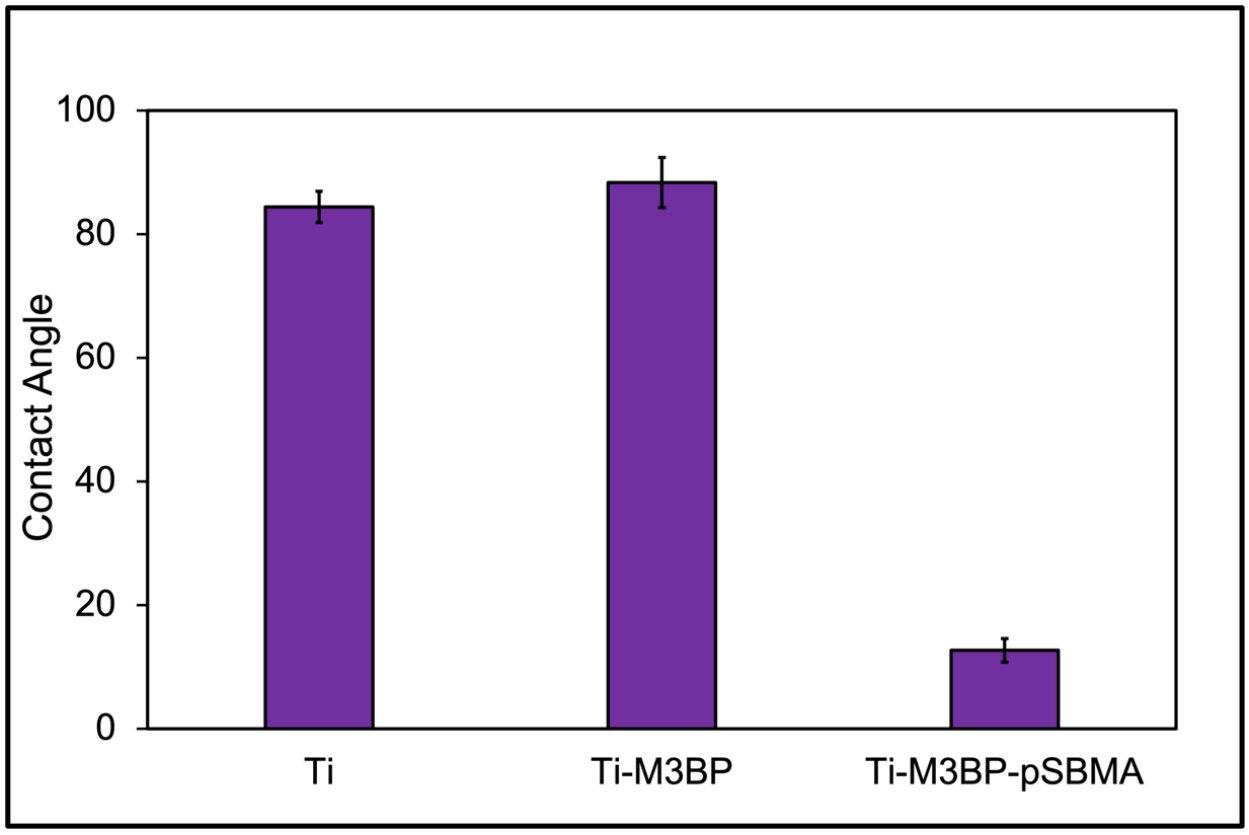

Figure 3.15. Contact angle measurements on titanium substrates, measured before and after pSBMA grafting (n=6).

3.4.4 PROTEIN ADSORPTION MEASUREMENT USING RADIOLABELED HSA

As detailed in chapters 1 and 2, non-specific protein adsorption can trigger FBR resulting in the formation of an insulating fibrous capsule around the implant, rendering it futile.[26–28] Protein adsorption values as low as 17 ng/cm^2 were measured on pSBMA grafted RPU surfaces prepared using the M3BP initiator approach. These values were 87% lower than that of bare substrates (Figure 3.16). The amount of protein adsorbed on RPU-M3BP samples was much higher with a value of ~100 ng/cm^2. Even though these values are lower than that of the bare substrates they are unacceptable metrics for non-fouling criteria. This observation confirms that the low protein adsorption on the pSBMA grafted sample is due to the hydrophilic pSBMA coating and not the underlying M3BP layer, which is hydrophobic and characterized by high values of contact angle. The significant reduction in the amount of protein adsorbed on pSBMA grafted surfaces can be attributed to the super-hydrophilic nature of zwitterionic molecules and their ability to form a full-coverage, uniform and stable hydration layers. The tightly structured hydration layers at the interface resist protein adsorption and inhibit foreign body response.[29,30]

Even though the protein adsorption results herein are 3-4 times higher than the protein adsorption values of 3-5 ng/cm^2 necessary for a material to be classified ‘non-fouling’, the initial results are promising.[27,28,31] These values are also comparable to the 10.5 ng/cm^2 values achieved for similar surfaces developed using the methodologies discussed in Chapter 2. There is potential to further reduce protein adsorption values to below the 5 ng/cm^2 with further optimization of this concept. These considerations thus illustrate the potential of the M3BP initiator approach of this chapter to prepare robust non-fouling coatings with enhanced biocompatibility.

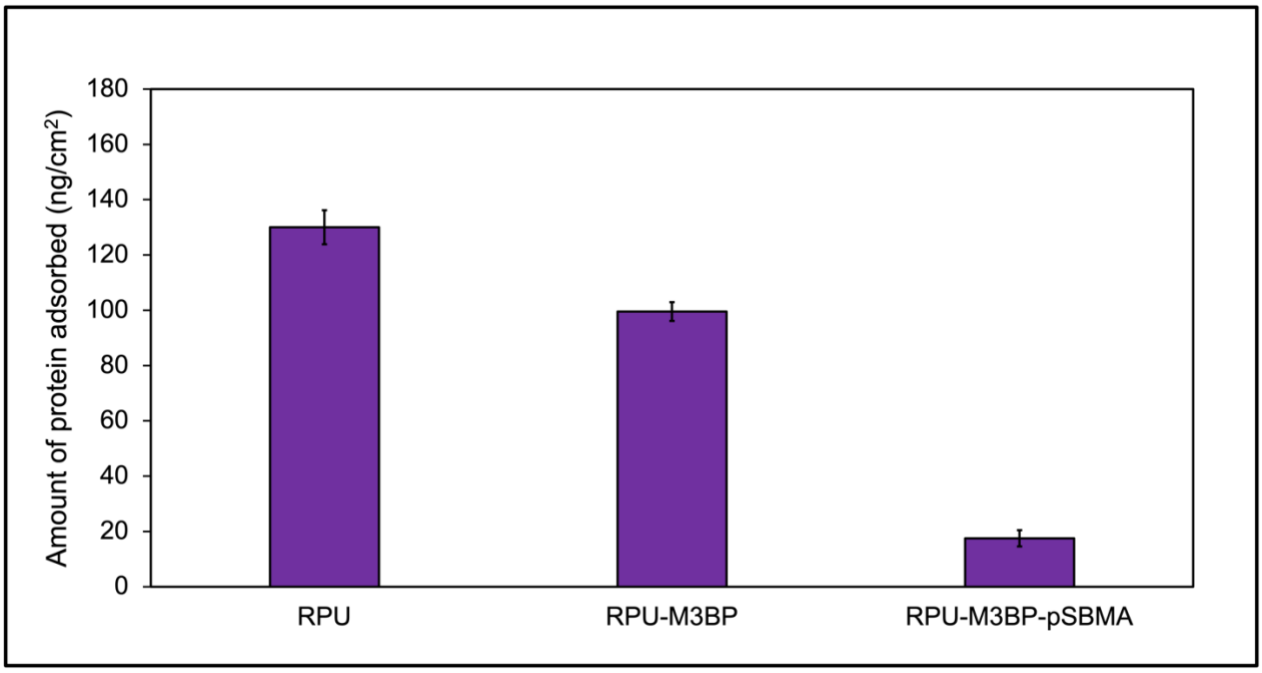

Figure 3.16. Protein adsorption on various RPU surfaces, measured using radiolabeled human serum albumin (n=4).

3.4.5 CYTOTOXICITY ASSESSMENT USING NIH-3T3 FIBROBLASTS

Sample cytotoxicity was assessed using procedures discussed in section 3.4.5. A qualitative evaluation of the samples using visual microscopic inspection indicated non-toxic response of the fibroblasts to extracts from RPU-M3BP-pSBMA and Ti-M3BP-pSBMA samples relative to latex controls.

3.5 SUMMARY AND CONCLUSIONS

A modified surface functionalization protocol which involves plasma deposition of ARGET ATRP polymerization initiators has been successfully demonstrated for biomedically relevant polymeric and metallic substrates. This approach builds on the methods introduced in Chapter 2 by combining the surface activation and initiator immobilization steps into a single, solvent-free synthesis. In choosing the initiator molecule, methyl 3-brompropionate (M3BP) was

selected as the initiator monomer based on adaptation of past work on glass substrates, which showed the ability to grow pHEMA brushes on M3BP-coated surfaces in under 15 min. The M3BP-coated RPU and titanium substrates in this work were successfully demonstrated to graft pSBMA brushes, leading to hydrophilic and non-fouling coatings while providing a method for initiator immobilization that eliminates harsh organic solvents which affect the mechanical integrity of polymeric implants.

The coated surfaces were characterized and analyzed based on the methods defined in Chapter 2. In particular, the proposed approach results in surface bromine composition values in close agreement with theoretical expectations. In addition, the films are resistant to delamination even after prolonged and vigorous chemical exposure. After the removal of physically adsorbed bromine compounds, the film thickness remains unchanged even after multiple wash steps, signifying strong and covalently attached coatings. Water contact angles on modified surfaces reduce from 84º to 13º on titanium substrates, indicating significant hydrophilicity. In addition, the fact that the intermediate brominated surfaces exhibit an increase in contact angle (88º) indicates that the hydrophilic action is primarily due to the introduction of super-hydrophilic pSBMA brushes. The protein adsorption trends are also consistent with this observation, wherein the final pSBMA-coated surfaces exhibit a substantially lower protein adsorption (~15 ng/cm^2) vis-à-vis the M3BP-coated surfaces (~100 ng/cm^2), suggesting antifouling effects of zwitterionic coatings by means of strong interfacial hydration layers.

There is substantial scope for improvement of this proof-of-concept. In particular, the plasma deposition process parameters can be varied further to improve the quality and density of the bromine layer, which can improve the density of the pSBMA coating and thus adsorption metrics, thereby bring the surfaces closer to the 5 ng/cm^2 threshold to be classified ‘non-fouling’

for biomedical applications. In addition, ARGET ATRP reaction parameters - namely reaction time, ratio of the monomer-catalyst-ligand-reducing agent system, composition of the solvent system, and the use of salts for faster monomer dissolution - can also be optimized to ensure full utilization of the deposited bromines and thereby improve hydrophilicity metrics. A third area of interest is the testing of M3BP initiator for grafting other monomers of interest, including CBMA. *In vivo* testing can also help evaluate the biocompatibility of these surfaces vis-à-vis those prepared by more conventional means. Despite these considerations however, this method represents a substantial simplification of conventional surface modification techniques such as those introduced in Chapter 2. The ability to achieve comparable non-fouling metrics while eliminating the need for deleterious organic solvents is expected to result in non-trivial improvements in the overall performance and lifetime of a range of polymeric biomedical implants.

3.6 REFERENCES

(1) Hoffman, A. S. Ionizing Radiation and Gas Plasma (or Glow) Discharge Treatments for Preparation of Novel Polymeric Biomaterials. In Polymers in Medicine; 1984; pp 141–157. https://doi.org/10.1007/3-540-12796-8_12.

(2) Yasuda, H. Glow Discharge Polymerization. Journal of Polymer Science: Macromolecular Reviews 1981, 16, 199–293.

(3) Biederman, H.; Slavínská, D. Plasma Polymer Films and Their Future Prospects. Surf Coat Technol 2000, 125 (1–3), 371–376. https://doi.org/10.1016/S0257-8972(99)00578-2.

(4) Mecwan, M. M.; Dong, X.; Shi, G. H.; Ratner, B. D. Plasma Polymerized HMDSO Coatings for Syringes To Minimize Protein Adsorption. J Pharm Sci 2021, 110 (4), 1710–1717. https://doi.org/10.1016/j.xphs.2020.10.057.

(5) Matyjaszewski, K.; Patten, T. E.; Xia, J. Controlled/'living' Radical Polymerization. Kinetics of the Homogeneous Atom Transfer Radical Polymerization of Styrene. J Am Chem Soc 1997, 119 (4), 674–680. https://doi.org/10.1021/ja963361g.

(6) Matyjaszewski, K.; Hongchen, D.; Jakubowski, W.; Pietrasik, J.; Kusumo, A. Grafting from Surfaces for “Everyone”: ARGET ATRP in the Presence of Air. Langmuir 2007, 23 (8), 4528–4531. https://doi.org/10.1021/la063402e.

(7) Simakova, A.; Averick, S. E.; Konkolewicz, D.; Matyjaszewski, K. Aqueous ARGET ATRP. Macromolecules 2012, 45 (16), 6371–6379. https://doi.org/10.1021/ma301303b.

(8) Hong, D.; Hung, H. C.; Wu, K.; Lin, X.; Sun, F.; Zhang, P.; Liu, S.; Cook, K. E.; Jiang, S. Achieving Ultralow Fouling under Ambient Conditions via Surface-Initiated ARGET ATRP of Carboxybetaine. ACS Appl Mater Interfaces 2017, 9 (11), 9255–9259. https://doi.org/10.1021/acsami.7b01530.

(9) Kaßel, M.; Gerke, J.; Ley, A.; Vana, P. Surface Modification of Wood Flour via ARGET ATRP and Its Application as Filler in Thermoplastics. Polymers (Basel) 2018, 10 (4), 1–16. https://doi.org/10.3390/polym10040354.

(10) Mecwan, M. M.; Taylor, M. J.; Graham, D. J.; Ratner, B. D. Highly Reactive Haloester Surface Initiators for ARGET ATRP Readily Prepared by Radio Frequency Glow Discharge Plasma. Biointerphases 2019, 14 (4), 041006. https://doi.org/10.1116/1.5110163.

(11) Lewis, K. B.; Ratner, B. D. Plasma-Deposited Polymer Coatings for Scanning Tunneling Microscope Tips. Journal of Vacuum Science & Technology B: Microelectronics and Nanometer Structures 1992, 10 (5), 2331. https://doi.org/10.1116/1.586063.

(12) Kim, D. D.; Takeno, M. M.; Ratner, B. D.; Horbett, T. A. Glow Discharge Plasma Deposition (GDPD) Technique for the Local Controlled Delivery of Hirudin from Biomaterials. Pharmaceutical Research. 1998, pp 783–786. https://doi.org/10.1023/A:1011987423502.

(13) Pata, V.; Dan, N. The Effect of Chain Length on Protein Solubilization in Polymer-Based Vesicles (Polymersomes). Biophys J 2003, 85 (4), 2111–2118. https://doi.org/10.1016/S0006-3495(03)74639-6.

(14) Ostaci, R. V.; Damiron, D.; al Akhrass, S.; Grohens, Y.; Drockenmuller, E. Poly (Ethylene Glycol) Brushes Grafted to Silicon Substrates by Click Chemistry: Influence of PEG Chain Length, Concentration in the Grafting Solution and Reaction Time. Polym Chem 2011, 2 (2), 348–354. https://doi.org/10.1039/c0py00251h.

(15) Sin, M. C.; Sun, Y. M.; Chang, Y. Zwitterionic-Based Stainless Steel with Well-Defined Polysulfobetaine Brushes for General Bioadhesive Control. ACS Appl Mater Interfaces 2014, 6 (2). https://doi.org/10.1021/am4041256.

(16) Badoux, M.; Billing, M.; Klok, H. A. Polymer Brush Interfaces for Protein Biosensing Prepared by Surface-Initiated Controlled Radical Polymerization. Polymer Chemistry. Royal Society of Chemistry June 21, 2019, pp 2925–2951. https://doi.org/10.1039/c9py00163h.

(17) Löpez, G. P.; Ratner, B. D.; Tidwell, C. D.; Haycox, C. L.; Rapoza, R. J.; Horbett, T. A. Glow Discharge Plasma Deposition of Tetraethylene Glycol Dimethyl Ether for Fouling-resistant Biomaterial Surfaces. J Biomed Mater Res 1992, 26 (4), 415–439. https://doi.org/10.1002/jbm.820260402.

(18) Chen, J. Y.; Tian, R. L.; Leng, Y. X.; Yang, P.; Wang, J.; Wan, G. J.; Zhao, A. S.; Sun, H.; Huang, N. Effect of Ar Plasma Etching of Ti-O Film Surfaces on Biological Behavior of Endothelial Cell. Surf Coat Technol 2007, 201 (15), 6901–6905. https://doi.org/10.1016/j.surfcoat.2006.09.110.

(19) Ko, Y. C.; Ratner, B. D.; Hoffman, A. S. Characterization of Hydrophilic-Hydrophobic Polymeric Surfaces by Contact Angle Measurements. J Colloid Interface Sci 1981, 82 (1), 25–37.

(20) Horbett, T. A. Adsorption of Proteins from Plasma to a Series of Hydrophilic-Hydrophobic Copolymers. II. Compositional Analysis with the Prelabeled Protein Technique. J Biomed Mater Res 1981, 15 (5), 673–695. https://doi.org/https://doi.org/10.1002/jbm.820150506.

(21) Kuo, T. Y.; Chung, Y. C. Surface-Initiated Polymerization of Mussel-Inspired Dopamine for Hydrophilic Coatings. Mater Adv 2021, 2 (17), 5686–5690. https://doi.org/10.1039/d0ma00908c.

(22) Fontes, C. M.; Achar, R. K.; Joh, D. Y.; Ozer, I.; Bhattacharjee, S.; Hucknall, A.; Chilkoti, A. Engineering the Surface Properties of a Zwitterionic Polymer Brush to Enable the Simple Fabrication of Inkjet-Printed Point-of-Care Immunoassays. Langmuir 2019, 35 (5), 1379–1390. https://doi.org/10.1021/acs.langmuir.8b01597.

(23) Cheng, C. H.; Liu, H. C.; Lin, J. C. Surface Modification of Polyurethane Membrane with Various Hydrophilic Monomers and N-Halamine: Surface Characterization and

Antimicrobial Properties Evaluation. Polymers (Basel) 2021, 13 (14). https://doi.org/10.3390/polym13142321.

(24) Dugan, J. M.; Colominas, C.; Garcia-Granada, A. A.; Claeyssens, F. Spatial Control of Neuronal Adhesion on Diamond-Like Carbon. Front Mater 2021, 8. https://doi.org/10.3389/fmats.2021.756055.

(25) Čolović, B.; Kisić, D.; Jokanović, B.; Rakočević, Z.; Nasov, I.; Petkoska, A. T.; Jokanović, V. Wetting Properties of Titanium Oxides, Oxynitrides and Nitrides Obtained by DC and Pulsed Magnetron Sputtering and Cathodic Arc Evaporation. Materials Science- Poland 2019, 37 (2), 173–181. https://doi.org/10.2478/msp-2019-0031.

(26) Zhang, L.; Cao, Z.; Bai, T.; Carr, L.; Ella-Menye, J. R.; Irvin, C.; Ratner, B. D.; Jiang, S. Zwitterionic Hydrogels Implanted in Mice Resist the Foreign-Body Reaction. Nat Biotechnol 2013, 31 (6), 553–556. https://doi.org/10.1038/nbt.2580.

(27) Lin, X.; Jain, P.; Wu, K.; Hong, D.; Hung, H. C.; O'Kelly, M. B.; Li, B.; Zhang, P.; Yuan, Z.; Jiang, S. Ultralow Fouling and Functionalizable Surface Chemistry Based on Zwitterionic Carboxybetaine Random Copolymers. Langmuir 2019, 35 (5), 1544–1551. https://doi.org/10.1021/acs.langmuir.8b02540.

(28) Horbett, T. A. Protein Adsorption on Biomaterials. In Biomaterials: Interfacial Phenomena and Applications; Cooper et al., Ed.; American Chemical Society: Washington, D.C., 1982; pp 233–244.

(29) Vogler, E. A. Protein Adsorption in Three Dimensions. Biomaterials 2012, 33 (5), 1201–1237. https://doi.org/10.1016/j.biomaterials.2011.10.059.

(30) Sengupta, T.; Razumovsky, L.; Damodaran, S. Energetics of Protein-Interface Interactions and Its Effect on Protein Adsorption. Langmuir 1999, 15 (20), 6991–7001. https://doi.org/10.1021/la990235s.

(31) Zhang, Z.; Chen, S.; Chang, Y.; Jiang, S. Surface Grafted Sulfobetaine Polymers via Atom Transfer Radical Polymerization as Superlow Fouling Coatings. Journal of Physical Chemistry B 2006, 110 (22), 10799–10804. https://doi.org/10.1021/jp057266i.

Chapter 4. LUBRICATION ASSESSMENT OF PREPARED pSBMA SURFACES

Abstract: The lubricity of biomedical implants is an important determinant of overall performance and lifetime. In addition to performance deterioration due to surface fouling, some biomedical implants also experience wear and degradation due to surface friction between sliding surfaces, which also limits implant lifetime. High surface friction of implants that experience relative dynamic motion around surrounding tissue and tendons can cause wear and abrasion on the tissue or tendons, which can cause further injury and hinder the smooth functioning of implants. Surface modifications by means of covalently attached super-hydrophilic polymer coatings can reliably increase the surface lubricity due to the formation of strong interfacial hydration sheaths around the polymer chains, adding to surface fluidity. To this end, this chapter discusses the evaluation of the lubrication properties of the poly (sulfobetaine methacrylate) coatings grafted on titanium and silicon wafers using the methodologies discussed in chapter 2 (methodology 1) and chapter 3 (methodology 2). The fabricated surfaces are evaluated for friction coefficients in the 'hydrated' state, measured using a nanoindenter. For the coated titanium surfaces prepared using methodology 1, the average friction coefficient is measured to be 0.07 compared to 0.52 for uncoated titanium, corresponding to a 7.5x reduction, and in line with literature reports. For surfaces prepared using methodology 2, friction coefficient values as low as 0.05 were measured, indicating a >10x reduction in the surface friction. As already discussed in detail in previous chapters, the prepared coatings are robust, exhibit good *in vitro* stability and significantly reduce non- specific protein adsorption. These observations indicate the ability of the proposed protocols to create strong hydration effects and minimize sliding friction for materials relevant for medical implants, thus helping increase their efficiency and prolonging lifetime.

4.1 INTRODUCTION

The lubricity of biomedical implants is an important consideration in overall performance and longevity, especially for implants experiencing dynamic motion relative to surrounding tissue. Natural cartilage between sliding biological joints is known to result in extremely low friction coefficients (<0.01) and ensure smooth sliding of surfaces with minimal abrasion and wear.[1–3] This is attributed to the formation of chemical complexes involving hydrophilic proteins, natural polysaccharides and phospholipid compounds.[4] The synergistic effects due to multiple species, including the dense extra cellular matrix and the confined interfacial water by charged species in the surface-active phospholipids, provide the necessary hydrophilicity to ensure sufficient lubrication, also termed 'hydration lubrication'.[5,6] In designing biomedical devices and implants, it is necessary to mimic these effects by way of surface modification with suitable chemical analogs.[5] This is of particular significance in the current work due to the specific function of the implants under study of Balasubramanian et al., which involve the sliding of implants on tendons to create a differential mechanism for fixing finger flexion.[7,8]

Engineering implant surfaces to achieve comparably low friction coefficients is thus an active area of research.[6] Multiple medically relevant substrate materials grafted with zwitterionic polymer coatings including PC, CBMA, and SBMA derivatives have been proven to mimic this 'articular lubrication'.[1,5,9,10] In addition, these molecules also substantially reduce protein adsorption.[11–15] The lubricating action is correlated with the increased hydrophilicity and wettability, which also prevents non-specific adsorption and fouling as discussed previously. Studies of PC-based zwitterionic polymers on cross-linked UHWMPE have observed a linear relationship between friction coefficient and contact angle, which in turn is a function of the grafting density. These studies also revealed the ability of zwitterionic polymer brush coatings to

achieve over 7x reductions in friction coefficient over bare substrates.[9,16,17] Other works have reported friction coefficients of the order of 10^{-3} - 10^{-4} in aqueous media, including copolymer coatings containing pSBMA which have also achieved low friction coefficients in various biological media (10^{-2}). It is noteworthy that the chemical attachment based on 'grafting-from' polymerization methods are indicated to provide increased lubricity relative to physisorption approaches, signifying the salience of the polymer brush structures in terms of modifying the energetics of hydration. This background indicates the potential of the methods described in this dissertation to replicate and improve upon these metrics.[18]

The remarkable lubrication properties of hydrophilic surfaces grafted with polymer brushes are typically attributed to the 'hydration lubrication' model. Water can retain substantial bulk fluid behavior even down to ultrathin films. This means when the water molecules form 'hydration sheaths' around charged species, they still produce a fluid-like response to shearing action, while the strong solvation (hydration) forces prevent the water from being 'squeezed out' from between two sliding surfaces even when large normal loads are applied. The combined effect of these two properties is significantly increased lubricity and the ability to achieve ultralow friction coefficients.[19,20]

In the case of superhydrophilic surfaces consisting of zwitterionic polymer brushes, the presence of charged brush structures results in additional synergistic effects that further enhance lubricity. Zwitterionic polymers are highly hydrated with many water molecules, forming 'hydration sheaths.[19,21,22] At high grafting density, favorable conformational changes due to the relative rigidity of the brush structures result in nearly vertical brushes which form even stronger hydration layers with the surrounding water. Polymer brushes grafted using covalent methods are more robust in this regard, resisting shear and delamination even at relatively high loadings (0.5

MPa), in addition to achieving increased brush density.[23] Secondarily, in the case of polymer brushes, steric and entropic effects and osmotic pressure effects also contribute towards lubricity.[6,19] Similar to PC-based polymers that have been the focus of much of past work, SBMA also possess robust functional groups with the ability to maintain favorable conformations in biological media, and thus it is reasonable to expect resistance to large normal loads while preserving hydration lubrication, thus ensuring low levels of friction coefficient.[16] In addition, the robust ARGET ATRP polymerization methods discussed herein are expected to ensure delamination-resistant coatings and thus enable operation even under biologically relevant loads.[24–26] Recent work using pSBMA based coatings has been demonstrated to achieve 90% reductions in friction coefficient for PDMS-based cochlear implants, signifying the potential of this work to achieve comparable performance for the specific implants of interest herein.[27]

This chapter thus discusses the systematic lubricity evaluation of the surfaces prepared using the protocols established in Chapters 2 and 3. Friction coefficients were studied on titanium and silicon wafer substrates. Friction coefficient measurements were made in 'hydrated' state for both bare and coated substrates. The measurements were performed using a nanoindenter using a dynamic scratch test at set loads. The extent of lubricity enhancement due to surface modification was then quantified based on the friction coefficient trends for bare and modified surfaces. As expected, the pSBMA-surfaces prepared using the methodologies discussed in chapter 2 (methodology 1) and chapter 3 (methodology 2) provide significant (~7-10x) reductions in friction coefficient, demonstrating the strong hydrophilicity and hydration lubrication action of the polymer coatings.

4.2 EXPERIMENTAL METHODS

4.2.1 SAMPLE PREPARATION

All samples were prepared on 1 inch titanium squares and silicon wafers. Samples were first thoroughly cleaned following the procedures previously described in section 2.3.1.1. Zwitterionic coatings of pSBMA were then synthesized on the substrates using the two methodologies described in chapters 2 and 3. In method 1, the surfaces were first activated by depositing a coating of 2-hydroxyethyl methacrylate (HEMA), followed by macroinitiator coupling and grafting pSBMA coatings via ARGET ATRP. These steps are discussed in sections 2.3.1.2, 2.3.1.3 and 2.3.1.4 of chapter 2. The pSBMA grafted samples prepared using this methodology are hereafter denoted as Ti-HEMA-pSBMA and Si-HEMA-pSBMA, for titanium and silicon wafer substrates, respectively. In method 2, a highly reactive haloester, methyl 3-bromopropionate (M3BP), was plasma deposited on the surface and the introduced bromine species were used as initiators for ARGET ATRP to synthesize pSBMA coatings. These procedures are described in section 3.3.1.2 and 3.3.1.3 of chapter 3. The pSBMA samples prepared using methodology 2 are hereafter denoted as Ti-M3BP-pSBMA and Si-M3BP-pSBMA for titanium and silicon wafer substrates, respectively.

4.2.2 FRICTION COEFFICIENT MEASUREMENT USING NANOINDENTER

The lubricity of the prepared surfaces was evaluated in terms of friction coefficients measured using the scratch test feature of nanoindenter. All measurements were performed on Hysitron TI 980 TriboIndenter (Bruker) instrument. To measure the friction coefficients, the ‘scratch test’ feature was used. The nanoindenter is equipped to measure lateral and normal forces

by means of a two-dimensional force transducer. All measurements were made using a conical diamond tip. A typical scratch procedure is depicted in Figure 4.1.

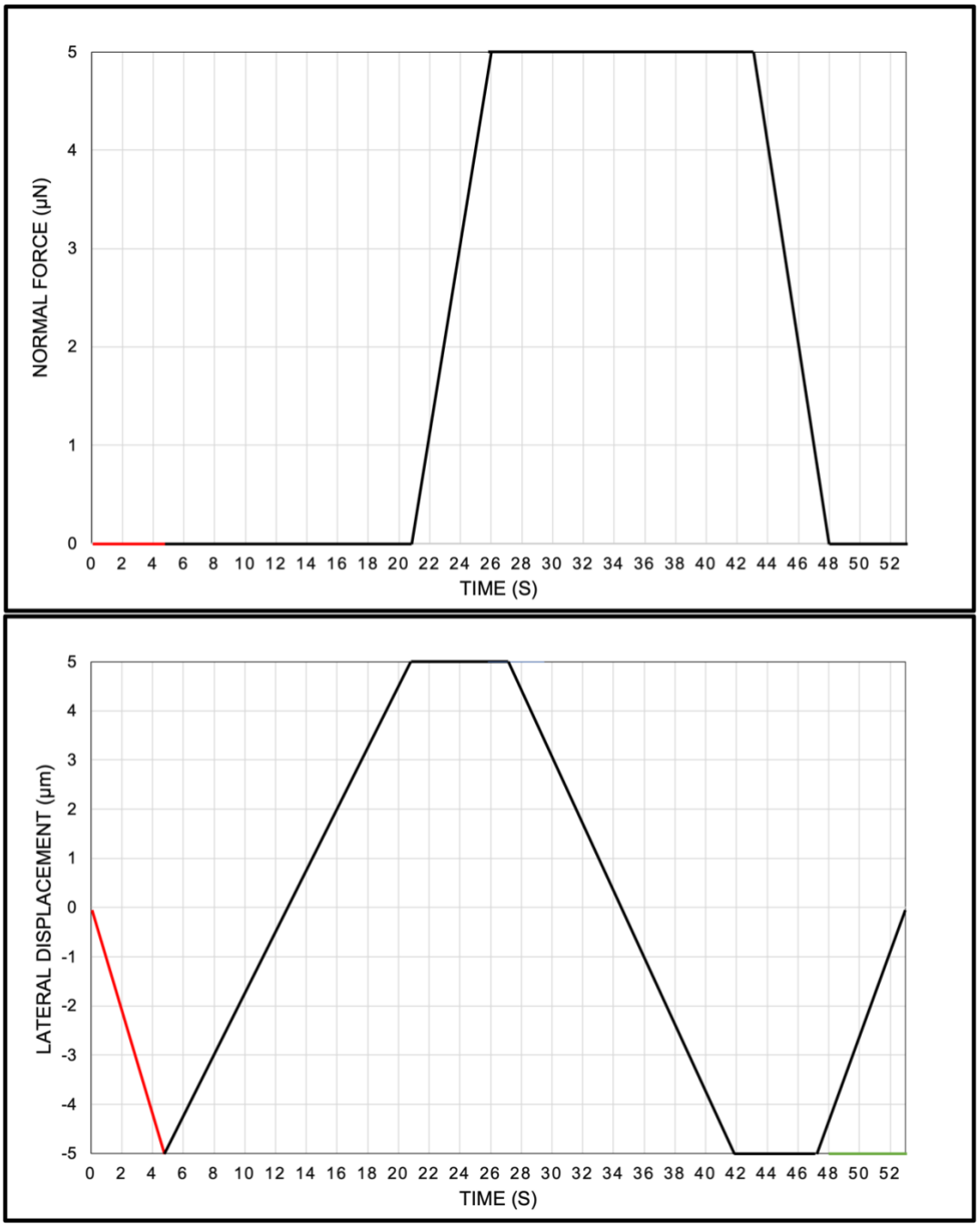

Figure 4.1. Schematic of the typical scratching procedure used for friction coefficient measurements on nanoindenter.

To perform a nanoscratch, a normal load is applied in a controlled fashion while measuring the force required by the tip moving laterally across the sample. 'Pre-load' is the load set to hold while the system pauses to allow the piezo scanner to settle and measure the system drift. For all measurements, the pre-load was set to 2 μN. All scratch tests were performed at constant load with a scratching speed of 0.4 μm/s and a scratch length of 10 μm. For a tip with radius r = 4.7 μm, an angle of 64.69° and a typical 15 μN load, this corresponds to a pressure of ~0.12 MPa, which is comparable to physiologically relevant conditions.[28] Tilt correction was performed on the scratch data before analysis to correct for the effect of sample tilt. As depicted in Figure 1, the tip was then translated by a fixed distance at zero load. The tip remained stationary as the applied load ramped up to the test value, following which it was held constant, and the tip translated back to its initial position at the fixed value of load. The applied load was linearly decreased back to zero while the tip remained stationary, completing the data acquisition. The reproducibility of the data was confirmed by testing each sample at least n=3 times. The data points for each scratch test were time-averaged over the scratch duration, neglecting any evident outliers.

4.3 RESULTS AND DISCUSSION

Following surface preparation, successful surface functionalization with stable and uniform coatings of pSBMA molecules was confirmed *via* measurement of surface composition using XPS and surface wettability through contact angle measurements. The non-fouling properties of the prepared surfaces were also evaluated using radiolabeled human serum albumin adsorption and are discussed in the previous chapters. The results of these studies indicated significantly increased surface wettability for surfaces grafted with pSBMA coatings, confirming the ability of prepared surfaces to form strong hydration sheaths at the interface. The increased surface hydrophilicity was then evaluated for its effect on the lubrication properties of the surfaces

by measuring the dynamic friction coefficients (FC) of the samples. These measurements were performed using a scratch test on a nanoindenter.

Prior to FC measurements, all samples were soaked in cell culture medium for 24 h and incubated at 37°C. Immediately before the measurements, the samples were removed from the media and air dried to remove any visible water from the surface. This was done to prevent any damage to the nanoindenter tip and transducer from the free water. Samples were soaked in cell culture medium to replicate biologically relevant conditions and mimic the complex environment around the implants in the host body. All data was collected at a constant load which translates to a ~0.12 MPa pressure applied on the coatings at the tip. The pressure values are comparable to the loads experienced by implants in the physiological systems. Loads higher than 30 μN resulted in excessively deep scratches on the coated silicon surfaces, leading to coating delamination along the length of the scan. This phenomenon was not observed for similarly coated titanium surfaces (Figure 4.2). This is possibly due to the presence of thick oxide layers underneath the functionalized coatings. To keep measurements consistent across both substrates, 15 μN was chosen as the constant load for all data acquisition.

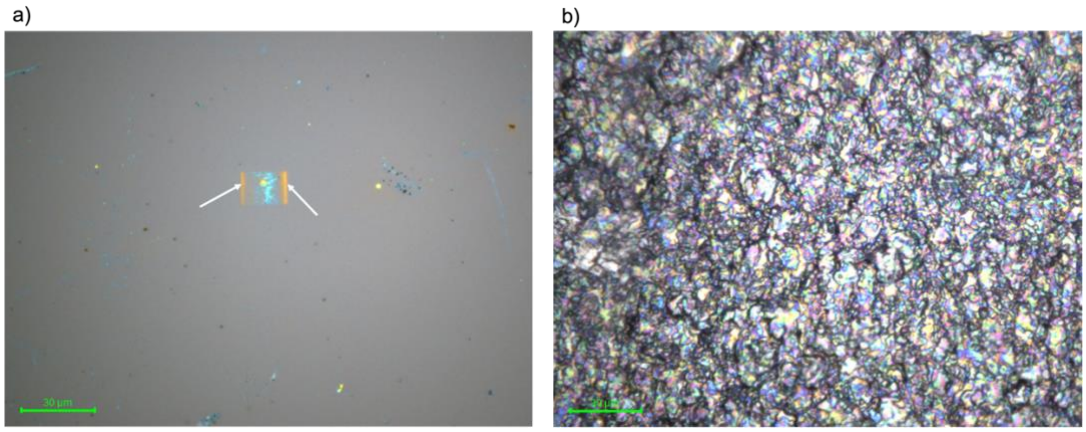

Figure 4.2. Optical images of a) coated silicon wafer and b) coated titanium surface. Two scratches 10 μm apart are visible on the silicon wafer surface, indicating delamination due to excessively high applied loads.

Friction coefficients measured for pSBMA grafted titanium surfaces prepared using methodologies 1 and 2 are depicted in Figure 4.3. All measurements were taken on surfaces hydrated from soaking in the cell culture medium. The friction coefficients of pSBMA grafted titanium surfaces prepared using the two approaches (Ti-HEMA-pSBMA and Ti-M3BP-pSBMA) exhibited comparable values. The average friction coefficient for Ti-HEMA-pSBMA was measured to be 0.07 and that for Ti-M3BP-pSBMA was 0.05. These values were respectively ~7.5x and 10.5x lower than the value measured for a bare titanium surface (0.52). Comparable values were also measured on silicon substrates with both Si-HEMA-pSBMA and Si-M3BP-pSBMA surfaces exhibiting a friction coefficient of 0.08 in comparison to 0.22 for a bare silicon substrate (Figure 4.4). The relatively higher friction coefficient for bare titanium surface can be attributed to the presence of a thick and rough inherent oxide layer. The difference in the surface roughness of silicon and titanium surfaces is also apparent in the optical images depicted in Figure 4.2.

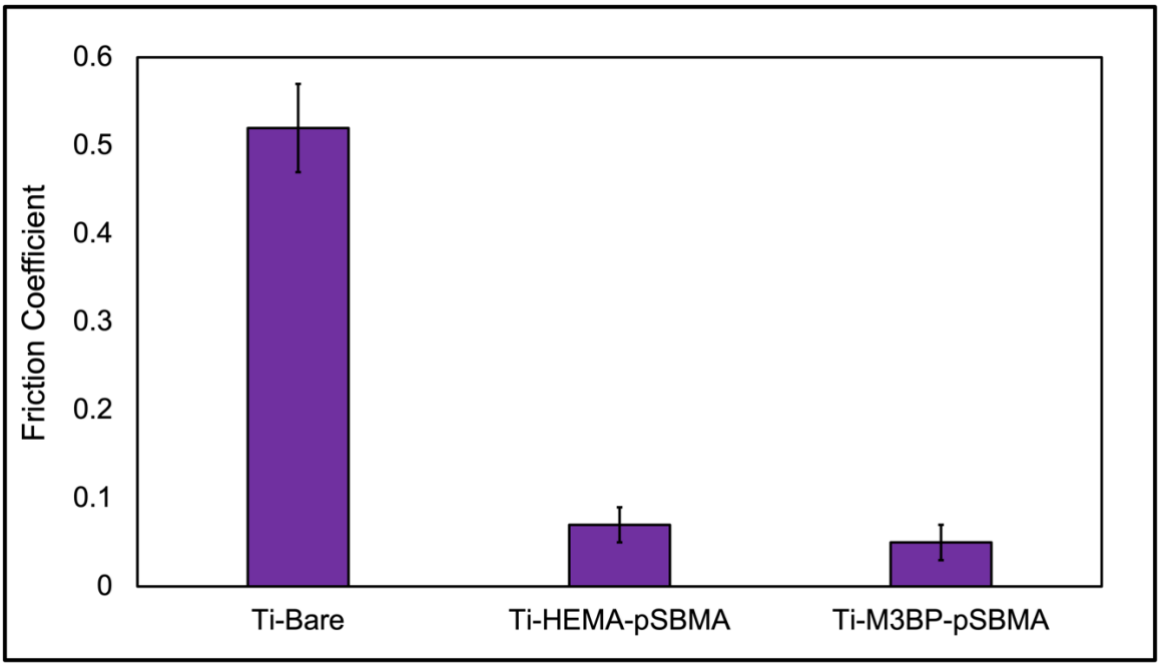

Figure 4.3. Friction coefficients of hydrated titanium substrates before and after grafting pSBMA coatings, measured using nanoindenter (n=3).

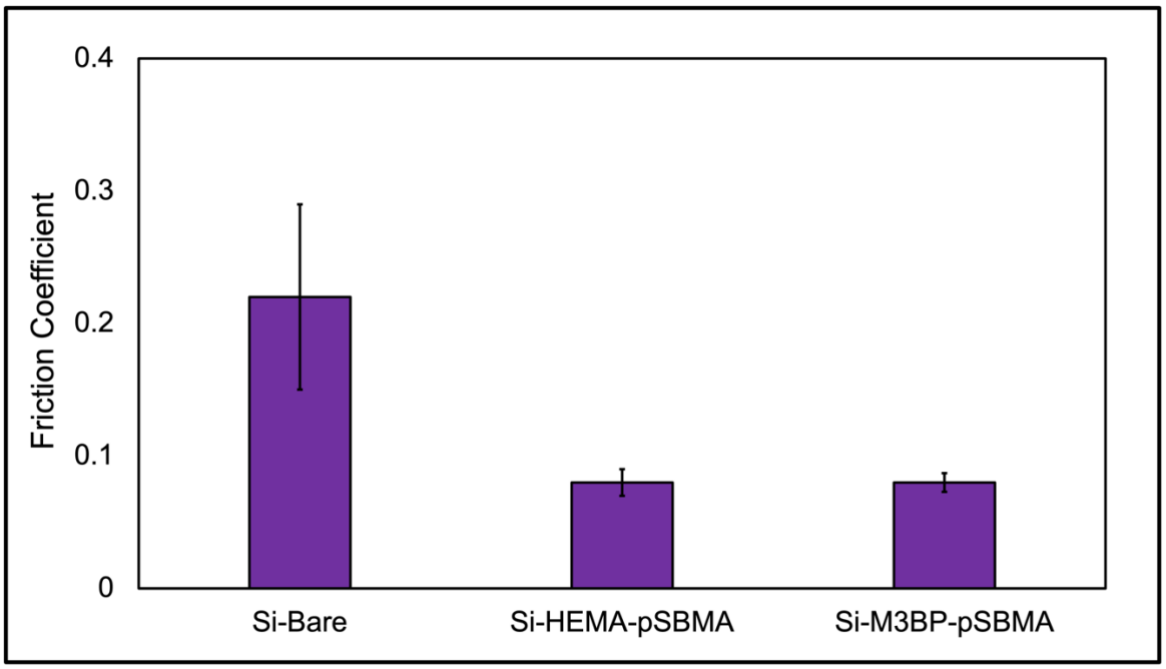

Figure 4.4. Friction coefficients of hydrated silicon substrates before and after grafting pSBMA coatings, measured using nanoindenter (n=3).

There is a significant difference in the friction coefficients of bare and pSBMA-grafted titanium surfaces despite the high roughness of the underlying titanium surface. This observation further confirms the ability of the pSBMA coatings to form strong, and stable hydration which uniformly cover the coated surfaces, improving surface lubricity. Upon soaking in water, the zwitterionic polymer chains tend to extend vertically due to the osmotic pressure repulsion between adjacent polymer chains, also causing the coating layer to slightly swell. The extended conformation of the polymer chains further improves the stability and strength of the attached hydration layer.[23] The dynamic profiles for friction coefficients are depicted in Figure 4.5. The coated surfaces exhibit substantially more uniform profiles with minimal local variations in contrast to the rougher bare surface. The reduced local variations in friction coefficients of

pSBMA- functionalized surfaces further confirm the uniformity of the polymer coatings, and thus the interfacial hydration sheaths formed around the polymer brush structures.[28]

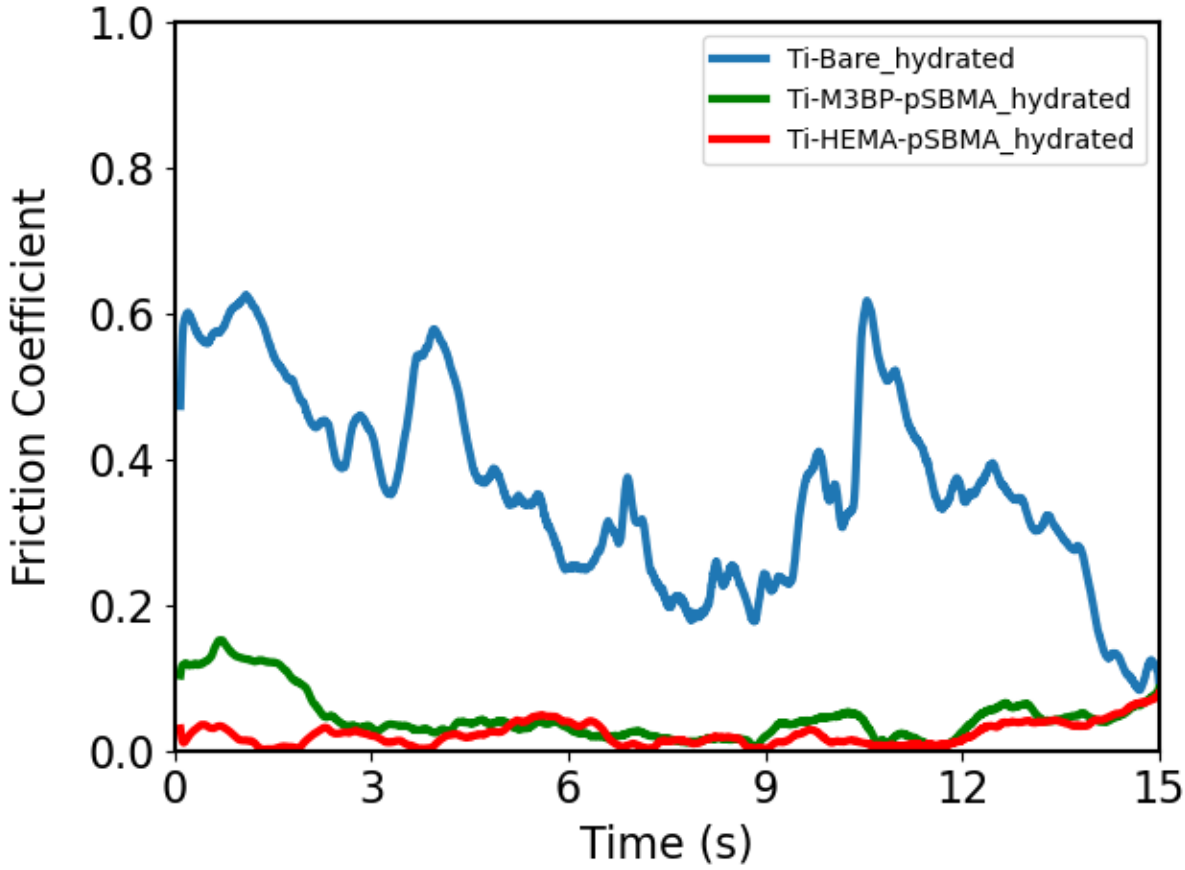

Figure 4.5. Representative dynamic friction coefficient profiles of bare and pSBMA-coated titanium surfaces showing reduced local variations for the functionalized samples. It must be noted that the dynamic measurements correspond to different points on the surface as the tip translates.

To further confirm the effect of hydration on the lubricity of the coatings, friction coefficients were also measured for the samples in dry state and after redrying, i.e. drying again after the hydration step. The results for titanium surfaces are summarized in Figure 4.6 for samples prepared using methodology 1 and in Figure 4.7 for methodology 2.

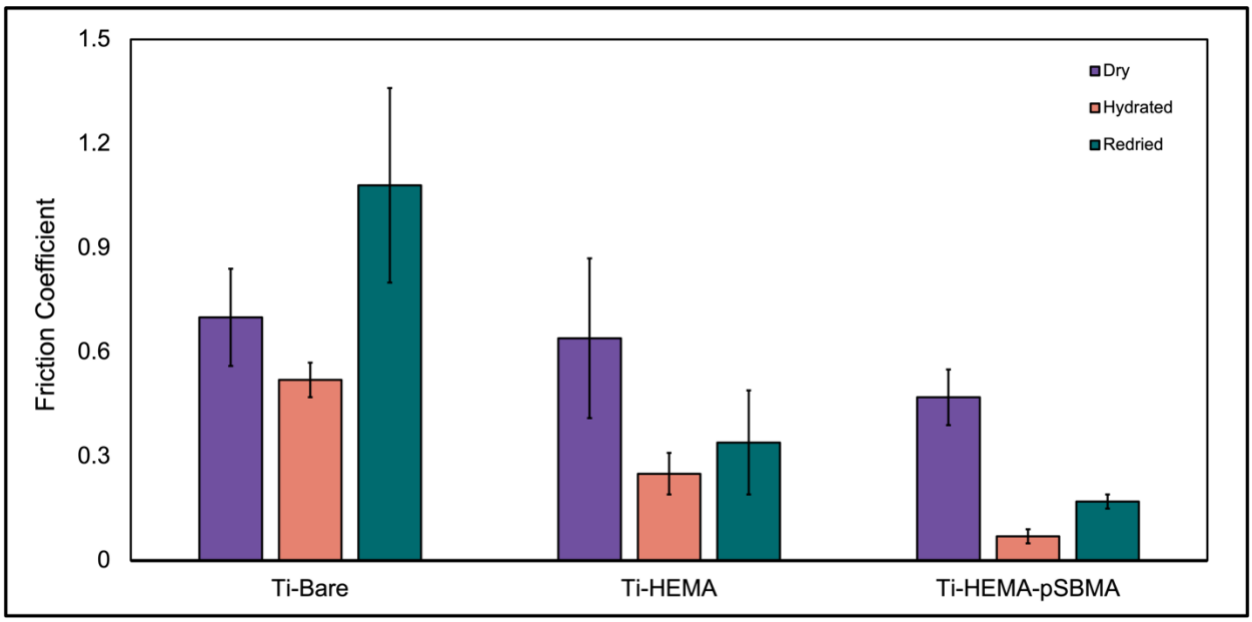

Figure 4.6. Friction coefficients of titanium surfaces functionalized using methodology 1, measured for dry, hydrated and redried samples (n=3).

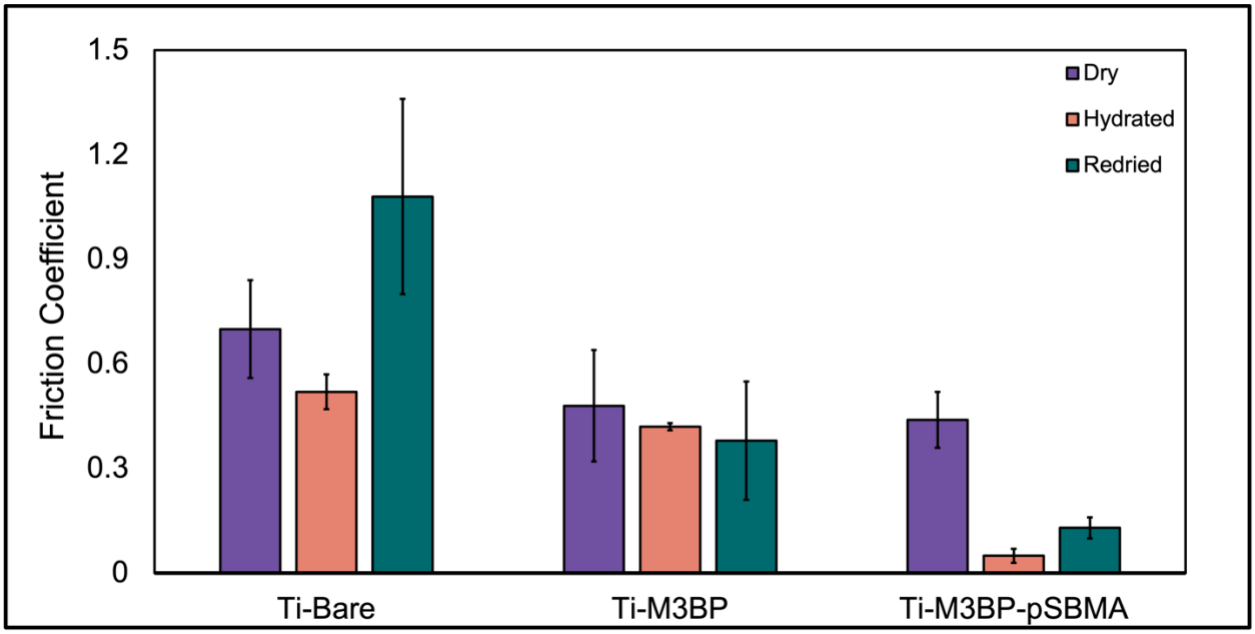

Figure 4.7. Friction coefficients of titanium surfaces functionalized using methodology 2, measured for dry, hydrated, and redried samples (n=3).

The same samples were used for measuring the friction coefficients in all three hydration states. The friction coefficients were first measured after thoroughly drying the sample immediately following ARGET ATRP sample preparation (dry). The samples were then soaked in cell culture medium for 24 h and incubated at 37°C, at the end of which the friction coefficients were measured again (hydrated). Samples were air dried before loading them into the nanoindenter to remove any visible surface water. Following these measurements, the samples were dried again by keeping under vacuum for 24 h (redried). Friction coefficients were then measured on the redried samples.

Dry and redried surfaces expectedly exhibited higher friction coefficients in comparison to hydrated surfaces, especially for the pSBMA-grafted surfaces. For titanium surfaces prepared using methodology 1, a small decrease was observed in the friction coefficient of dry titanium after the deposition the HEMA coating, which further reduced upon pSBMA grafting. The changes were, however, much more significant for the same samples in the hydrated state. The friction coefficient of bare titanium was 0.52 which reduced by almost 2x to a value of 0.25 after HEMA deposition. Friction coefficients as low as 0.07 were measured for Ti-HEMA-pSBMA surfaces, exhibiting approximately 87% reduction in comparison to Ti-Bare samples. The >2x reduction in friction coefficient for Ti-HEMA samples can be explained based on the hydrophilic nature of the abundant hydroxyl groups present on HEMA-coated surfaces and their ability to form hydration layers via hydrogen bonding. The more prominent changes for pSBMA further confirm that the combined effect of electrostatic interactions and hydrogen bonding can create hydration layers that are more uniform and offer better surface coverage, confirming the super-hydrophilic nature of zwitterionic sulfobetaine molecules. The friction coefficients increased again upon redrying the samples, confirming the effect of hydration induced lubricity. However, the friction coefficient

values for redried samples were still much lower than the values obtained for dry samples. This could possibly be due to incomplete drying in 24 h in addition to the lingering effect of hydration on the hydrophilic HEMA and pSBMA-functionalized samples, which can retain hydration for longer periods.

Similar trends were also observed for samples prepared using methodology 2, with the exception of Ti-M3BP samples which did not show any significant change upon hydration or drying. This can be explained based on the hydrophobic nature of the bromine molecules present in abundance on the surfaces. The pSBMA coated samples exhibited a >88% reduction in friction coefficient after hydration, values like pSBMA samples prepared using methodology 1 (~85%). Similar trends were observed for samples prepared on silicon wafers, for dry, hydrated, and redried samples respectively. The average friction coefficients in dry, hydrated and redried state for bare and functionalized silicon wafers are depicted in Figure 4.8 for methodology 1 and Figure 4.9 for methodology 2.

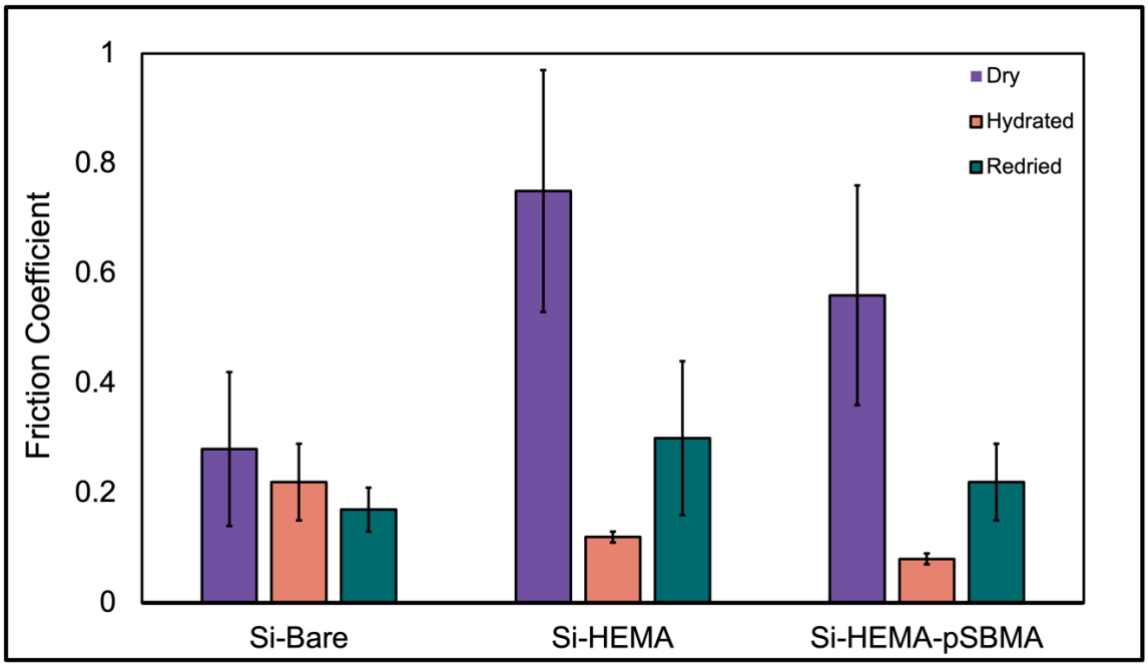

Figure 4.8. Friction coefficients of silicon surfaces functionalized using methodology 1, measured for dry, hydrated, and redried samples (n=3).

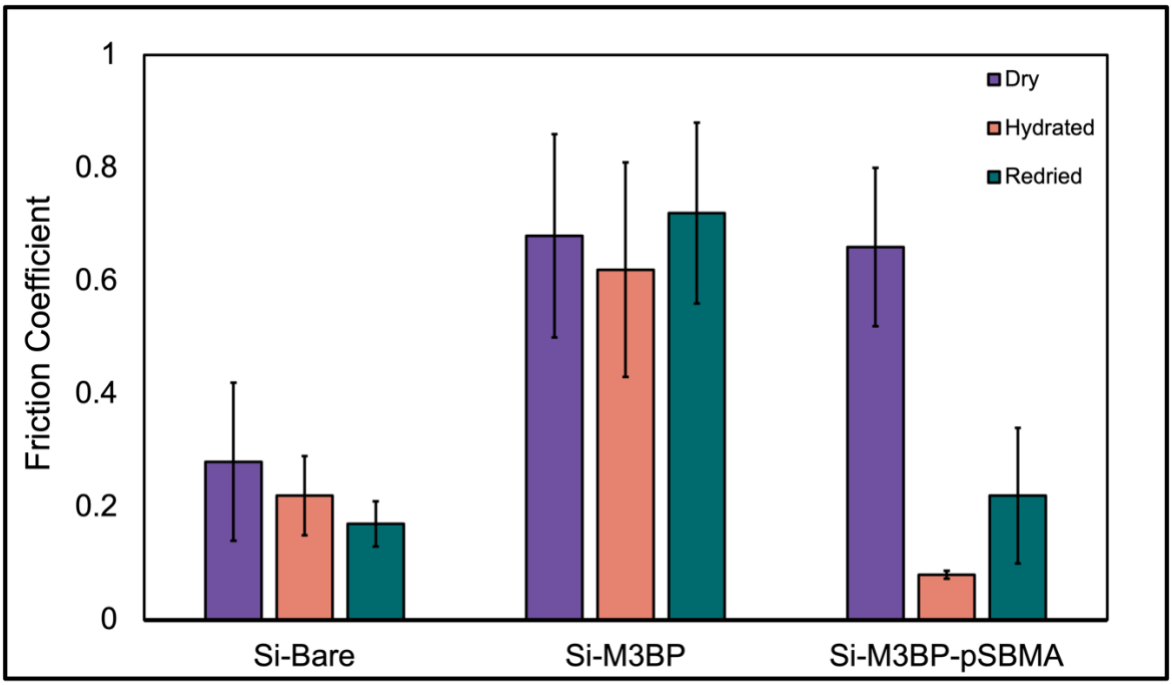

Figure 4.9. Friction coefficients of silicon surfaces functionalized using methodology 2, measured for dry, hydrated, and redried samples (n=3).

4.4 SUMMARY AND CONCLUSIONS

The surface lubrication performance of coated implant materials prepared using the protocols outlined in chapters 2 and 3 has been investigated. Silicon wafers and titanium substrates were used for this study, and the friction coefficients were measured using nanoindenter in the hydrated state at a reasonably relevant loading (0.12 MPa). The coated surfaces exhibited substantial reductions in friction coefficient over the bare samples, indicating improved lubricity on account of strong interfacial hydration effects and resulting fluidity of the adhered water. In particular, the Ti-HEMA-pSBMA samples were measured to have an average friction coefficient of 0.07 while the Ti-M3BP-pSBMA surfaces exhibited average friction coefficients of ~ 0.05. These values represent a 7-10x reduction over the bare Ti (0.52) and signify the ability of both methodologies to achieve high-quality hydrophilic coatings which result in friction coefficients

substantially close to that of biological environments.[1,16,23] In addition, representative dynamic profiles of friction coefficients revealed minimal variance for the hydrated coated samples, which indicates uniform coatings and is expected to have attendant advantages for overall implant longevity.

There is scope for refinement and improvement of these results to establish performance in more realistic scenarios. In particular, the tests performed herein were at a fixed value of the normal load, whereas biological environments are characterized by substantial temporal variations in loadings on implants. Thus repeating the measurements at prolonged higher loadings (~ 0.5 – 1 MPa) is a straightforward extension of this work. In addition, these tests will also establish the mechanical stability and abrasion resistance of these coatings, which have been known to delaminate at excessively high loadings.[4] It is also important to perform friction coefficient measurements in truly 'wet' conditions to mimic actual biological environments. For these tests, given the limitations of the nanoindenter, the friction coefficient measurements were performed after 'wetting'. Friction coefficient measurements in the truly 'wet' state can help obtain a more detailed understanding of lubrication performance in conditions closer to the *in vivo* environment of the implant and improve the accuracy of the friction coefficient measurements.

4.5 REFERENCES

(1) Wei, Q.; Liu, X.; Yue, Q.; Ma, S.; Zhou, F. Mussel-Inspired One-Step Fabrication of Ultralow-Friction Coatings on Diverse Biomaterial Surfaces. Langmuir 2019. https://doi.org/10.1021/acs.langmuir.9b00421.

(2) Caligaris, M.; Ateshian, G. A. Effects of Sustained Interstitial Fluid Pressurization under Migrating Contact Area, and Boundary Lubrication by Synovial Fluid, on Cartilage Friction. Osteoarthritis Cartilage 2008, 16 (10), 1220–1227. https://doi.org/10.1016/j.joca.2008.02.020.

(3) Oungoulian, S. R.; Durney, K. M.; Jones, B. K.; Ahmad, C. S.; Hung, C. T.; Ateshian, G. A. Wear and Damage of Articular Cartilage with Friction against Orthopedic Implant Materials. J Biomech 2015, 48 (10), 1957–1964. https://doi.org/10.1016/j.jbiomech.2015.04.008.

(4) Ishihara, K. Biomimetic Materials Based on Zwitterionic Polymers toward Human-Friendly Medical Devices. Sci Technol Adv Mater 2022, 23 (1), 498–524. https://doi.org/10.1080/14686996.2022.2119883.

(5) Kyomoto, M.; Moro, T.; Yamane, S.; Watanabe, K.; Hashimoto, M.; Tanaka, S.; Ishihara, K. Hydrated Phospholipid Polymer Gel-Like Layer for Increased Durability of Orthopedic Bearing Surfaces. Langmuir 2019, 35 (5), 1954–1963. https://doi.org/10.1021/acs.langmuir.8b01494.

(6) Lin, W.; Klein, J. Recent Progress in Cartilage Lubrication. Advanced Materials 2021, 33 (18), 2005513. https://doi.org/https://doi.org/10.1002/adma.202005513.

(7) Mandich, J.; Casebier, J.; Francis, J.; Chandramouli, S.; Balasubramanian, R.; Warnock, J. Implantable Mechanisms for Orthopedic Surgery: Validation Using Biomechanical Simulation and Cadaver Study in Chicken Foot. In Proceedings of the Veterinary Orthopedics Society; 2017.

(8) Le, A. J.; Casebier, J.; Mandich, J.; Larson, M. K.; Warnock, J.; Sweeney, J.; Balasubramanian, R. Evaluation of Postoperative Healing for Novel Tendon-Transfer Surgery Using an Implantable Passive Mechanism: A Pilot In Vivo Study. In Proceedings of the Veterinary Orthopedics Society; 2017.

(9) Nakano, H.; Noguchi, Y.; Kakinoki, S.; Yamakawa, M.; Osaka, I.; Iwasaki, Y. Highly Durable Lubricity of Photo-Cross-Linked Zwitterionic Polymer Brushes Supported by Poly(Ether Ether Ketone) Substrate. ACS Appl Bio Mater 2020, 3 (2), 1071–1078. https://doi.org/10.1021/acsabm.9b01040.

(10) Milner, P. E.; Parkes, M.; Puetzer, J. L.; Chapman, R.; Stevens, M. M.; Cann, P.; Jeffers, J. R. T. A Low Friction, Biphasic and Boundary Lubricating Hydrogel for Cartilage Replacement. Acta Biomater 2018, 65, 102–111. https://doi.org/10.1016/j.actbio.2017.11.002.

(11) Zhang, Z.; Chao, T.; Chen, S.; Jiang, S. Superlow Fouling Sulfobetaine and Carboxybetaine Polymers on Glass Slides. Langmuir 2006, 22 (24), 10072–10077. https://doi.org/10.1021/la062175d.

(12) Zhang, Z.; Chen, S.; Chang, Y.; Jiang, S. Surface Grafted Sulfobetaine Polymers via Atom Transfer Radical Polymerization as Superlow Fouling Coatings. Journal of Physical Chemistry B 2006, 110 (22), 10799–10804. https://doi.org/10.1021/jp057266i.

(13) Chang, Y.; Chen, S.; Zhang, Z.; Jiang, S. Highly Protein-Resistant Coatings from Well-Defined Diblock Copolymers Containing Sulfobetaines. Langmuir 2006, 22 (5), 2222–2226. https://doi.org/10.1021/la052962v.

(14) Sin, M. C.; Sun, Y. M.; Chang, Y. Zwitterionic-Based Stainless Steel with Well-Defined Polysulfobetaine Brushes for General Bioadhesive Control. ACS Appl Mater Interfaces 2014, 6 (2). https://doi.org/10.1021/am4041256.

(15) Lin, X.; Jain, P.; Wu, K.; Hong, D.; Hung, H. C.; O'Kelly, M. B.; Li, B.; Zhang, P.; Yuan, Z.; Jiang, S. Ultralow Fouling and Functionalizable Surface Chemistry Based on Zwitterionic Carboxybetaine Random Copolymers. Langmuir 2019, 35 (5), 1544–1551. https://doi.org/10.1021/acs.langmuir.8b02540.

(16) Kyomoto, M.; Moro, T.; Miyaji, F.; Hashimoto, M.; Kawaguchi, H.; Takatori, Y.; Nakamura, K.; Ishihara, K. Effect of 2-Methacryloyloxyethyl Phosphorylcholine Concentration on Photo-Induced Graft Polymerization of Polyethylene in Reducing the Wear of Orthopaedic Bearing Surface. J Biomed Mater Res A 2008, 86A (2), 439–447. https://doi.org/https://doi.org/10.1002/jbm.a.31511.

(17) Chen, M.; Briscoe, W. H.; Armes, S. P.; Cohen, H.; Klein, J. Polyzwitterionic Brushes: Extreme Lubrication by Design. In European Polymer Journal; 2011; Vol. 47, pp 511–523. https://doi.org/10.1016/j.eurpolymj.2010.10.007.

(18) Kyomoto, M.; Moro, T.; Iwasaki, Y.; Miyaji, F.; Kawaguchi, H.; Takatori, Y.; Nakamura, K.; Ishihara, K. Superlubricious Surface Mimicking Articular Cartilage by Grafting Poly(2-Methacryloyloxyethyl Phosphorylcholine) on Orthopaedic Metal Bearings. J Biomed Mater Res A 2009, 91A (3), 730–741. https://doi.org/https://doi.org/10.1002/jbm.a.32280.

(19) Klein, J. Hydration Lubrication. Friction 2013, 1 (1), 1–23. https://doi.org/10.1007/s40544-013-0001-7.

(20) Klein, J.; Raviv, U.; Perkin, S.; Kampf, N.; Chai, L.; Giasson, S. Fluidity of Water and of Hydrated Ions Confined between Solid Surfaces to Molecularly Thin Films. Journal of Physics Condensed Matter 2004, 16 (45). https://doi.org/10.1088/0953-8984/16/45/008.

(21) Leng, C.; Hung, H. C.; Sun, S.; Wang, D.; Li, Y.; Jiang, S.; Chen, Z. Probing the Surface Hydration of Nonfouling Zwitterionic and PEG Materials in Contact with Proteins. ACS Appl Mater Interfaces 2015, 7 (30), 16881–16888. https://doi.org/10.1021/acsami.5b05627.

(22) Wu, J.; Lin, W.; Wang, Z.; Chen, S. Investigation of the Hydration of Nonfouling Material Poly(Sulfobetaine Methacrylate) by Low-Field Nuclear Magnetic Resonance. Langmuir 2012, 28 (4), 2137–2144. https://doi.org/10.1021/la203827h.

(23) Superlubricity Achieved with Zwitterionic Brushes in Diverse Conditions Induced by Shear Actions. Macromolecules 2021, 54 (12), 5719–5727. https://doi.org/10.1021/acs.macromol.1c00430.

(24) Matyjaszewski, K.; Hongchen, D.; Jakubowski, W.; Pietrasik, J.; Kusumo, A. Grafting from Surfaces for "Everyone": ARGET ATRP in the Presence of Air. Langmuir 2007, 23 (8), 4528–4531. https://doi.org/10.1021/la063402e.

(25) Hong, D.; Hung, H. C.; Wu, K.; Lin, X.; Sun, F.; Zhang, P.; Liu, S.; Cook, K. E.; Jiang, S. Achieving Ultralow Fouling under Ambient Conditions via Surface-Initiated ARGET ATRP of Carboxybetaine. ACS Appl Mater Interfaces 2017, 9 (11), 9255–9259. https://doi.org/10.1021/acsami.7b01530.

(26) Kaßel, M.; Gerke, J.; Ley, A.; Vana, P. Surface Modification of Wood Flour via ARGET ATRP and Its Application as Filler in Thermoplastics. Polymers (Basel) 2018, 10 (4), 1–16. https://doi.org/10.3390/polym10040354.

(27) Bennion, D. M.; Horne, R.; Peel, A.; Reineke, P.; Henslee, A.; Kaufmann, C.; Guymon, C. A.; Hansen, M. R. Zwitterionic Photografted Coatings of Cochlear Implant Biomaterials Reduce Friction and Insertion Forces. Otology & Neurotology 2021, 42 (10).

(28) Raviv, U.; Giasson, S.; Kampf, N.; Gohy, J. F.; Jéröme, R.; Klein, J. Lubrication by Charged Polymers. Nature 2003, 425 (6954), 163–165. https://doi.org/10.1038/nature01970.

Chapter 5. SUMMARY AND FUTURE WORK

5.1 SUMMARY

This dissertation has presented a comprehensive description and application of two surface modification techniques aimed at improving the biocompatibility of polyurethane and titanium, both of major salience for biomedical implants as part of a tendon transfer mechanism for treating ulnar median palsy. The first method (Chapter 2) involves a combination of RFGD plasma surface activation of the substrate, followed by surface initiated ARGET ATRP grafting of superhydrophilic zwitterionic pSBMA brushes. The surfaces prepared thus were subjected to extensive characterization using XPS, and the surface compositions thus obtained exhibited close agreement with theoretical values, confirming successful chemical transformation at the surface. The biocompatibility of the surfaces was evaluated using radiolabeled adsorption tests, and the coated surfaces exhibited a 93% reduction in adsorbed protein over bare surfaces. In addition, multiple vigorous chemical exposure and wash tests revealed negligible changes in surface elemental composition and film thickness, testifying to the chemical robustness of the coatings and good *in vitro* performance. *In vivo* implantation in mouse and chicken models also provided promising results, revealing minimal inflammation and foreign body capsule formation vis-à-vis bare implants.

Building on this work, chapter 3 discussed the use of a highly reactive haloester, methyl 3-bromopropionate (M3BP) as an initiator for ARGET ATRP for grafting pSBMA coatings. Bromine species surface localized by plasma deposition of M3BP were explored as initiators for ARGET ATRP for grafting zwitterionic molecules. The prepared surfaces were characterized in a similar manner to those prepared in chapter 2. After confirming the deposition of a stable M3BP layer, rich in bromine species, the surface wettability, chemical composition, robustness, and *in*

vitro stability were evaluated for the synthesized pSBMA coatings. The pSBMA coatings showed an 87% reduction in adsorbed protein over bare surfaces, results comparable to those obtained for similar surfaces prepared using methodologies discussed in chapter 2. This methodology also exhibits the added advantage of being compatible with a variety of materials used in biomedical devices and implants, irrespective of surface chemistry or geometry. The favorable results thus obtained using this solvent-free initiator deposition approach show promise for further development for creating functionalized surfaces of various chemistries. The solvent-free approach also simplifies the overall protocol and eliminates the use of solvents with potentially deleterious effects on substrate mechanical properties.

The lubrication performance of the superhydrophilic surfaces prepared using the above discussed methodologies was evaluated in chapter 4. Friction coefficients as low as 0.07 were achieved for pSBMA coatings grafted on titanium substrates using methodologies discussed in chapter 2, signifying a ~7x reduction over bare titanium surfaces. For surfaces prepared using methods discussed in chapter 3, friction coefficients values were ~0.05, a ~10x reduction in comparison to bare titanium substrates. In addition to the effect of surface functionalization, the effect of hydration or fluidity of water on surface lubricity was also explored. These results indicate the formation of uniform hydration sheath layers on the surfaces grafted with pSBMA, by means of stable polymer brush structures with suitable surface density, orientation, and robustness to ensure friction coefficients comparable to natural joints under physiological conditions.

5.2 FUTURE WORK

Some potential research extensions are now outlined to further improve the performance of these coatings and to help realize their potential as simple and scalable surface modification approaches. It is required to bring down protein adsorption levels from ~10 ng/cm^2 to <5 ng/cm^2

for wider applicability in real-world applications. There is scope for further optimization of the brush grafting density by exploring alternative initiator molecules and immobilization methods. By controlling the initiator density, the grafting density and molecular weight of the polymer chains can be tuned.[1] By creating gradients of hydroxyl group density on the surface of titanium, followed by the immobilization of an initiator such as bis[2-(2′-bromoisobutyryloxy) undecyl] disulfide, the initiator density on the surface can be tuned, which can further help tune the grafting density and molecular weight of polymer chains. The solubility of monomers like SBMA are ionic strength dependent and can be increased by the introduction of salts like sodium chloride, which can further help tune the chain length and molecular weight.[2] Other zwitterionic monomers such as CBMA, which are known to have better hydrophilic properties owing to the shorter separation between charged moieties, can also be explored as non-fouling coatings using the discussed methodology.[3]

The above refinements including addition of salts and using CBMA monomers can be examined for the M3BP-based approach as well. For M3BP-based approaches, it is particularly worthwhile to examine the effect of M3BP surface concentration on ultimate brush density and correlated hydrophilicity metrics.[4–6] In particular, it is possible to blend M3BP vapors with an inert species such as methyl propionate, which leads to a competitive adsorption effect, and the relative reactant amounts can be manipulated to vary the bromine surface composition from 0% to the theoretical maximum of 14%. The characterization of these surfaces based on standard hydrophilic measures can then provide useful insights into the effect of initiator amounts on the quality of surface modification. In addition, evaluating the *in vivo* performance of the prepared surfaces discussed in chapter 3 is an immediate future work.

There is also scope for significant extension of the lubrication results. In particular, the experiments herein were performed after 'wetting' the sample due to the limitations of the nanoindenter equipment. A simple extension is testing friction coefficients in actual biological fluids, mimicking the biological and physiological environment of the implants using a surface force apparatus. Additionally, more accurate estimates of friction coefficients will result by performing measurements at higher loadings to verify the shear resistance and robustness of the coatings. The friction coefficient evaluations can also be refined by subjecting the coatings to cyclic loadings and sliding tests, both of which simulate actual implant operation.[7]

These results collectively illustrate the potential of these treatments to be adapted for coating biomedical implants at scale, and the methodologies introduced herein represent a suite of simple but versatile and effective surface treatments applicable to an array of relevant materials used for biomedical implants. In conjunction with the suggested improvements, this work has the potential to achieve non-trivial progress towards FBR mitigation, hasten further development of medical implants, and ultimately help improve quality of life.

5.3 REFERENCES

(1) Ahmed, S. T.; Leckband, D. E. Protein Adsorption on Grafted Zwitterionic Polymers Depends on Chain Density and Molecular Weight. Adv Funct Mater 2020, 30 (30), 2000757. https://doi.org/https://doi.org/10.1002/adfm.202000757.

(2) Delgado, J. D.; Schlenoff, J. B. Static and Dynamic Solution Behavior of a Polyzwitterion Using a Hofmeister Salt Series. Macromolecules 2017, 50 (11), 4454–4464. https://doi.org/10.1021/acs.macromol.7b00525.

(3) Zhang, Z.; Finlay, J. A.; Wang, L.; Gao, Y.; Callow, J. A.; Callow, M. E.; Jiang, S. Polysulfobetaine-Grafted Surfaces as Environmentally Benign Ultralow Fouling Marine Coatings. Langmuir 2009, 25 (23), 13516–13521. https://doi.org/10.1021/la901957k.

(4) Lorusso, E.; Ali, W.; Leniart, M.; Gebert, B.; Oberthür, M.; Gutmann, J. S. Tuning the Density of Zwitterionic Polymer Brushes on PET Fabrics by Aminolysis: Effect on Antifouling Performances. Polymers (Basel) 2020, 12 (1), 1–14. https://doi.org/10.3390/polym12010006.

(5) Mecwan, M. M.; Taylor, M. J.; Graham, D. J.; Ratner, B. D. Highly-Reactive Haloester Surface Initiators for ARGET ATRP Readily Prepared by Radio Frequency Glow Discharge Plasma. Biointerphases 2019, 14 (4), 041006. https://doi.org/10.1116/1.5110163.

(6) Kyomoto, M.; Moro, T.; Miyaji, F.; Hashimoto, M.; Kawaguchi, H.; Takatori, Y.; Nakamura, K.; Ishihara, K. Effect of 2-Methacryloyloxyethyl Phosphorylcholine Concentration on Photo-Induced Graft Polymerization of Polyethylene in Reducing the Wear of Orthopaedic Bearing Surface. J Biomed Mater Res A 2008, 86A (2), 439–447. https://doi.org/https://doi.org/10.1002/jbm.a.31511.

(7) Wei, Q.; Liu, X.; Yue, Q.; Ma, S.; Zhou, F. Mussel-Inspired One-Step Fabrication of Ultralow-Friction Coatings on Diverse Biomaterial Surfaces. Langmuir 2019. https://doi.org/10.1021/acs.langmuir.9b00421.

Appendix A. GRAFTING PSBMA BRUSHES ON POLYPROPYLENE USING RFGD PLASMA AND ATRP

A.1 SUBSTRATE PREPARATION

For the fabrication of polypropylene (PP) substrates, medical-grade PP was used. PP discs were prepared by first heat pressing PP pellets into a 0.5 mm thick sheet and then punching 8 mm discs. The substrates were then cleaned by sonication in n-hexane, methylene chloride, acetone, and methanol for 15 min each. This cycle was repeated three times and solvents were changed between each cycle. The samples were dried under vacuum and placed in a desiccator until further use.

A.2 SURFACE ACTIVATION USING RFGD PLASMA

The surfaces were activated using the procedure used for RPU-70 as described under section 2.3.1.2. The HEMA-functionalized samples are denoted as PP-HEMA.

A.3 IMMOBILIZATION OF MACROINITIATOR

BIBB was immobilized on the HEMA-activated surfaces using initiator immobilization protocols used for titanium, as described under section 2.3.1.3. The samples are labeled as PP-HEMA-BIBB.

A.4 SURFACE INITIATED ATRP OF SBMA

The PP samples were prepared using conventional ATRP. The polymerization reaction was performed in a schlenk tube under an argon atmosphere with CuBr-bpy as the catalyst-ligand system. The ratio of the SBMA: CuBr: bpy system was fixed at 10: 1.5: 1.5. A fixed amount of SBMA (200 mg) and an appropriate amount of bpy were first dissolved in 10 ml of 1:1 mixture of

dimethyl sulfoxide and DI water and were then transferred to a dry schlenk tube under constant stirring. The reaction mixture was degassed by freeze-thaw method, running at least three cycles, to get rid of any trapped air bubbles in the mixture. The schlenk tube under vacuum was then connected to the schlenk line and purged with argon followed by the addition of CuBr and the PP-HEMA-BIBB discs. The reaction tube was then again purged with argon and sealed. The reaction was allowed to progress for 24 h at room temperature. The samples (PP-HEMA-pSBMA) were then collected and washed with a 1:1 mixture of water and methanol to remove any unreacted chemicals and then dried under vacuum.

A.5 SURFACE ANALYSIS

The elemental composition of the prepared samples was analyzed with XPS on a Surface Science Instruments S-Probe photoelectron spectrometer. The details of the procedure are described in section 2.3.2.1. The contact angle and protein adsorption were also measured as described in section 2.3.2.3 and section 2.3.2.4, respectively.

A.6 SURFACE MODIFICATION AND PROTEIN ADSORPTION RESULTS

Table A 1. Summary of the surface composition of bare and functionalized PP surfaces as obtained by survey scans from XPS (n=3).

Sample	**Elemental composition (%)**				
	C 1s	**O 1s**	**Br 3d**	**N 1s**	**S 2p**
PP	100 ± 0.02	0.44 ± 0.01	-	-	-
PP-HEMA	69 ± 0.7	31 ± 0.7	-	-	-
PP-HEMA-BIBB	73 ± 0.8	21± 0.6	5.7 ± 0.2	-	-
PP-HEMA-pSBMA	68 ± 0.6	23 ± 0.5	-	3.8 ± 0.07	4.6 ± 0.3

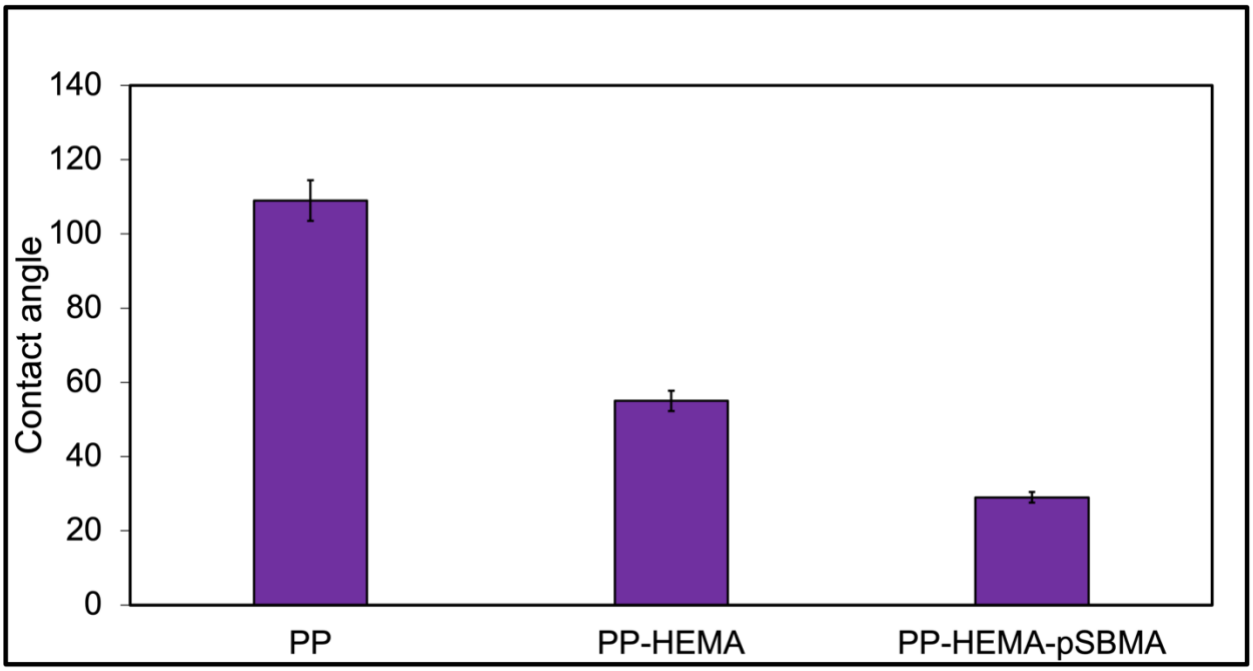

Figure A 1. Contact angle measured on PP surfaces before and after functionalization (n=6).

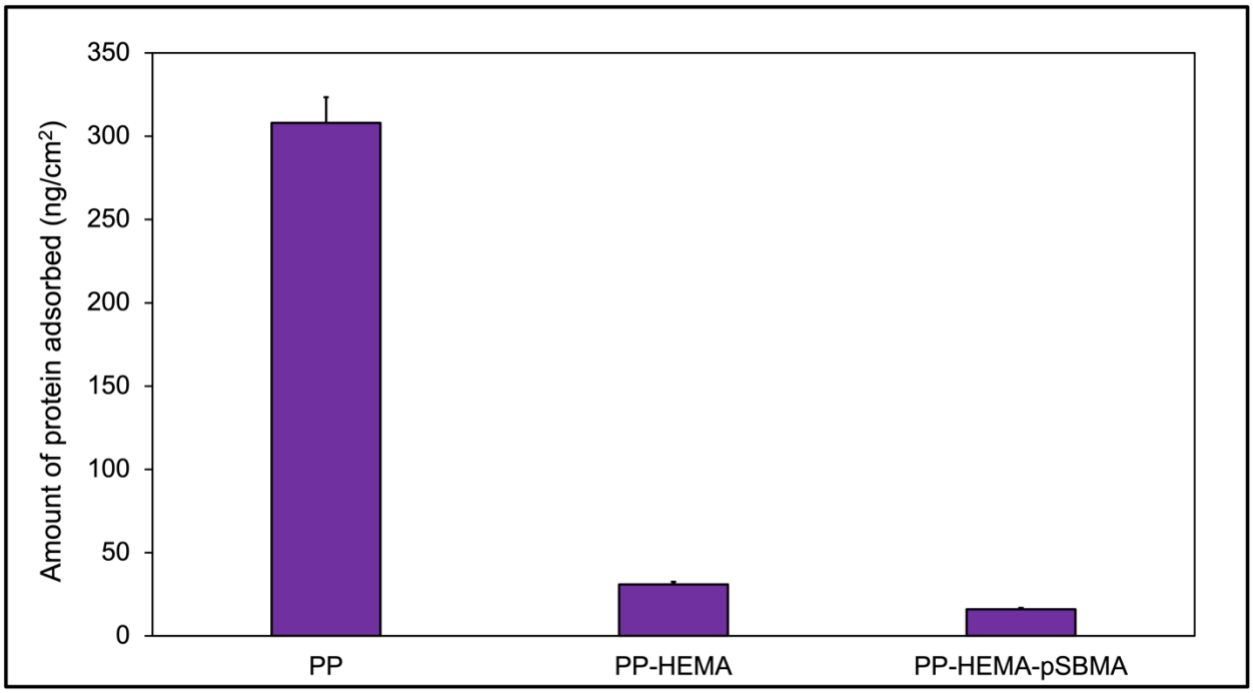

Figure A 2. Protein adsorption measured on PP surfaces before and after functionalization (n=4).

Appendix B. PROTEIN ADSORPTION MEASUREMENTS ON ACRYLATE

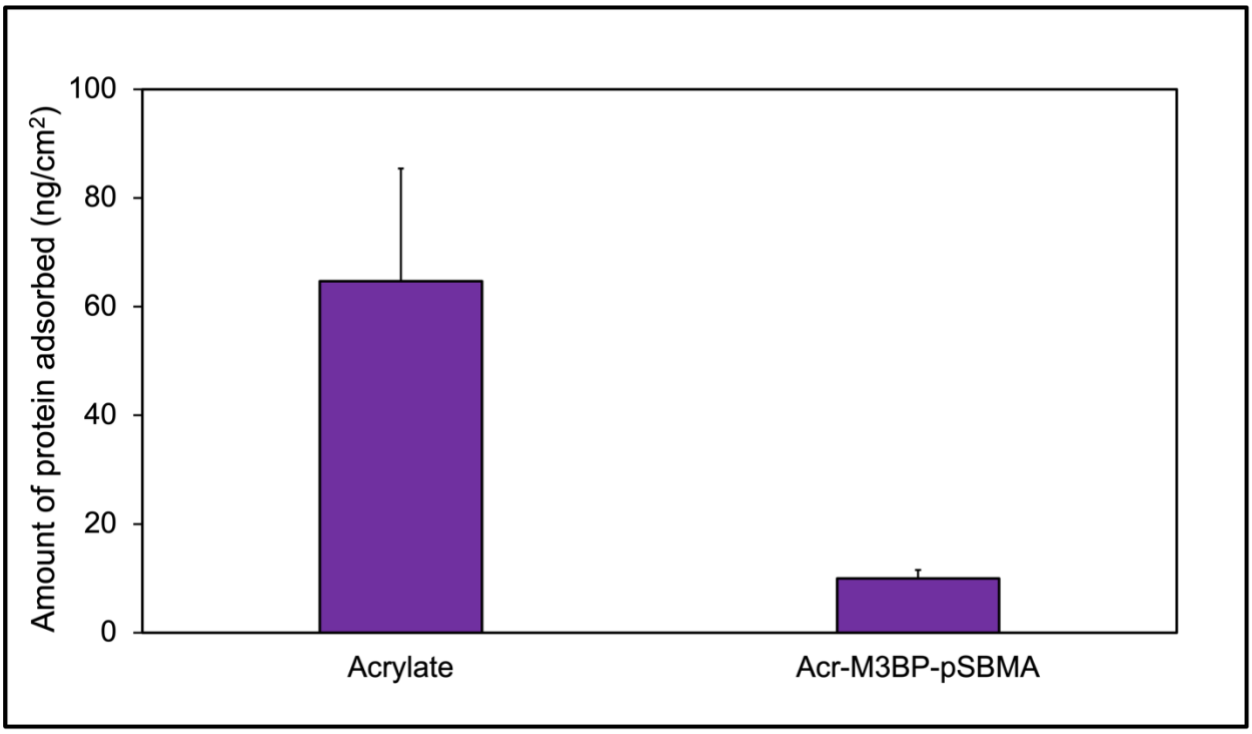

Figure B 1. Protein adsorption measured on acrylate surfaces before and after grafting pSBMA coatings using plasma deposited M3BP as initiator for ARGET ATRP (n=4).

VITA

Prabhleen Kaur was born in Jalandhar, Punjab, India on August 11, 1990 to parents Jasbir Singh and Parminder Kaur. Prabhleen's interest in science began from an early age, thanks to her surgeon parents. It was further solidified in high school when she learnt about nanotechnology. Prabhleen earned her Bachelor of Engineering in Chemical Engineering from DSSBUICET, Panjab University, India in 2013. Soon after she moved to the USA to pursue her Master of Engineering in Chemical and Biomolecular Engineering from Cornell University, where she worked under the guidance of Prof. Yong Lak Joo on nanostructure manufacturing and controlling the distribution of conductive nanofiller in nanofibers using air assisted electrospinning and electrospraying. Prabhleen joined the Ph.D. program in Chemical Engineering at the University of Washington in fall 2016 and worked under the guidance of Prof. Buddy Ratner. Her research at UW focused on developing non-fouling and lubricious biomaterials for applications in medical devices. After earning her Ph.D. in December 2022, Prabhleen plans to begin her scientific career in industrial research and development. Apart from science and research, Prabhleen enjoys baking and exploring new coffee shops around town.